DEVELOPMENT OF SAFE AND EFFECTIVE MAGNETIC RESONANCE CONTRAST AGENTS FOR BLOOD POOL IMAGING AND CANCER DIAGNOSIS

by

Zhen Ye

A dissertation submitted to the faculty of
The University of Utah
in partial fulfillment of the requirements for the degree of

Doctor of Philosophy

Department of Pharmaceutics and Pharmaceutical Chemistry

The University of Utah

May 2016

The University of Utah Graduate School

STATEMENT OF DISSERTATION APPROVAL

The dissertation of **Zhen Ye**

has been approved by the following supervisory committee members:

Hamidreza Ghandehari	, Chair	**02/17/2016** Date Approved
Jindrich Kopecek	, Member	**01/06/2016** Date Approved
Dennis Parker	, Member	**01/06/2016** Date Approved
James Herron	, Member	**02/18/2016** Date Approved
Carol Lim	, Member	**02/22/2016** Date Approved

and by **David Grainger** , Chair/Dean of

the Department/College/School of **Pharmaceutics and Pharmaceutical Chemistry**

and by David B. Kieda, Dean of The Graduate School.

ABSTRACT

The current commercialized Gd(III)-based magnetic resonance (MR) contrast agents are small molecules characterized with short blood half-life and nonspecific tissue distribution. The accuracy of MR diagnosis involving clinical contrast agents is often hindered because of a short diagnostic window and low selectivity of target tissues. Macromolecular Gd(III)-based contrast agents are more effective than small molecular agents for blood pool imaging with high relaxivity and limited vascular extravasation. However, the clinical translation of macromolecular contrast agents is impeded by the potential safety concerns associated with their slow excretion and prolonged tissue retention. Polydisulfide Gd(III) complexes have been developed as biodegradable macromolecular MR contrast agents to facilitate the excretion of Gd(III) chelates and alleviate the safety concerns. The agents can be readily degraded and excreted via renal filtration with minimal tissue retention. However, the reported polydisulfide Gd(III) complexes are based on linear Gd(III) chelates of a DTPA derivative, which has poor kinetic stability. In this research, two alternative polydisulfides have been developed to minimize the stability issue of the linear Gd(III) ligand. Firstly, polydisulfide Mn(II) complexes were developed as gadolinium-free biodegradable macromolecular MRI contrast agents. Two polydisulfide Mn(II) complexes based on Mn-DTPA and Mn-EDTA were synthesized and characterized. Both agents showed comparable relaxivity to the reported polydisulfide Gd(III) complexes. The degradations of both polydisulfide

Mn(II) complexes were demonstrated through in vitro incubation with endogenous free thiols. In vitro transmetallation study revealed higher kinetic inertness of the Mn-DTPA-based agent. In vivo MR evaluation showed preferential contrast enhancement of Mn(II) agents in the liver and myocardium. Secondly, polydisulfides based on the more stable macrocyclic Gd(III) chelates were developed and evaluated. Two polydisulfide Gd-DOTA conjugates with charge differences were synthesized and characterized. Both agents showed improved relaxivity, and efficient degradability. Both in vitro and in vivo transmetallation study revealed higher kinetic inertness of the macrocyclic polydisulfide agents than the previously reported linear agents. The effect of charge on pharmacokinetics and biodistribution was compared and discussed.

TABLE OF CONTENTS

ACKNOWLEDGMENTS

I would first like to send my greatest gratitude to my parents, who are in China, for their emotional support and encouragement while I pursued my goals.

I would also like to thank my committee members, Dr. Carol Lim, Dr. Dennis Parker, Dr. Hamid Ghandehari, Dr. James Herron, and Dr. Jindrich Kopecek, for their support, guidance, and criticism throughout my graduate career. In addition, I would like to thank my colleagues, Dr. Zhuxian Zhou, Dr. Erlei Jin, Dr. Guanping Yu, Mrs. Xiaoyue Shi, Mr. Anthony Malamas, and Mr. Anthony Puntel, as well as my mentors, Dr. Xueming Wu, Dr. Mingquin Tan, Dr. Chengcai Luo, and Dr. Shouyu Yin, for their help with my experiments and providing me with inspirations. I would also like to thank Dr. Eun-Kee Jeong from University of Utah and Dr. Chris Flask and Dr. Mark Grisworld from Case Western Reserve University for their help in MR imaging. Furthermore, I would like to thank my best friend, Fei Wu, for motivating and encouraging me through difficult times.

Most importantly, I would like to thank my mentor and thesis advisor, Dr. Zheng-Rong Lu, for his guidance and help during my graduate career.

This research was supported by NIH grant R01 EB00489.

CHAPTER 1

INTRODUCTION

The development of contrast agents for magnetic resonance imaging (MRI) has been rapidly growing with the expanding clinical needs of MRI, which plays a critical role in routine medical diagnosis. As a noninvasive diagnostic modality, MRI is versatile in providing extensive information of tissues, including their anatomical structure and functional conditions (1-3). Compared to other imaging modalities, MRI has an advantage in providing high-resolution image qualities without the exposure of patients under ionization radiation. Contrast agents have been applied to further extend the clinical potential of MRI. To date, over one third of clinical MR diagnoses are carried out with the administration of contrast media, among which gadolinium (Gd)-based agents have remained the dominant choice in clinical practices (4-6). These Gd(III)-based commercialized agents were small molecular Gd(III) chelates with low tissue selectivity, short blood retention, and fast renal elimination (5, 6). Such unfavorable features have hindered the application of clinical agents in the more advanced diagnostic challenges, such as early detection of cancer.

The concept of Gd(III)-based macromolecular contrast agent stems from the early 1990s in an effort to push the clinical potential of MR imaging, especially in the area of blood pool imaging, including MR angiography and cancer prognosis (7-10). The

increase of molecular size has led to dramatically different physiological behaviors of the macromolecular agents from the small molecular agents. These agents have limited extravasation from the vasculature and longer blood retentions, thus providing blood pool specific images with a longer diagnostic window (7). In addition, the macromolecular contrast agents generally exhibit higher relaxivity than that of the small molecular agents due to reduced molecular rotational tumbling (5). Given these favorable features, research interests on macromolecular contrast agents have been expanding over the past decade, but their further clinical translation is hindered mainly due to safety considerations associated with inefficient elimination (11).

This chapter will briefly cover reviews on the principle of MRI and contrast agents, as well as the advantage and limitation of clinical and experimental macromolecular Gd(III)-based contrast agents in terms of efficacy and safety. In the end, the rationale for our previous and current research on clinically oriented biodegradable macromolecular contrast agents will be summarized.

Magnetic Resonance Imaging

Until the early 1970s, the phenomenon of nuclear magnetic resonance was only used as an analysis tool to detect local molecular environment and identify compounds in chemistry (2). Today, the same principle is utilized as a noninvasive technique to detect the internal structure of living subjects. MRI takes advantage of the vast information in nuclei signals and uses it as a clinical diagnostic tool for disease detection. In comparison to other imaging techniques such as computed tomography (CT) and positron emission tomography (PET), MR imaging can provide deep tissue penetration without the

requirements of radioactive tracer or radiation exposure. In addition, MRI provides high spatial and contrast resolution and is currently the primary imaging tool for soft tissue anatomy (1).

Working Principles of MRI

Spin of Nuclei and Precession in Magnetic Field

MRI generates images from the signals produced by the nuclei of hydrogen atoms in common molecules of the human body such as water and fat. These hydrogen atoms have unpaired protons that add spin to the nuclei. Spin is the intrinsic property of protons and has its individual axis around which the protons rotate. Since proton is positively charged, the spin creates a magnetic moment to the proton, which acts like a small magnet. When exposed to a large external magnetic field (B_0) generated by the MRI machine, the magnetic moments of protons are affected by B_0. In order to achieve minimum energy state, a torque will act on each nucleus and align them parallel or antiparallel with the external magnetic field. As the axis of each nuclei spin aligns with the external magnetic field, their magnetic moments undergo a process called precession. The frequency of this nuclei precession is called the Larmor frequency, ω_L, which is proportional to the strength of the magnetic field, B_0 :

$$\omega_L = \gamma B_0 \qquad (1)$$

where γ is the gyromagnetic ratio of the nucleus of interest.

Radio Frequency Excitation and Signal Collection

The sum of the net magnetic moments of all the nuclei in a given tissue can be represented by the vector sum of their magnetic moments as nuclear magnetization, denoted M, which can be divided into transverse and longitudinal components. The Radio Frequency (RF) receiver coil detects the rotation of the traverse component of M. As the magnetic flux of the transverse component oscillates in the receiver coil, an electrical signal is generated as the MR signal. Upon equilibrium, the nuclei precess at random phases, causing the transverse components of M to cancel out and leaving the longitudinal components as the net equilibrium magnetization, M_0. M_0 occurs as a slight excess of nuclei preferentially align parallel instead of antiparallel with the external field to minimize the energy requirement. This process can be described by equation (2):

$$\frac{N\uparrow}{N\downarrow} = e^{-\gamma h B_0 / k_B T} \qquad (2)$$

where $N\uparrow/N\downarrow$ is the ratio of numbers of nuclei parallel versus antiparallel with the external field, h is Plank's constant, k_B is Boltzmann's constant, and T is the absolute temperature of the sample. The equation illustrates that the equilibrium magnetization M_0 is related to the strength of the external magnetic field. In order to manipulate this net magnetization, an excitation pulse at the Larmor frequency is applied, inducing the net magnetization to tip away from the longitudinal direction to the tranverse direction, as shown in Figure 1.1. The excitation pulse in the form of a magnetic field, $B_1(t)$, causes the transverse magnetization to rotate. The rotation continues after $B_1(t)$ is switched off, producing an alternative voltage that can be detected by the RF receiver coil, which will eventually disappear when the net magnetization decays back to M_0.

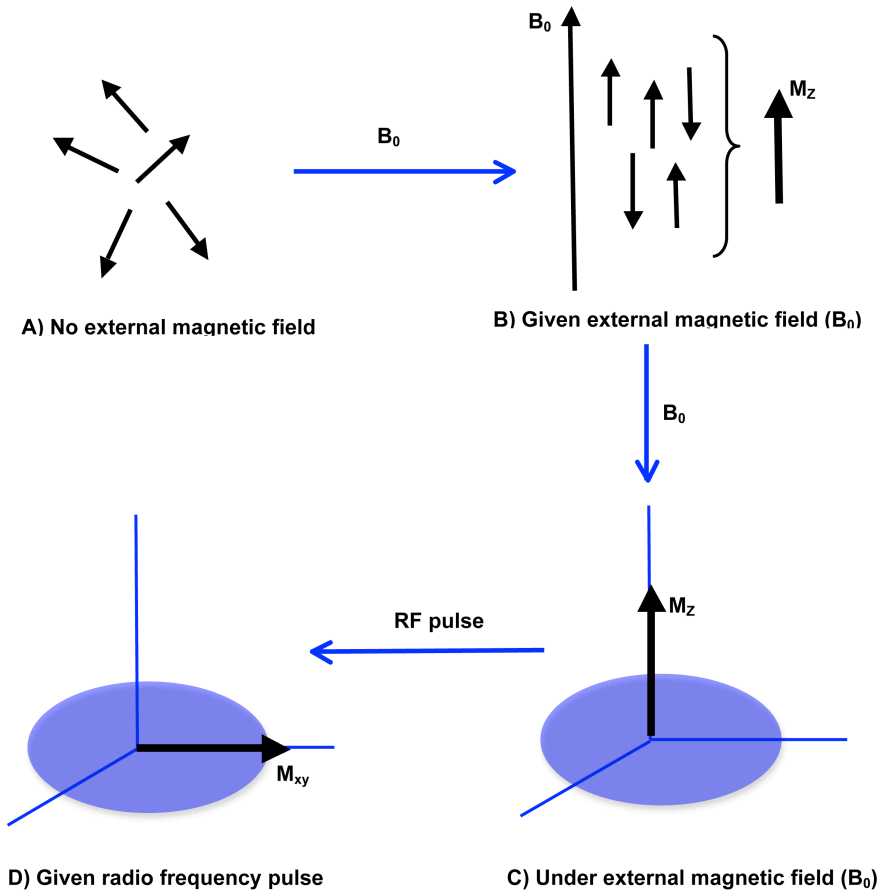

Figure 1.1. Schematic of the change in net magnetization vector, M_0, during MR scans

T_1 and T_2 Relaxation

Due to intramolecular and intermolecular forces, the excited nuclei will eventually relax back to its equilibrium state, which is termed longitudinal relaxation. As the timescale for longitudinal relaxation to occur is designated T_1, the longitudinal relaxation is also called T_1 relaxation. T_1 relaxation is caused by interactions between the nuclei and their environment, and thus varies with different molecules and tissue types to which the nuclei are subjected. Therefore, T_1 is determined by the tumble of a molecule

in its surrounding environement. The T_1 value is shortest as the tumbling rate is closest to the Larmor frequency. In order to obtain signal contrast, excitation and signal collection is performed repeatedly during an MR scanning, and the degree of longitudinal magnetization recovery between each excitation is different. Therefore, the repetition time (TR) of successive excitation becomes important to determine different tissue types, as tissue with long T_1 value cannot regain full magnetization during short TR excitation. In general, MR images acquired during short TR are called 'T_1-weighted' images.

The amplitude of the transverse component of the magnetization depends on the phase coherence of the nuclei. Similar to longitudinal relaxation, the transverse component will decay as well after the initial excitation. However, the transverse relaxation occurs at a faster rate than the longitudinal relaxation. There are generally two sources of dephasing that lead to transverse relaxation. One of them comes from the interaction of the local magnetic fields between the neighboring molecules. The time that it takes is known as T_2. Molecules in constant motion counteract the effect of local magnetic fields and therefore have a slower T_2 relaxation. Macromolecules hence exhibit very short T_2 value since they cannot move freely in their environment. The other source of dephasing comes from the inhomogeneity of the external magnetic field applied. The time value of this process is denoted T_2^*. The ability to be magnetized by the external fields varies among molecules. Depending on their electron configuration, ferromagnetic materials such as most metals are more susceptible to magnetization than diamagnetic and paramagnetic materials. Both T_2 and T_2^* relaxation can be utilized to gain image contrast.

MR Contrast Agents

In order to improve image contrast between normal and diseased tissues, there has been a surge in the development of induced-image contrast using exogenous contrast agents. In the late 1970s, paramagnetic agents were first discovered to enhance tissue discrimination by altering the relaxation time of water protons (4). From a physical point of view, the MR contrast agents can be classified into T_1 and T_2 agents according to the relaxation time they predominantly influence. Contrast agents that mainly affect the T_1 relaxation rate of protons is termed T_1 agents. During the scanning of T_1-weighted images using MR sequences with comparatively short repetition time (TR), the T_1 agents increase the signal intensities of the target tissues and generate positive contrast. The T_2 contrast agents mainly affect the T_2 relaxation of protons. They are used in T_2-weighted imaging scanning with MR sequences of relatively long echo time (TE). The T_2-weight imaging scans will result in decreased signal intensities in the target tissues, leading to darkening of target contrast.

Paramagnetic or superparamagnetic metal species, such as manganese (Mn), iron (Fe), and the lanthanides, possess high magnetic moments that can significantly enhance the relaxation of excited nuclei. They have been considered promising candidates for MR contrast agents. So far, only three metal species, Mn(II), gadolinium (Gd), and Fe(III), have successfully entered clinical application, among which Mn(II) and Gd(III) are T_1 agents and Fe(III) is T_2 agent (5, 12, 13). Gd(III)-based contrast agents are most widely used in clinical applications among all current clinical available MR contrast agents. Over the past decades, Gd(III) continues to be the dominant choice in the development of MR contrast agents due to its superior relaxation enhancing property granted by the large

number of unpaired electrons on its outermost shell and its symmetrical molecular structure (4, 5). Free Gd^{3+} ions have been characterized with high relaxivity, but are too toxic to be given directly (14, 15). Highly stable Gd(III) chelates have been developed to minimize the acute toxicity of Gd^{3+} (5).

Design Rationale for MR Contrast Agents

In general, contrast agents are designed to achieve three major goals regarding effectiveness and safety. Firstly, the agent should generate adequate relaxivity enhancement to increase the sensitivity of MR imaging at acceptable dose. In particular, the agents should be able to increase the relaxation rate of target tissues in order to cause enough contrast for detection. Secondly, the contrast agents should possess certain tissue specificity in order to discriminate the tissue of interest from normal tissues. Thirdly, the contrast agents need to be biocompatible and safe to apply. In the case of Gd(III)-based contrast agents, their ligand structure need to have higher affinity to the Gd^{3+} ions over the endogenous metal ions to minimize their possible interference in vivo for safety purposes. In addition, the Gd(III) complexes also need to be readily excreted after the MR examination to ensure minimal tissue retention of the agents. The efficacy requirement can conflict with the safety need when designing a contrast agent. For instance, agents with rapid clearance might have short blood retention for effective MR evaluation, whereas agents with high relaxivity might exhibit longer tissue accumulation. Therefore, successful design of clinical applicable contrast agents should balance the considerations between efficacy and safety.

Small Molecular Commercial Gd(III)-based Contrast Agents

Chemical Structure

The current clinically available Gd(III)-based MR contrast agents are small molecular Gd(III) complexes, formed between Gd(III) and different polyamino-polycarboxylic ligands (4-6). Based on ligand structure, the current commercial Gd(III)-based contrast agents can be categorized into two distinct categories: 1) the 'linear' chelates based on acyclic triamine (diethylenetriamine) derivatives, including Gd-DTPA (Magnevist®), Gd-DTPA-BMA (Omniscan®), Gd-DTPA-BMEA (OptiMARK®), Gd-BOPTA (MultiHance®), Gd-EOB-DTPA (Primovist®), and MS-325 (Vasovist®); 2) the 'macrocyclic' chelates based on the twelve-membered tetraazamacrocyclic cyclen (1,4,7,10-tetraazacyclododecane) derivatives, including Gd-DOTA (Dotarem®), Gd-HP-DOTA (ProHance®), and Gd-BT-DOTA (Gadovist®) (5). In both types of chelates, Gd^{3+}, with nine coordination sites, is trapped in the cavity of the polyamino-polycarboxylic ligands with eight coordination bonds, leaving one coordination site for inner sphere water binding (4, 5). Depending on the charge of their corresponding ligands, the overall Gd(III) complexes are either electronically neutral (nonionic) or charged (ionic). Thus, the current clinical Gd(III)-based agents can be further devided into four catogeries: the ionic linear, the nonionic linear, the ionic macrocyclic, and the nonionic macrocyclic chelates (Figure 1.2).

All linear Gd(III) agents are formed between Gd^{3+}- and DTPA-derived ligands with open-chain structure. As shown in Figure 1.2, the ionic linear chelates, including Gd-DTPA, Gd-BOPTA, Gd-EOB-DTPA, and MS-325, contain three amino nitrogen atoms and five negatively charged monodentate carboxylic oxygen atoms that bind with Gd^{3+},

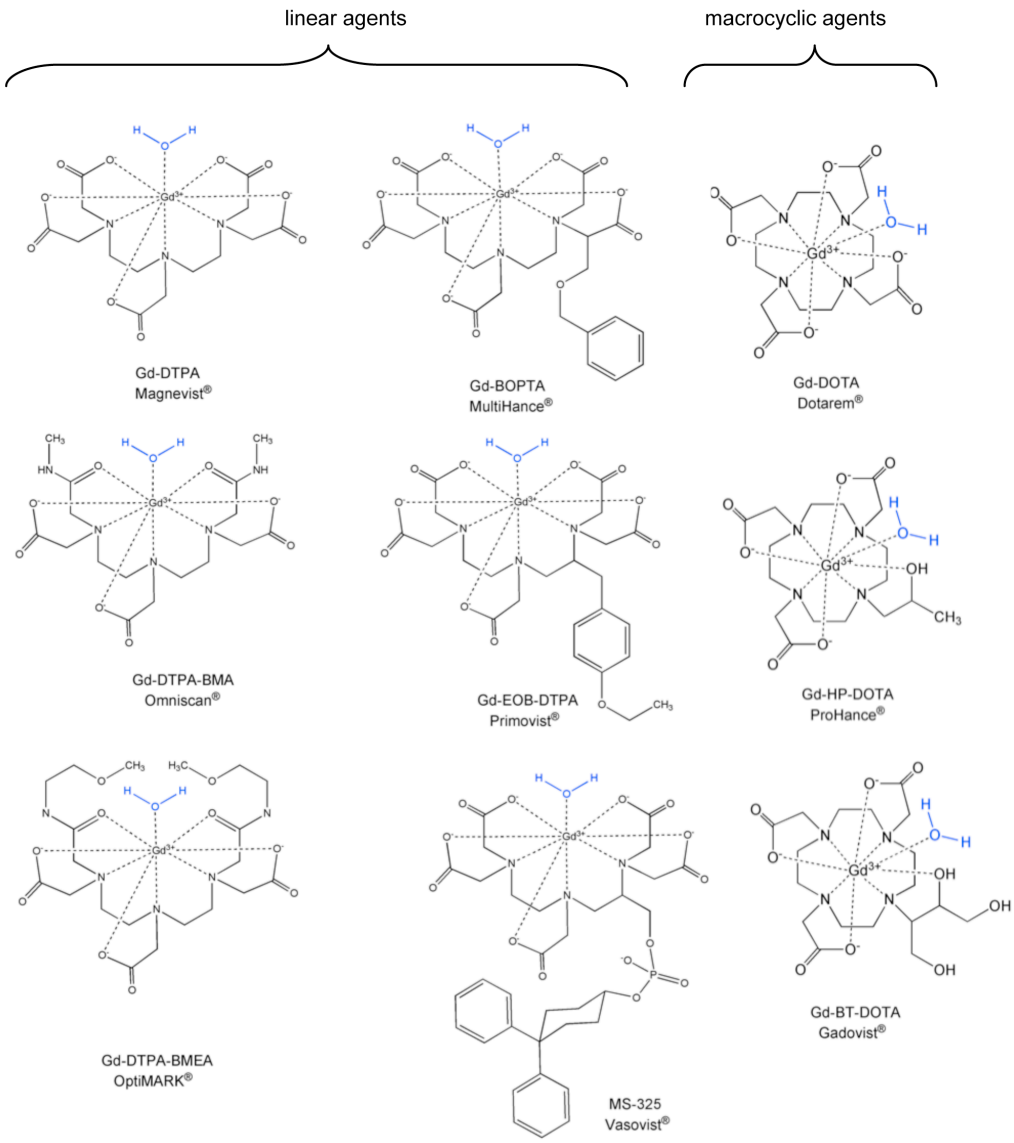

Figure 1.2. Structure of clinical Gd(III)-based contrast agents

resulting in two overall negative charges of the Gd(III) complexes. The negative charges of the overall chelates may result in lower dose tolerance due to increased osmolality and viscosity of the injection solution (5, 16-18). As a result, the ionic Gd(III) chelates are generally formulated with positively charged cations, such as the amino sugar meglumine (with Gd-DTPA and Gd-BOPTA) and Na^+ (with Gd-EOB-DTPA and MS-325), to form neutralized solution with lower osmolality and viscosity (16). The nonionic linear Gd(III) chelates, including Gd-DTPA-BMEA and Gd-DTPA-BMA, were originally developed to lower the osmolality of the injection solution as well. The structure of the nonionic linear Gd(III) is similar to their ionic analogue, except that two of the ionic bonds between Gd^{3+} and the negatively charged carboxylic oxygen in the ionic chelates are substituted by the weaker nonionic bonds between Gd^{3+} and the neutral carbonyl oxygen atoms in the nonionic chelates (Figure. 1.2).

The macrocyclic Gd(III) chelates are formed between Gd^{3+} and DOTA derivatives with 12-membered macrocycilc polyaminocarboxylates ring. The ionic macrocyclic Gd(III) chelate, Gd-DOTA, has four amino nitrogen atoms and four monodentate carboxylic oxygen atoms that bind to Gd^{3+}, leading to a negative overall charge of the complex. In comparison, one of the negatively charged carboxylic oxygens in the ionic Gd-DOTA is replaced by less powerful electron donor oxygen atoms such as the alcoholic oxygen for nonionic macrocyclic Gd(III) chelates, including Gd-HP-DO3A and Gd-BT-DO3A. For Gd-HP-DO3A, a hydroxypropyl group is used to substitute one carboxylate group of Gd-DOTA, whereas a bulky 2,3-dihydroxy-(1-hydroxymethyl)-propyl group was used for the replacement in Gd-BT-DO3A (Figure 1.2).

Chelate Stability-Safety of Gd(III)-based Contrast Agents

Free Gd^{3+} is highly toxic. It is structurally similar to Ca^{2+}, and can act as a potent inhibitor for many types of voltage-gated calcium channels and calcium dependent enzyme activities at very low concentrations (in the range of nano- to micromolar concentrations) (14, 15). Consequently, a small amount of free Gd^{3+} ions can cause inhibition of calcium-involved physiological functions such as smooth, skeletal, cardiac muscle contraction, nervous influx transmission, blood coagulation, liver function, etc. (14, 15). In addition, free Gd^{3+} is known to depress the reticuloendothelial system (15), inhibit phagocytosis of Kupffer cells (19, 20), and increase the expression of certain hepatic cytokines (21). The acute toxicity of free Gd^{3+} can be substantially alleviated through chelation of Gd(III) using appropriate coordinating ligands (5). For instance, the intravenous LD_{50} of Gd-DOTA in mice (10.6 mmol/kg) was 30-fold higher than that of $GdCl_3$ (0.35 mmol/kg) under similar conditions, indicating significant increase of drug safety after complexation (22). Chelate stability is therefore a crucial factor influencing the safety profile of Gd(III)-based contrast agents.

Chelate stability is generally described using two concepts: thermodynamic stability and kinetic inertness (or kinetic stability). For Gd(III) chelates, thermodynamic stability emphasizes the extent of complex formation under certain conditions at equilibrium. It is often quantified using stability constants, indicating the bonding energy between Gd(III) and its corresponding ligands. Thermodynamic stability is independent of how equilibrium is reached and hence gives no information of the reaction process. Kinetic inertness, on the other hand, focuses on the course of complex formtion and therefore mainly deals with reaction rates and mechanisms (23, 24).

Thermodynamic Stability

The thermodynamic stability of Gd(III) chelates reflects the affinity of Gd^{3+} and its ligand. When Gd(III) is complexed, a thermodynamic equilibrium occurrs between the metal [Gd], its ligand [L] and the chelate [GdL]:

$$[Gd] + [L] \leftrightarrows [GdL] \quad (1)$$

From the equilibrium equation, the thermodynamic stability constant is defined as:

$$K_{therm} = [GdL] / ([Gd]*[L]) \quad (2)$$

In general, the stability of Gd chelate is expressed in the form of log K_{therm}. The higher the value of log K_{therm}, the more stable is the chelate, and the lower chance of free Gd^{3+} and free ligands release at equilibrium, both of which are poorly tolerated in vivo.

Since K_{therm} applies only at at highly basic conditions where the ligand is not protonated, a more appropriate description, the conditional thermodynamic constant log K_{cond} that takes into account the protonation forms of the free ligand at physiological pH (pH=7.4), was introduced. At equilibrium, K_{cond} is defined as (25):

$$K_{cond} = [GdL] / [Gd]\{[L] + [HL] + [H_2L] + \ldots + [H_nL]\} \quad (3)$$

where [HL], $[H_2L]$, and $[H_nL]$ are the different protonation species of the free ligands. From equation (2) and (3), the relationship between the theoretical (K_{therm}) and conditional thermodynamic constants (K_{cond}) are derived as:

$$K_{cond} = K_{therm} [L] / L_T \quad (4)$$

where L_T is the total concentration of the uncomplexed ligands at physiological pH, $\{[L] + [HL] + [H_2L] + \ldots + [H_nL]\}$. Since all Gd(III) ligands have significant extent of protonation at pH 7.4, the conditional thermodynamic constant log K_{cond} is always substantially lower than the theoretical thermodynamic constants log K_{therm}, as shown in

Table 1.1.

Although the current clinical Gd(III) agents are classically considered highly stable with large thermodynamic constants, their log K_{therm} and log K_{cond} can be dramatically different due to structural impact. For Gd(III) complexes, ionic bonding is the predominant chemical force that keeps the chelates intact . Therefore, stability of Gd(III) chelates essentially reflects the extent of electrostatic interactions between the Gd^{3+} and the donor groups of the ligand (e.g., Polyaza-carboxylate). Such interactions are mainly influenced by two structural factors, molecular configuration (complex conformation), and chelate ionicity (ligand basicity).

As demonstrated in Table 1.1, the thermodynamic stability constants of the macrocyclic Gd(III) chelates are similar or 2-3 magnitude higher than those of the linear chelates, indicating the macrocyclic effect on chelate stability (28, 29). In comparison to the linear ligands, the macrocyclic ligands provide a more rigid and compact cavity for

Table 1.1 Structure and thermodynamic constants of clinical Gd(III)-based contrast agents (5, 6, 17, 26, 27).

Trademark	Abbreviation	Structure	Ionicity	Log K_{therm}	Log K_{cond}
Magnevist®	Gd-DTPA	Linear	Ionic	22.1	17.7
MultiHance®	Gd-BOPTA			22.6	18.4
Primovist®	Gd-EOB-DTPA			23.5	18.7
Vasovist®	MS-325			22.1	18.9
Omniscan®	Gd-DTPA-BMA		Nonionic	16.9	14.9
OptiMARK®	Gd-DTPA-BMEA			16.6	15.0
Dotarem®	Gd-DOTA	Macrocyclic	Ionic	25.6	19.3
ProHance®	Gd-HP-DOTA		Nonionic	23.8	17.1
Gadovist®	Gd-BT-DOTA			21.8	14.7

the entrappment of Gd^{3+} (30). This pre-organized conformation is found well suited for Gd^{3+}, incorporating the transitional metal ions tightly with coordination bonds provided by the oxygen and nitrogen donors. NMR experiments have demonstrated this high rigidity of the DOTA structure, which requires relatively high activation energy to break the barrier for both complexation and de-complexation reactions (31). Therefore, the conformation of the macrocyclic ligand assures high thermodynamic stability of its corresponding ligands (32, 33). Structures of the pendant arms that have certain impacts on the rigidity of the ligand can consequently affect the thermodynamic stability of macrocyclic chelates (34). In comparison, the linear ligands exhibit higher flexibility and are more susceptible to conformational change and loss of Gd^{3+} in solution. Overall, the conformational differences between the two structures have a major influence on their thermodynamic stabilities.

The influence of chelate ionicity, or ligand basicity, can also be derived from Table 1.1. Ligand basicity is a quantitative depiction of the electronegative intensities on the polyaza-carboxylate scaffolds, which directly affect the charge-charge interactions between the ligands and the Gd^{3+} ions and thus the thermodynamic stability of the resulting chelates (29, 35). The overall basicity of a ligand (pK_b) is caculated as the summary of the protonation constants of each donor atom of the ligand (29). The value of K_{therm} varies through modifications of the pendant arms of DTPA and DOTA, which are carried out to enable different functionalities and pharmacokinetic patterns of the corresponding Gd(III) chelates. Ligand modifications include substitution of the carboxylic acids on the pendant arms of DTPA or DOTA with amides, alcohols, and phenols for clinical agents. These modifications often decrease the basicity of the ligands

and result in weaker chelates. As a result, the original forms of both linear and macrocyclic chelates (Gd-DTPA, Omniscan®, and Gd-DOTA, Doteram®) are characterized with higher thermodynamic stability than their respective derivatives. For linear chelates, the diamide derivatives, Gd-DTPA-BMA (Omniscan®), and Gd-DTPA-BMEA (OptiMARK®), compromise two negatively charged donor atoms of the original ligand and lead to significant decrease of log K_{therm} from 22 to 15~19 as shown in Table 1.1. In contrast, the thermodynamic stability of macocyclic chelate is only slightly affected after replacement of one acetate group with an alcohol-containing group (e.g., Gd-HP-DOTA, ProHance®, and Gd-BT-DOTA Gadovist) (29, 36).

In addition to clinical agents, the effect of basicity on thermodynamic stability was also observed for a variety of experimental ligand derivatives. For the macrocyclic chelates, modification of the pendant arms can affect the basicity of the nitrogen atoms on the macrocyclic ring and lead to change of thermodynamic stability of the chelates. For instance, the replacement of four acetate pendant arms of DOTA with methylphosphonic acid improves log K_{therm} due to increased basicity of the four donor nitrogen atoms (37, 38), yet introduction of four monoesters of methylphosphonic acid for the replacement resulted in weaker macrocyclic chelates due to decreased nitrogen basicity (39-42). However, this impact on nitrogen basicity was found minor when the substitution happened on single pendant arms of the macrocyclic chelates (43, 44). This also explains the relatively minor change of thermodynamic stability of Gd-HP-DOTA and Gd-BT-DOTA from Gd-DOTA as mentioned above. Similar effects also apply to the DTPA chelates, of which double or multiple modifications of the pendant arm result in greater change of thermodynamic stability than that resulted from single modification.

In summary, the thermodynamic stability of Gd(III) chelates is affected by the ligand basicity, which is determined by the number and structure of the modified pendant arms of DTPA or DOTA.

The thermodynamic stability constants of Gd(III) chelates (log K_{therm} and log K_{cond}) are important parameters in terms of formulation, since formulation solutions have adequate time to equilibrate during their relatively long shelf-life (generally 2-3 years for the marketed Gd(III)-based contrast agents). From the thermodynamic point of view, Gd(III) agents with relatively low conditional stability are generally formulated with an excess of free ligands or different salts to reduce the chance of Gd^{3+} dissociation in the pharmaceutical solutions over their shelf lives (5, 6).

Although the thermodynamic stability constants, log K_{therm} and log K_{cond}, appear accurate in predicting the stability of Gd(III) complexes under simple in vitro conditions, they are insufficient to depict the actual inertness of Gd(III) agents when exposed to the much more complicated in vivo environment. After intravenous injection, the clinical agents are exposed to the blood and other body fluids that are composed of relatively complex and intricate milieus with enormous amount of endogenous ligands and metal species (17) . The presence of these ingredients can greatly threaten the stability of Gd(III) agents via competitive reactions. Endogenous metal cations such as Fe^{3+}, Zn^{2+}, Ca^{2+}, and Cu^{2+} can replace Gd(III) from its chelate, causing the release of Gd^{3+} ion which can then be complexed with metal-binding proteins and small endogenous ligands such as citrate, glutaminate, CO_3^{2-}, OH^-, PO_4^{3-}, etc. This phenomenon of in vivo metal-metal exchange reaction is termed “transmetallation” and regarded as the main mechanism of in vivo de-chelation for Gd(III) complexes (17, 24).

In order to study the in vivo fate of Gd(III) complexes from the thermodynamic aspect, thermodynamic selective constant (K_{sel}) is introduced to describe the chance of transmetallation according to the following equation (25, 45-47):

$$GdL + [M]^{2+} \leftrightarrows Gd^{3+} + [ML]^{-} \quad (5)$$

where M is the bivalent metal cation that substitutes Gd^{3+} from the original chelate. Different definitions of K_{sel} have been reported in the literature (5, 25, 33, 35). A simplified interpretation takes into account the differences in thermodynamic stability constants between the Gd(III) chelates (GdL) and the corresponding metal complexes (ML), and defines the thermodynamic selective constant K_{sel} at equilibrium using the following equation:

$$\log K_{sel} = \log K_{GdL} - \log K_{ML} \quad (6)$$

The thermodynamic stability constants of chelates between endogenous metal and various Gd(III) ligands are listed in Table 1.2. In addition, more complicated definitions have been developed, trying to cover all possible competition reactions such as the binding of released Gd^{3+} with endogenous ligands (48).

Table 1.2 Thermodynamic stability constant log K_{ML} of several metal complexes (5).

Ligand L	Log K_{therm} (GdL)	Log K_{therm} (ZnL)	Log K_{therm} (CaL)	Log K_{therm} (CuL)
DTPA	22.1	18.3	10.7	21.4
DTPA-BMA	16.9	12.0	7.2	13.0
DOTA	25.8	21.0	17.2	22.6
HP-DOTA	21	19.4	14.8	22.8

Differences in vitro and in vivo approaches have been reported using the thermodynamic selective constant (K_{sel}) to predict the in vivo toxicity of Gd(III)-based contrast agents. However, none of these methods correlate well with the actual in vivo stability of various Gd(III) complexes. The thermodynamic stability approaches are limited due to two major reasons. Firstly, the actual in vivo equilibrium between the endogenous ingredients and Gd(III) complexes is too complicated to be well simulated via current thermodynamic models. More importantly, the prediction of thermodynamic approaches can be biased since the methods are based only on the final state of thermodynamic equilibrium without consideration of the dissociation processes. For chelates with high thermodynamic stability, such as the macrocyclic Gd(III) complexes, the actual time to reach equilibrium can be dramatically longer than the excretion time of the agents due to their high in vivo kinetic inertness. In such cases, the thermodynamic models are of little physiological importance, whereas the kinetics of chelate dissociation are critical in understanding the in vivo stability of Gd(III) agents.

Kinetic Inertness

Compared to thermodynamic stability, kinetic inertness is more relevant to the in vivo fate of Gd(III)-based contrast agents by exploring the rate and mechanisms of chelate dissociation reaction. As mentioned in the thermodynamic stability section, the dissociation of Gd^{3+} can occur via two major mechanisms: dechelation and transmetallation.

Dechelation kinetics. Dechelation is the simplest route of dissociation for Gd(III) complex, described as:

$$GdL \leftrightarrows Gd^{3+} + L \quad (7)$$

The reaction can happen through two mechanisms: spontaneous or proton-assisted dissociation (47). The rate of dissociation (k_{diss}) and dissociation half-life ($T_{1/2}$) are often used as quantitative parameters to evaluate the dechelation process. Various in vitro studies have been carried out to determine the dissociation rate of different Gd(III) chelates. In general, the dissociation is slow at physiological pH and increases as pH decreases (49). In consequence, the measurement of dissociation rate is normally carried out at very acidic conditions (pH ≈1.0 or 3.0) to amplify the phenomenon (50). In such acidic mediums, the dissociation of Gd(III) chelates appeared as a pseudo-first-order reaction with the dissociation rate defined as:

$$\text{Dissociation rate} = k_{diss}\,[H^+][GdL] \quad (8)$$

Since $[H^+]$ is considerably larger than [GdL], it can be considered as constant $[H^+]_0$, then the equation can be simplified as:

$$\text{Dissociation rate} = k_{obs}\,[GdL] \quad (9)$$

where

$$k_{obs} = k_{diss}\,[H^+]_0 \quad (10)$$

The dissociation rate k_{obs} is determined as the slope of the curves $\ln[GdL]_t = f(t)$ (50).

Although the reported values of k_{obs} and $T_{1/2}$ for a specific Gd(III) chelate varies depending on the experimental conditions and methods (50-54), a general relationship between chelate structure and dissociation rate is observed. The dissociation of the linear chelates is dramatically faster than that of the macrocyclic chelates, indicating relatively high kinetic lability of the linear chelates. Among the linear chelates, the nonionic bisamide linear chelates Gd-DTPA-BMA (Omniscan®) and Gd-DTPA-BMEA

(OptiMark®) exhibit faster dissociation than the ionic chelates (55, 56). Such influence of ionic strength on dissociation rates is observed but not as significant for the macrocyclic chelates in comparison to that for the linear chelates (24). The order of dissociation rates among the macrocyclic Gd(III) agents is: Gd-HP-DOTA > Gd-BT-DOTA > Gd-DOTA, indicating higher kinetic inertness of the ionic macrocyclic chelate than that of the ionic macrocyclic chelates (24). Between the two nonionic chelates, the dissociation rate of Gd-BT-DOTA is slightly lower than that of Gd-HP-DOTA, indicating higher kinetic inertness of Gd-BT-DOTA. This is possibly due to the bulky side chain of Gd-BT-DOTA that provides higher steric hindrance against the conformational change required for dechelation (57).

Transmetallation kinetics. Transmetallation is generally considered as the major route of Gd^{3+} loss in vivo given the intricate physiological environment Gd(III)-based contrast agents are subjected to after application. Transmetallation of Gd(III) chelates leads to Gd^{3+} release through replacement of chelated Gd(III) by endogenous metal cations such as Zn^{2+}, Cu^{2+}, Ca^{2+}, and Fe^{3+}. The exchange reactions can happen via two mechanisms: 1) spontaneous or proton-assisted dechelation of Gd^{3+} followed by rapid complexation between the free ligands and endogenous metal ions; 2) direct attack of endogenous metal cations on the Gd(III) chelates (49). Although transmetallation of Gd(III) chelates is of significant physiological relevance, it is more complicated to depict than the dechelation kinetics. Both in vitro and in vivo studies have been conducted to understand the structural impact of Gd(III) chelates on transmetallation (17, 24).

All reported in vitro studies tried to quantify the extent of transmetallation through incubation of Gd(III) chelates with solutions containing the endogenous metal cation

species (24, 47, 50, 55, 58, 59). Various direct or indirect methods have been applied to measure the loss of Gd^{3+} after in vitro incubation. In one study, different types of Gd(III) chelates were incubated with equimolar of Zn^{2+} or Cu^{2+} in a phosphate solution for 15 minutes. If transmetallation happened in this case, the dissociation of Gd^{3+} would then react with the phosphate anions to form precipitated $GdPO_4$. Based on this assumption, the amount of precipitated $GdPO_4$ was measured as an indication of transmetallation (50). The results demonstrated that the macrocyclic chelates Gd-DOTA and Gd-HP-DOTA were kinetically inert against Zn^{2+} or Cu^{2+} transmetallation, whereas significant loss of Gd^{3+} were observed for the linear chelates Gd-DTPA and Gd-DTPA-BMA. Similarly, some other in vitro transmetallation studies were carried out under different experimental conditions, all leading to the same conclusion that macrocyclic chelates were kinetically more stable against transmetallation than the linear chelates (24).

Despite direct measurement of the precipitated $GdPO_4$, another in vitro relaxometric approach is developed to indirectly quantify the loss of Gd^{3+} after incubation of Gd(III) chelates with Zn^{2+} in phosphate solutions at physiological pH (60, 61). Since the precipitated Gd(III) species ($GdPO_4$) have negligible impact on the relaxation rate of water, a decrase of relaxation rate over time $R_1(t)$ would be observed if transmetallation happened, the magnitude of which is related to the proportion of the precipitated $GdPO_4$. According to this rationale, the time-course of $R_1(t)/R_1(t=0)$ is drawn and compared for different clinical Gd(III) chelates. Three distinct classes of Gd(III) chelates with different stability against in vitro transmetallation are concluded from the graph: the most kinetically stable macrocyclic chelates (Gd-DOTA, Gd-HP-DOTA, and Gd-BT-DOTA), the moderate kinetically stable ionic linear chelates (Gd-DTPA, Gd-

EOB-DTPA, Gd-BOPTA, and MS325), and the least kinetically stable nonionic linear chelates (Gd-DTPA-BMA and Gd-DTPA-BMEA).

Various in vitro incubation studies of Gd(III) chelates have arrived at the same conclusions regarding the structural impact on transmetallation. Consistent with the trend found on thermodynamic stability, chelate conformation and ionicity are demonstrated as the two major structural factor influencing kinetic stabilily of Gd(III) chelates, of which the impact of chelate conformation is predominant. In general, linear chelates are more susceptible to transmetallation than macrocyclic chelates due to their flexible backbone structure, providing relatively high conformational mobility (62). In order to improve the kinetic stability of linear chelates, bulky functional groups, such as in the case of Gd-EOB-DTPA, Gd-BOPTA, and MS325, are introduced to increase the steric hindrance for conformational change (63). As mentioned in the previous section, chelate ionicity reflects the bonding between Gd^{3+} and its corresponding ligands, among which ionic bonding is the strongest. As a result, the ionic complexes are generally more stable against transmetallation than their nonionic analogues for both macrocyclic and linear Gd(III) chelates.

In vivo, the Gd(III)-based contrast agents are subjected to a much more complicated environment in comparison to the conditions of in vitro transmetallation studies. Disparate from in vitro, dissociation of Gd^{3+} in vivo can be a result of synergetic effects of multiple factors such as endogenous ions, enzymes, and other biological elements. Therefore, the in vitro data are not adequate to predict the kinetic stability of Gd(III)-based contrast agents in vivo. Since dissociation of Gd^{3+} cannot be directly measured in vivo, the kinetics of Gd(III) chelates on animals or human after

administration of various Gd(III) agents are infered through assessment of long-term tissue Gd(III) deposition and analysis of blood samples and urine metabolites (24).

Tissue retention of Gd(III) has been used to determine the in vivo stability of Gd(III) chelates. For most clinical Gd(III) agents, the majority of injected chelates would be excreted intact through renal elimination within 24 hours after administration, resulting in similar pharmacokinetics and biodistribution patterns (50, 51). The data begin to separate a week after administration, showing distinct tissue depositions among various Gd(III) chelates, which is interpreted as the result of different Gd^{3+} release from the chelates. Once dissociation happened, Gd^{3+} would complex with endogenous anions such as citrates and phosphates, and then be transported and deposited in different tissues. Thus, the amount of Gd(III) retention in tissues is considered to correlate with the extent of Gd^{3+} dissociation among different Gd(III) chelates, indicating their kinetic stability in vivo.

Various preclinical animal studies have been conducted to trace the residual Gd(III) in healthy mice or rats after administration of Gd(III) chelates using Gd isotopes such as ^{153}Gd and ^{154}Gd (50, 51, 59, 64). In one study, for instance, the tissue deposit of ^{153}Gd-labelled formulations of Gd-DTPA, Gd-DTPA-BMA, Gd-DOTA, and Gd-HP-DO3A on mice and rats were monitored at various time-points post injection for up to 14 days (65). Significant differences were demonstrated for the whole body, liver, and femur Gd(III) residuals 14 days post administration of various Gd(III) chelates. In comparison, the macrocyclic chelates Gd-DOTA and Gd-HP-DOTA showed minimal Gd(III) retention, the ionic linear chelate Gd-DTPA exhibited slightly higher Gd(III) deposit and the nonionic linear chelate Gd-DTPA-BMA resulted in the greatest Gd(III) residual, three

times higher than that of Gd-DTPA. However, since the residual Gd(III) species cannot be identified using the isotope approach, this study alone was not adequate to verify Gd^{3+} dissociation as the cause of long-term Gd(III) retention. The authors then compared the tissue retentions of Gd(III) between formulated and unformulated Gd-DTPA-BMA as an indirect approach to demonstrate the relationship between Gd^{3+} dissociation and Gd(III) deposition. The results demonstrated that addition of extra Gd(III) ligands Na[Ca-DTPA-BMA] in the formulated solution dramatically reduced the whole body Gd(III) retention from 1 % to 0.3 % of the injected dose, suggesting association between in vivo Gd^{3+} and long-term Gd(III) deposit in tissues. Other similar studies have been carried out, leading to results indicating the same order of in vivo stability among various Gd(III) chelates as: macrocyclic chelates > ionic linear chelates > > nonionic linear chelates, which was consistent with the conclusions from in vitro kinetic studies (24).

The human relevance of these animal data was demonstrated in clinical studies with patients of normal renal function, the impairment of which may lead to dramatic increase of Gd(III) retention as renal filtration was the major excretion route for Gd(III) chelates (66, 67). In one study, the authors analyzed Gd(III) residuals in the bones of patients receiving hip transplant 4 days after contrast-enhanced MRI, during which either Gd-HP-DO3A or Gd-DTPA-BMA was administered at clinical dose (0.1 mmol/kg) (66). The Gd(III) bone retention was measured using inductively coupled plasma (ICP) atomic emission and ICP mass spectroscopy in the consecutive study (67). The results demonstrated significantly higher deposit of Gd(III) in the bones of patients receiving Gd-DTPA-BMA than that of patients receiving Gd-HP-DOTA. This difference could indicate greater in vivo kinetic lability of Gd-DTPA-BMA over Gd-HP-DOTA. However,

it was inadequate to confirm Gd^{3+} dissociation due to limitation of the analytical methods that only provide information on the Gd(III) element rather than the species of Gd(III) deposits. Nevertheless, as shown in animal studies, the clinical studies also demonstrated higher Gd(III) retention of the linear chelates, especially the nonionic linear chelates than that of the macrocyclic chelates, indicating a similar trend of in vivo stability among various Gd(III) agents.

Transmetallation has been regarded as the major route of in vivo Gd^{3+} dissociation from Gd(III) chelates. It was extensively investigated in both animal and clinical studies (58, 68-72). Theoretically, transmetallation can happen between Gd(III) chelates and any endogenous cations with good affinity to Gd(III) ligands, such as Zn^{2+}, Cu^{2+}, Ca^{2+}, and Fe^{3+}. In practice, only the Zn^{2+}-mediated transmetallation of Gd(III) chelates has been confirmed by current in vivo transmetallation studies, possibly due to the readily accessibility of Zn^{2+} in blood. Among the various endogenous cations, Zn^{2+} is the most availabe due to its relatively high blood concentration (55-125 μmol/L) and good ligand affinity. In comparison, Cu^{2+} level is low (1-10 μmol/L) in plasma, Ca^{2+} ions have relatively low ligand affinity, and Fe^{3+} ions are tightly bound to plasma proteins (69, 73). By far, most in vivo transmetallation have been demonstrated through analysis of plasma or urine Zn(II) content before and post administration of Gd(III) chelates. In both animal and clinical studies, significant increase of urine Zn(II) level was observed for the linear chelates, whereas no detectable Zn(II) was discovered for the macrocyclic chelates (17). One clinical study on healthy patients showed almost 3-fold higher of the urine Zn(II) content post application of Gd-DTPA-BMA than that of post application of Gd-DTPA (58), indicating dramatically greater extent of transmetallation for the nonionic

linear chelates in comparison to the ionic linear chelates. Similar results were demonstrated in other clinical and animal studies (11, 17). In summary, both animal and clinical studies verified that dissociation of Gd^{3+} can be caused by Zn^{2+} transmetallation in vivo. The order of susceptibility of in vivo transmetallation among different chelates is: nonionic chelates > ionic chelates > macrocyclic chelate, which is consistent with the conclusions from in vitro transmetallation studies.

In Summary

Chelate stability is a critical factor determining the safety of Gd(III)-based contrast agents. It is structural dependent, and can be described thermodynamically or kinetically. The thermodynamic approach uses stability constants to describe the equilibrium state between chelation and dissociation of the Gd(III) chelates, and thus has a practical relevance in terms of formulation where the solutions have enough time to equilibrate during the relatively long shelf-life. In comparison, kinetic stability focuses on the process of chelate dissociation by describing the rate and mechanisms of the reactions. It has more physiological relevance since most clinical Gd(III) chelates have inadequate time to equilibrate during their short in vivo retention. The structure and stability relationships have been studied in both thermodynamic and kinetic studies.

Molecular configuration and chelate ionicity are concluded as the two major factors determining both the thermodynamic and kinetic stability of Gd(III) chelates. Between the two factors, molecular configuration or molecular conformation is of primary importance. The macrocylic chelates are generally more stable than the linear chelates. The release of Gd^{3+} from macrocyclic chelates requires breaking of multiple

coordination bonds simultaneously, whereas the dissociate takes place more easily for linear chelates through sequential bond breaking (18). The ionicity factor, or ligand basicity, reflects the strength of the coordination bonds between Gd^{3+} and its corresponding ligand. All clinical Gd(III) chelates contain at least three carboxylic donor oxygen atoms for Gd^{3+} complexing. The nonionic chelates have three carboxylate groups and one or two alcoholic or phenol donor groups for Gd^{3+} complexing, whereas the ionic chelates contain more than three carboxylate donor groups. Since ionic bonding requires the highest energy to break in comparison to other chelation bonds, the ionic chelates are more stable than their nonionic analogues because of their extra ionic bonds. Based on the two structural aspects, the order of stability for current clinical Gd(III) agents can be deduced as: macrocyclic ionic chelates > macrocyclic nonionic chelates >linear ionic chelates >linear nonionic chelates. In practice, the impact of ionicity is more significant among linear chelates than that among macrocyclic chelates in both thermodynamic and kinetic studies of Gd(III) chelates. The order of stability among different clinical agents were summarized as macrocyclic chelates > ionic linear chelates >> nonionic linear chelates.

Relaxivity- Efficacy of Gd(III)-based Contrast Agents

The efficacy of Gd(III)-based contrast agents is measured in terms of relaxivity. According to the Solomon-Bloembergen-Morgan theory, relaxivity is affected by various structural factors such as the molecular rotational correlation time, the electron relaxation time, and the water residence life time, among which the rotational correlation time is of predominant influence (4, 5). The rotational correlation time is longer with decreased

molecular tumbling, which can be achieved through enhancement of molecular size and solution viscosity (5). While the influence of solution viscosity is limited, the relaxivity of Gd(III)-based contrast agents can be significantly increase by enlarging the molecular size.

The influence of molecular size and solution viscosity on relaxivity have been demonstrated in the relaxivity studies of clinical agents. All clinical agents are small molecules with similar molecular size, resulting in similar relaxivity ranging from 3.0 mM^{-1} s^{-1} to 5.0 mM^{-1} s^{-1} when measured in aqueous solutions under the same field strength (4, 6, 16). Depending on whether the Gd(III) chelate can reversibly bound to plasma proteins after administration, the current clinical agents can be categorized as non-protein-binding and protein-binding agents. All marketed agents except MS325 are non-protein-binding agents, among which Gd-EOB-DTPA may weakly bind to plasma proteins in vivo via its aromatic lipophilic groups. The non-protein-binding agents exhibit similar relaxivities in water and in plasma since their molecular size remain the same. The plasma relaxivity of these agents can be slightly higher than relaxivities measured in water due to higher viscosity of the plasma leading to slightly increased rotational correlation time (61). Since the non-protein-binding agents with aromatic groups, including Gd-BOPTA and Gd-EOB-DTPA, have slightly higher molecular weight and possibly weak plasma protein affinity, they have been shown to exhibit slightly higher plasma and water relaxivity than those of the other non-protein-binding agents. In comparison, the relaxivity of the protein-binding agent MS325 is dramatically increased when exposed in blood where MS325 reversibly binds to plasma proteins, especially albumin, resulting in significantly larger molecules with slower rotational correlation

time (74, 75).

In summary, the efficacy of Gd(III) chelates is related to their corresponding relaxivity which is predominantly determined by the rotational correlation time of the chelate molecule. In comparison, larger molecules of Gd(III) chelates have significantly slower molecular rotation in solution. Therefore, they are characterized with dramatically higher relaxivity than that of small molecules. This is demonstrated by the significant differences in plasma relaxivity between the protein-binding and non-protein-binding clinical agents.

Pharmacokinetics and Biodistribution

The pharmacokinetics and biodistribution of clinical Gd(III)-based contrast agents are different depending on different structures. The non-protein-binding agents are small molecules characterized with nonspecific extracellular distribution and fast elimination post intravenous injection, whereas the protein-binding agent MS325 has limited extravasation and comparably slower excretion due to significant increase of molecular size through reversible plasma protein binding of the chelate after administration (11, 75, 76). Renal filtration is the predominant elimination pathway for all clinical agents (11). While most agents are exclusively excreted renally, the non-protein-binding agents with aromatic groups, including Gd-BOPTA and Gd-EOB-DTPA, can also be cleared via the hepatobiliary system (77, 78). As the major elimination route for Gd(III) chelates, the pharmacokinetics and biodistribution of clinical agents can be greatly affected when patients receiving the contrast agents suffer from impaired kidney function (79-81).

Based on different elimination pathway, the non-protein-binding agents can be

further divided into two groups, the extracellular fluid (ECF) agents that exclusively excreted from renal filtration and ECF plus liver agents that can also be eliminated hepatically (11). All non-protein-binding agents are small molecules that can rapidly and freely distribute to the extracellular space. Their steady-state volume of distribution from various pharmacokinetics studies ranged from 210-280 mL/kg, consistent with extracellulara distribution (77-80, 82-88). Both ECF and ECF plus liver agents can be rapidly eliminated in healthy objects. In comparison to the nonspecific ECF agents, the ECF plus liver agents Gd-BOPTA and Gd-EOB-DTPA can be favorably taken up by hepatocytes, resulting in relatively better liver enhancement (11). In patients with normal renal function, the terminal half life for blood elimination is about 1.5 hours for all ECF agents, 1.5–2 hours for Gd-BOPTA, and 1 hour for Gd-EOB-DTPA (78). The slightly longer blood retention of Gd-BOPTA may be a result of its weak protein binding, whereas significant liver elimination of Gd-EOB-DTPA may lead to its relatively shorter blood retention. In moderately renal impaired patients, the half-lives of all non-protein-binding agents have increased to 4-8 hours (79, 80, 87). In patients with severe renal damage, the reported half-lives of these agents were in the range of 18-34 hours, approximately 12-22 times higher than that in patients with normal renal function (79, 80, 87). Significantly prolonged retention of Gd(III) chelates in renal insufficient patients may lead to greater in vivo Gd^{3+} dissociation and deposit, and consequently higher possibility of Gd^{3+} related side effects.

The protein-binding agent MS325 exhibits distinct pharmacokinetics and biodistribution from the non-protein-binding agents due to significant increase of size after intravenous injection (89). MS325 has been developed and applied as blood pool

imaging agents due to its limited extravasation through reversible plasma protein binding (5, 74, 75). Correspondingly, the steady-state volume of distribution for MS325 is 148 ± 16 mL/kg (89). Renal filtration is the main excretion pathway for MS325. In test subjects with normal renal function, its terminal blood half-life is 18.5 hours, considerably higher than other non-protein-binding clinical agents (90). Pharmacokinetics studies demonstrate that moderate to severe renal impairment resulted in significantly prolonged blood retention of MS325 and consequently 2- to 3-fold increase of its terminal half-life (90).

In summary, the pharmacokinetics and biodistribution of clinical Gd(III)-based contrast agents vary depending on the structure and size of the chelate, as well as the renal functions of patients. Most clinical agents are small molecules with nonspecific extracellular distribution and rapid elimination, mainly through renal filtration. One exception is the protein-binding agent MS325 that reversibly bound to plasma proteins after application, resulting in confined intravascularly distribution, prolonged blood retention, and slower excretion. Considerably increased in vivo retention and decreased excretion are also discovered in patients with severe renal dysfunction receiving the non-protein-binding agents due to inefficient elimination. As mentioned in the stability section, prolonged in vivo retention may result in elevation of in vivo Gd^{3+} dissociation that consequently leads to increased potential risks for Gd(III) chelates.

Adverse Reaction

Nephrogenic systemic fibrosis (NSF) is a complex and fatal disorder found mainly in patients with marked impairment of renal function receiving Gd(III)-based contrast

agents (91-93). It is a fairly new syndrome without thorough understanding, and has not been reported until 2000 (94). NSF is characterized by thickening, induration, and tightening of the skin with subcutaneous edema, and may lead to joint contractures and immobility in severe cases (91, 95). In addition, NSF may also result in complications with multiple organs such as the lungs, heart, liver, kidneys, and muscles, and consequently causing death through the scarring of body organs (95-98). The severity of the disease is patient dependent.

The cause of NSF was not clear until a report in 2006 suggesting possible association between NSF and the administration of Gd(III)-based contrast agents, which was further confirmed by various follow-up studies (99, 100) . Despite exposure of Gd(III) chelates, other factors such as renal dysfunction in patients also contribute to the cause of NSF. Although the mechanism of NSF is still not clear, a correlation between NSF lesions and increased Gd^{3+} dissociation through delayed excretion of the agents was indicated in many studies. The majority of NSF cases have been reported with the nonionic Gd-DTPA-BMA and Gd-DTPA-BMEA. Other cases have been documented with ionic linear agent Gd-DTPA, but not with the macrocyclic agents. Combining the fact that NSF has been found only in severe renal impaired patients administered with the less stable linear chelates, the epidemiology suggests an important impact of chelate stability on the pathogenesis of this condition. The long retention of unstable chelates can lead to release of Gd^{3+}, and consequently NSF. Given the severity of NSF and its potential association with Gd(III)-based contrast agents, the food and drug administration of the USA (FDA) has issued warnings on the labels of current clinical Gd(III)-based contrast agents.

Limitation of Clinical Agents

All commercial Gd(III)-based contrast agents except the protein-binding agent MS325 are nonspecific small molecular agents with similar relaxivity. The small size of these agents rendered short blood retention and rapid elimination of the chelates through renal filtration. The fast renal clearance of the clinical agents minimizes the potential in vivo release of Gd^{3+} that can consequently result in long-term Gd(III) tissue deposit, and thus assures relatively good safety profile of these agents in clinical application (6). On the other hand, the nonspecificity and short blood retention of the non-protein-binding small molecular agents provide low tissue discrimination and limited time window (approximately 5 minutes) for effective MR diagnosis of the more challenging tasks such as early detection of cardiovascular dysfunction and cancer (5).

Macromolecular Gd(III)-based Contrast Agents

Both natural and synthetic polymeric systems have been widely used in biomedical applications as carriers for various drugs and targeting ligands (101). The diverse functionalities of marcomolecules make them suitable candidates for MR contrast agents as well. In comparison to small molecular Gd(III) chelates, macromolecular agents have considerably slower molecular tumbling due to dramatic increase of size, resulting in superior relaxivity (5, 7) . As demonstrated with the protein-binding agent MS325, the increase of size can also lead to limited extravasation and prolonged blood retention, providing blood pool imaging with longer diagnostic window (75, 102, 103). In addition, macromolecules can carry a large payload of Gd(III) chelates and targeting ligands, enabling tissue-specific imaging with lower dose. The combined properties of high

relaxivity, long blood retention, and better tissue specificity make maromolecular Gd(III)-based contrast agents promising for a wider range of imaging challenges such as MR angiography and tumor prognosis (8-10, 104, 105).

A wide range of Gd(III)-based marcomolecuar MR contrast agents has been developed such as linear polymers, dendrimers, liposomes, micelles, and nanoparticles (101, 106). These macromolecular contrast agents generally have molecular weights over 20 kDa and hydrodynamic diameter over 1-2 nm. The pharmacokinetics and biodistrubution profile vary among different macromolecular agents as their size and ligand attachments change.

Different Types of Macromolecular Gd(III)-based Contrast Agents

Linear Polymeric-based Gd(III) Contrast Agents

Early research utilized natural linear polymers such as the plasma protein, serum albumin, as the macromolecular platform for Gd(III) labling (107, 108). While proteins are abundantly available with high homogeneity, they are associated with problems such as limited Gd(III) loading sites, immunogenic effects, and insufficient clearance (7, 109). To overcome these problems, instead of chemically attaching Gd(III) chelates to proteins, the protein-binding agent MS325 have been developed as small molecules that can reversibly bound with plasma proteins after application for clinical blood pool imaging (74, 75, 102). In comparison to proteins, synthetic linear polymers are more versatile carriers for Gd(III)-based contrast agents. Various linear polymer-based macromolecular Gd(III) contrast agents, such as polysaccharides, polyethylene glycol (PEG), and different polyamino acids agents, have been developed and evaluated (80, 110-113).

Polysaccharides provide biocompatible linear platforms capable of carrying high payloads of Gd(III) chelates, among which dextran was first applied as macromolecular Gd(III) contrast agent (114, 115). It has been widely used as macromolecular delivery systems for various drugs due to its good water solubility and biodegradability (116). In one study, a 165 kDa dextran was shown to conjugate as many as 187 Gd(III) per molecule, demonstrating its high loading capacity for Gd(III) chelates (115). The high payloads of Gd(III) and large size of dextran-based Gd(III) agents should result in significantly increased relaxivity than that of the small molecular clinical agents (3.3 mM^{-1} s^{-1} at 1.5 T, 37 °C). This was verified in a separate study where the T_1 relaxivity of a 75 kDa dextran-Gd-DTPA conjugate was 10.5 $mM^{-1}s^{-1}$ (0.25 T, 37 °C) (117). However, dextran-based contrast agents have a high degree of polydispersity which makes the preparation of identical formulations difficult. Therefore, it may have inconsistent in vivo distribution and pharmacokinetics due to the differences between batches (118, 119). Other polysaccharides such as inulin, hydroxyehyl starch, and chitosan oligosaccharides have been investigated as carriers for Gd(III)-based contrast agents (120-122). In comparison with small molecular Gd(III) chelates, the polysaccharides agents all showed significantly improved image contrast due to enhanced T_1 relaxivity, and dramatically prolonged in vivo retention up to 7 days after administration due to slow clearance.

The potential of PEG Gd(III) conjugates as macromolecular contrast agents have been explored (123). Similar to polysaccharides, PEG has good biocompatibility and hydrophilicity for biomedical application. In addition, the narrow polydispersity of PEG facilitates repetition of identical formulations. A family of PEG diamines-Gd-DTPA complex with a wide range of molecular weights and linear or globular structures have

been developed and compared (123). These compounds were synthesized with molecular weights under 50 kDa. The studies showed that the blood retention of PEG Gd(III) conjugates lengthened as molecular weight of the polymers increased, which indicated the impact of molecular size on the pharmacokinetics of macromolecular contrast agents. Moreover, the studies also demonstrated the influence of polymeric rigidity on relaxivity as the globular PEG Gd(III) conjugates showed higher relaxivity than its linear polymer counterparts. It was proposed that the higher rigidity of globular structure led to increased water exchange rate and viscosity, both contributing to enhancement of relaxivity.

Polyamino acids, such as polyglutamic acid (PGA) and polylysine (PLL), have been investigated as another suitable polymeric Gd(III) loading platform (80, 110-112). Besides superior biocompatibility, both PGA and PLL are flexible with molecular weights. They have highly modifiable side groups for attachment of Gd(III) chelates and various targeting ligands. For instance, our group has developed PGA-1,6-hexanediamine-Gd-DOTA complex with molecular weights ranging from 28 kDa to 87 kDa (124). Size-dependent relaxivity and contrast enhancement was demonstrated in this study. Cancer-specific contrast enhancement was also observed with the PGA Gd(III) conjugate, indicating passive cancer targeting of the agent. In another study, PLL-Gd-DTPA conjugate was synthesized with 3-fold increase of relaxivity in comparison to Gd-DTPA (125). The PLL conjugate was further modified through PEGylation to achieve longer blood retention and even higher relaxivity for blood pool imaging (126).

Dendrimer-based Gd(III) Contrast Agents

Dendrimers have become popular drug carrier systems due to their defined structure and the availability of multivalent surface groups (127, 128). They have globular structures consisting of a core, an inferior section, and an outer surface. The multivalent groups on the outer surface enable attachment of different functional groups, thus facilitating modifications for various biomedical applications (128). For Gd(III)-based contrast agents, the large amount of surface groups such as amines and carboxylic acids not only provides high Gd(III) loading capacity, but also facilitates conjugation of various targeting groups, rendering dendrimer-based Gd(III) contrast agents promising in molecular imaging (129).

The size of dendrimers is an important parameter affecting the relaxivity, solubility, pharmacokinetics, and biodistribution of dendrimer-based Gd(III) contrast agents (129). As dendrimer size increases after each generation, the surface functional groups increase, resulting in higher Gd(III) loading. For instance, Gd(III) loading increased from 96 Gd(III) per molecule for a generation 5 (G5) polyamidoamine (PAMAM) dendrimer to 1860 (III) per molecule for a G10 PAMAM dendrimer (130). As more Gd(III) ions attach to each molecule, the MR signal is enhanced. The increase of size also contributes to enhancement of relaxivity due to slower molecular tumbling and increased Gd(III) loading. This was demonstrated in one study where the relaxivity increased from 20 mM^{-1} sec^{-1} for a G2 PAMAM Gd(III) conjugate to 28 mM^{-1} sec^{-1} for a G4 PAMAM Gd(III) conjugate (131). In comparison, another study reported the relaxivity for a G10 PAMA Gd(III) conjugate to be as high as 36 mM^{-1} sec^{-1} (130). In terms of pharmacokinetics, the excretion route differs with increase of size. Smaller

dendrimers are rapidly cleared through renal filtration and larger dendrimers tend to accumulate and are eliminated through liver (131). Besides dendrimer size, the pharmacokinetics of dendritic Gd(III) conjugate is also influenced by the core and interior section of dendrimers. It has been shown that increased hydrophilicity and flexibility of the core and interior facilitate renal clearance while increased hydrophobicity and rigidity of the inner structures may lead to longer blood retention and higher liver accumulation (132).

Targeted dendritic Gd(III) contrast agents have been developed for tissue-specific imaging (118, 133). Although the total relaxation per molecule for G5 and lower generation dendritic Gd(III) conjugates are beyond the expected threshold for molecular imaging, it is hypothesized that signal amplification of targeted tissues can be achieved through receptor-mediated internalization and recycling of targeted dendritic Gd(III) conjugates (134). For instance, folate were attached to a G4 and a G5 PAMAM Gd(III) agent to image tumors expressing high density of folate receptors (134, 135). Significant tumor contrast was observed in comparison to that of nontargeted dendritic Gd(III) conjugate and free Gd-DTPA in this study.

Although higher generation dendrimers provide higher Gd(III) loading and more versatile modifications, they are more complicated to prepare and have lower solubility. Dendritic nanocluster (DNC) systems have recently been developed to conquer these problems (136). DNCs are nanoparticles formed by crosslinking individual Gd(III)-labeled dendrimers, through which the highly soluble and easily synthesized lower generation dendrimers can be used to achieve high Gd(III) loading and relaxivity. It has been shown that 300,000 Gd(III) can be loaded to a 150 nm DNC, resulting in relaxivity

high enough for targeted molecular imaging (136).

Nanoparticle-based Gd(III) Contrast Agents

Liposomes are synthetic spherical vesicles with lipid bilayer membranes that have been widely used as macromolecular vehicles for various nutrients and pharmaceutical drugs (137). Its potential to carry Gd(III) chelates has been investigated through either encapsulating the chelates within liposomal vesicles or immobilizing the chelates on its surface (138-140). In comparison, liposomal encapsulation provides higher Gd(III) payloads than that from surface conjugation. However, the liposomes with encapsulated Gd(III) chelates are generally characterized with low relaxivity as its lipid bilayers limit the water accessibility of the encapsulated Gd(III) (141). Liposomes with surface-bound Gd(III) chelates experience better water exposure that contributes to improved relaxivity (139). The limitation of encapsulated liposomal-based Gd(III) contrast agents has recently been addressed through development of paramagnetic porous polymersomes with improved water permeability (142). In comparison to liposomes, more versatile structure and functionality can be achieved from polymersomes since they are easier to manipulate through polymer selection and design (143, 144). For polymersome encapsulated Gd(III) contrast agents, membrane permeability for water is achieved by introducing pores into the vesicle bilayer through two different approaches (145, 146). In both preparation methods, Gd(III) chelates are attached to dendrimers before encapsulation to prevent possible leaking of small molecular Gd(III) chelates from the porous vesicles. The resulting relaxivity is considerably higher in comparison to the liposomal encapsulated Gd(III) chelates.

Similar to liposomes, micellar-based Gd(III) contrast agents have been developed and evaluated as highly paramagnetic nanoparticle contrast agents (147-150). The micellar particles are synthesized through self-aggregation of Gd(III)-labeled amphiphilic compounds. Their hydrophobic parts orient towards the core of nanoparticle and the Gd(III)-labeled hydrophilic moieties are exposed to the aqueous solvent (147). It has been shown in one study that Gd(III)-labeled micelles formed in this approach exhibited relaxivity of 18.03 $mM^{-1}s^{-1}$ (20 MHz, 37 °C) (147). In addition to pre-attaching Gd(III) chelates to amphipilic units before micellar formation, Gd(III) loading can also be accomplished vice versa through postlabeling of preformed micelles (151). It has been shown that micellar Gd(III) contrast agents achieved through both methods exhibit similar relaxivities, which can be further improved through manipulation of the micellar structure such as cholesterol incorporation or structure modification of the conjugated Gd(III) chelates (148-150).

Another kind of nanoparticle-based Gd(III) contrast agents involves the application of perfluorocarbon (PFC) nanoemulsions. In this case, liquid PFC core is surrounded by a lipid monolayer that can be functionalized to contain various agents for imaging or therapeutic purposes (152). The Gd(III)-labeled PFC nanoemulsions requires a large amount of lipid Gd(III) chelates to stabilize the system which also result in to high Gd(III) loading. In one study, a loading capacity of up to 100,000 Gd(III) per PFC particle was demonstrated, showing relaxivity of 17.7 $mM^{-1}s^{-1}$ (1.5 T, 37 °C) (153). Higher relaxivity can be achieved through further modification of the nanoemulsion or the structure of lipid Gd(III) chelates (154-158). In addition, targeted Gd(III)-labeled PFC nanoemulsions can be synthesized through incorporation of various targeting ligands into

the PFC nanoemulsion systems. The targeted diagnostic agents are promising in areas such as tumor and atherosclerotic plaque MR imaging (155-157).

Safety Concerns of Gd(III)-based Macromolecular Contrast Agents

Although macromolecular Gd(III)-based contrast agents are promising in blood pool and tumor imaging, their clinical translation has been hindered due to several factors such as difficult quality control, lack of scalability, unfavorable pharmacokinetics, and inefficient elimination. Among them, the potential safety issues associated with slow excretion of macromolecular agents are the primary concern (11, 159). Since renal filtration is the primary elimination route for Gd(III)-based contrast agents, inefficient renal clearance can result in prolonged retention of Gd(III) chelates, and consequently increases the chance of in vivo Gd^{3+} release. The risk associated with long-term Gd(III) retention has been clinically demonstrated in the cases of severely renal impaired patients who developed NSF after administration of linear small molecular Gd(III) agents (92, 99). In comparison to small molecular clinical Gd(III) agents, the experimental macromolecular-based Gd(III) contrast agents tend to have significantly longer retentions even in healthy animals due to their relatively large sizes that prevent efficient renal clearance (11). The retention level and patterns of macromolecular Gd(III) agents on healthy objects, as shown in some studies, were similar to that of the linear clinical agents on renal insufficient patient (160). This indicated the potential risk of macromolecular agents. Therefore, to facilitate the clinical translation of macromolecular agents, efforts should be focused on improving the elimination of macromolecular agents while retaining their advantage in blood pool and tumor imaging.

Summary

The current clinical Gd(III)-based contrast agents are nonspecific small molecular monomeric Gd(III) chelates providing a limited diagnostic window for MR imaging (6). Over the past decade, various types of macromolecular Gd(III)-based contrast agents have been developed as MR imaging agents with higher potency for the more challenging diagnostic tasks such as early detection of tumor and angiogenesis staging (118, 159). In comparison to current clinical agents, macromolecular Gd(III)-based contrast agents exhibit higher relaxivity due to slower molecular tumbling and large Gd(III) payloads. Also, they provide longer diagnostic windows due to their prolonged in vivo retention. Moreover, the macromolecular agents, with versatile compositions, can be designed to achieve multiple functions besides diagnosis, such as targeting and treatment. Therefore, they are promising for clinical applications. However, the dramatic increase of molecular size has created potentially high safety issues due to inefficient excretion of the macromolecular agents, hindering their further development in clinical applications (11). To address this problem, a balance should be maintained between efficacy and safety during the design of macromolecular Gd(III)-based contrast agents in order to minimize the potential risks while retaining the advantages of macromolecular contrast agents.

Biodegradable Polymeric Gd(III)-based Contrast Agents

In our previous studies, polymeric contrast agents with efficient biodegradability were designed to alleviate the safety concerns associated with long-term in vivo deposition of macromolecular Gd(III)-based contrast agents while retaining their advantages in MR imaging (124, 161-164). The biodegradable polymeric contrast agents

were designed based on in vivo degradability of disulfide bonds (161). Two types of biodegradable polymeric Gd(III) complex systems have been developed through different disulfide incorporation approaches: the backbone-incorporation method which results in polydisulfides and the side-chain-incorporation approach that leads to disulfide-grafted polymers (163, 165) (Figure 1.3). The polydisulfides and disulfide-grafted poly(L-glutamic acid) (PGA) are derived from Gd-DTPA and Gd-DOTA, respectively. The safety and effectiveness of the two biodegradable imaging systems were systemically evaluated, and compared in our preliminary studies.

Synthesis and Characterization of the Disulfide-based Contrast Agents

The preparation of the disulfide-based biodegradable polymeric Gd(III) contrast agents can be summarized into two steps: 1) synthesis of polymeric ligands, including polydisulfides DTPA and PGA-cystamine-DOTA; 2) complexation of the ligands with

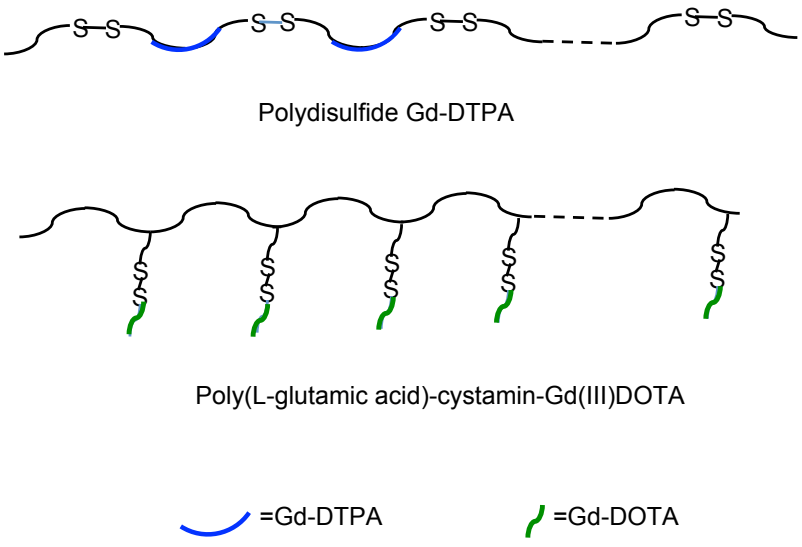

Figure 1.3. Structure design of disulfide-based contrast agents

Gd^{3+} (164). Chemical structure from each synthetic step was verified by H1-NMR and mass spectroscopy. The molecular weight, Gd(III) content, and relaxivity of the biodegradable contrast agents were determined as primary standards for the selection of suitable synthetic contrast agents for in vivo studies.

The polydisulfides Gd-DTPA were synthesized by copolymerization of disulfide-contained monomers and DTPA dianhydride (162). The ligand PGA-cystamine-DOTA, was obtained by conjugating cystamine-DOTA to the active ester of PGA (165). For the polydisulfide system, the impact of side chain structure on degradability was evaluated through comparison of three different polydisulfides with different side chain structures around the disulfide bonds: the polydisulfide with no side chains (Gd-DTPA cystamine copolymer, GDCC), with neutral side chains (Gd-DTPA cystine diethyl ester copolymer, GDCEP), and with negatively-charged side chains (Gd-DTPA cystine copolymer, GDCP). In addition, a nondegradable counterpart of GDCC, Gd-DTPA 1,6-hexanediamine copolymer (GDHC), which has no disulfide bonds, was synthesized for comparison purposes (166, 167). Similarly, a nondegradable control of PGA-cystamine-Gd-DOTA was also synthesized using the nondegradable spacer, 1,6-hexanediamine (168).

The average molecular weight of the synthetic polymeric contrast agents was determined by size exclusion chromatography (SEC). For macromolecular contrast agents, molecular size is an important factor affecting their elimination efficiency and tumor-diagnosing efficacy (105, 118, 169). The increase of size often results in improved relaxivity and tumor diagnosing effect, but can lead to prolonged retention with greater safety concerns (162, 166). Therefore, an ideal molecular weight of a biodegradable

system needs to be determined to assure proper balance between efficacy and safety. In our study, the polydisulfide Gd-DTPA and PGA-cystamine-Gd-DOTA with similar molecular weight (Mn≈60 kDa) were first synthesized and evaluated (163, 165). While both contrast agents showed similar tumor diagnosing effect, the polydisulfide Gd-DTPA showed better excretion post administration. This indicated it has better in vivo degradability and are therefore a safer choice than PGA-cystamine-Gd-DOTA for clinical application. Additional studies were then carried out to choose the optimal molecular weight for polydisulfides Gd-DTPA (162, 166, 167, 170). Polydisulfides with different molecular weight were obtained by adjusting the temperature, time, and solvent systems of the polymerization reactions. According to our study, polydisulfides Gd-DTPA ranging from 20-40 kD were optimal candidates for clinical application due to their good tumor diagnosis efficacy and comparably low in vivo accumulation.

Verification of Degradation

The degradation of the disulfide-based polymeric contrast agents was verified by in vitro incubation of the agents with aqueous solutions (pH 7.4) of free thiols (cysteine in our experiments) (163, 165). For polydisulfides Gd-DTPA, the influence of side chain structure around disulfide bonds were evaluated by comparing the degradation of GDCC, GDCEP, and GDCP with similar molecular weight (162, 166, 167, 170). The results demonstrated significantly different degradation profiles among the three structures. When incubating with plasma concentration of cystine solution (15 μM), GDCP showed no change in molecular weight over time; GDCEP showed comparably faster degradation, with a decrease of 6 %, 11 %, and 24 % of molecular weight at 5, 15, and 60 minutes

during incubation; GDCC demonstrated the most efficient degradation with 28 %, 33 %, and 50 % molecular weight decrease at 5, 15, and 60 minutes during incubation (163, 166, 167). The degradation of GDCP and GDCEP increased considerably when the concentration of cysteine was 10-fold higher (166). The slower degradation of GDCEP and GDCP illustrated the influence of side chain structures around the disulfide bonds on degradability of polydisulfides. For GDCEP, its relatively long neutral side chains (ethyl ester) may hinder the approach of free thiols to the disulfide bonds and result in slower degradation. For GDCP, the attack of cysteine may be restrained by electrostatic repulsion due to the negative charges of the carboxylic groups on both cysteine and the side chains of GDCP.

In comparison to GDCC, the PGA-disulfide grafted system showed relatively slower in vitro degradation, which was only observed with cysteine incubation at higher concentrations (100 μM) (161). The grafted polymeric structure of PGA-cystamine-Gd-DOTA and the steric hindrance of the DOTA side chain may confine the accessibility of disulfide bonds in solution and lead to inefficient degradation of the polymer.

The results of in vitro degradation study were consistent with in vivo observation, both showing more efficient degradation of the polydisulfides over the PGA-disulfide system (161, 164, 166, 171). For the polydisulfide system, degradation can be greatly affected by side chain strucutres around the disulfide bonds. Modificaion such as increase of side chain bulkiness or introduction of negatively charged side chains can lead to slower degradation of the polydisulfides. Overall, the degradability of disulfide-based polymeric systems depends mainly on the availability of highly accessible disulfide bonds in solution. In our case, the linear polydisulfide structure provides more spatial

freedom and thus higher accessibility of the disulfide bonds than that of the grafted polymeric disulfide structure. This effect rendered linear polydisulfide to be the better structure for further clinical development.

In Vivo MR Imaging

The tumor diagnosing efficacy of GDCC and PGA-disulfide-Gd-DOTA were evaluated on mice tumor xenograft models, in comparison with the clinical agent Ominiscan® (164, 165, 172). The MR studies were performed under similar conditions with both agents (164). The results showed that the tumor and blood pool enhancing effects of both disulfide incorporated polymers were between the efficacy of Ominiscan® and their respective nondegradable controls. Both polymers demonstrated improved diagnosing effect in comparison with the small molecular clinical agents (161, 165). Further analysis of in vivo MR imaging revealed longer blood retention of PGA-disulfide-Gd-DOTA than that of GDCC. The contrast enhancement of GDCC was close to baseline level after 30 minutes post injection, while significant contrast enhancement was still observable for the PGA-disulfide-grafted polymer up to 4 hours post injection. This can be explained by the slower in vivo degradation of the grafted polymeric system.

Long-term Accumulation Study

Evaluation of long-term tissue accumulation was performed among Ominiscan®, GDCC (18 kD), GDCC (60 kD), GDCEP, GDCP, and GDCH, as well as between PGA-cystamin-Gd-DOTA and its nondegradable counterpart, in different studies (161, 166, 167, 173). In all studies, the Gd(III)-based contrast agents were intravenously injected to

Sprague-Dawley rats at the standard clinical dose of 1.0 mmol-Gd/kg. The rats were kept for 10 days and then sacrificed to collect various tissues, including heart, lung, spleen, kidney, muscle, femur, and liver. The remaining Gd(III) content in each organ was measured using the inductively coupled plasma optical emission spectrometry (ICP-OES). The results showed that the order of tissue accumulation was: liver > muscle > kidney > femur > spleen > heart≈lung for all the polymeric agents, while negligible residues of Gd(III) was detected with the clinical agent. Although both types of biodegradable polymeric agents had significant decrease of tissue accumulation in comparison with their nondegradable controls, the disulfide-grafted agents exhibited significantly higher liver and spleen accumulation than the polydisulfides Gd-DTPA. Among the polydisulfides, GDCC with lower molecular weight (18 kD) showed minimal tissue accumulation, which was comparable to that of the clinical agent Omniscan®. Overall, the long-term accumulation studies showed that both biodegradable disulfide-based polymeric systems can greatly reduce long-term Gd(III) tissue deposit in comparison with the nondegradable polymers. However, the level of residual Gd(III) was still higher for most biodegradable systems than that of the clinical agents (173). Between the two disulfide-based polymeric systems, the polydisulfides were more efficiently eliminated than the disulfide-grafted polymers. It resulted in considerably less residual Gd(III) 10 days after administration of the agents. This indicated that the polydisulfides were the safer option for further clinical investigation (161, 171).

Kinetic Stability

GDCC (20-40 kD) was the most clinically promising biodegradable contrast agent we have developed. However, it was facing another potential safety issue due to the less stable linear chelate Gd-DTPA on which the polydisulfide agent was based. As mentioned in the previous section, low kinetic stability of the linear chelates, especially the nonionic linear chelates, could result in the release of free Gd^{3+} ions through transmetallation with endogenous metal ions such as Zn^{2+}, Cu^{2+}, and Ca^{2+} (17, 24). This risk of Gd^{3+} release increased with inefficient elimination of the agents, in the case of patients with severe renal impairment receiving clinical linear agents (81, 91) or in the case of patients with normal renal function receiving nondegradable macromolecular contrast agents (11). Although the biodegradable polymeric systems can significantly improve the elimination efficiency, they still lead to relatively higher long-term Gd(III) residues in comparison with that of the clinical agents. As a result, the nonionic linear chelate-based polydisulfide GDCC (20-40 kD) may result in greater loss of Gd^{3+} in comparison with the small molecular linear agents due to its relatively longer in vivo retention. To evaluate the extent of transmetallation of GDCC (20-40 kD), in vitro and in vivo studies have been carried out to understand the kinetic stability of GDCC in comparison with the clinical contrast agents: Ominiscan® (linear ionic), MultiHance® (linear nonionic), and ProHance® (macrocyclic) (174).

The transmetallation of GDCC was first verified through in vitro incubation study using phosphate buffered solutions (PBS) with or without the existence of endogenous metal ions under physiological pH and temperature (173). The results showed that approximately 15 % of Gd(III) was lost within 45 minutes post incubation with

endogenous metal ions, whereas no change in Gd(III) content was observed in negative control solution, indicating the occurrence of transmetallation for GDCC. To better simulate in vivo transmetallation, further in vitro assessment of transmetallation was carried out through incubation studies using fresh rat plasma for GDCC (31 kD) and different clinical agents as the majority plasma metal species are protein-bound instead of free ions. After incubation, ultrafiltration was used to separate the protein-bound metal species and the exogenous polymeric ligand-bound metal species based on their size differences. The measurement was carried out by incubation of plasma concentrations of various Gd(III) agents with fresh rat plasma at room temperature for 2 hours. The different molecular components of the plasma mixture was then separated by ultrafiltration and measured using ICP-OES. The degree of transmetallation was calculated based on the proportion of ligand bound metals versus protein bound metals. Our results showed that the transmetallation happened mainly between plasma Zn(II) and the contrast agents. The order of transmetallation of the tested agents with plasma Zn(II) was: Omniscan (linear nonionic) > MultiHance (linear ionic) ≈ GDCC > ProHance (macrocyclic).

In vivo transmetallation was assessed through analysis of metal metabolites in rat urines after administration of Gd(III)-based agents (173). In this study, the animals were injected with various Gd(III)-based agents at the clinical dose of 0.1 mmol Gd/kg, followed by collection of urine samples at 8 hours and 24 hours post injection. Urine samples collected 12 hours before administration of Gd(III) agents were used as negative controls. The collected urine samples were processed and analyzed to calculate transmetallation. Similar to what was shown from in vitro studies, in vivo analysis also

revealed Zn(II) as the major metal species responsible for the loss of Gd(III) from its ligand through transmetallation. Between the two time points, significant transmetallation was only observed at 8 hours post injection at the order of Ominiscan (linear nonionic) > MultiHance (linear ionic) > GDCC > ProHance (macrocyclic).

In summary, both in vitro and in vivo transmetallation study showed clear correlations between chelate structure and kinetic stability. Similar order of stability was observed among the four agents tested in both studies: macrocyclic chelate (ProHance®) > linear ionic chelate (MultiHance®) ≈ GDCC (31 kD) > linear nonionic chelate (Omniscan®). Although GDCC is based on linear nonionic chelates, the polymeric structure itself may produce steric hindrance against transmetallation with the endogenous Zn(II), making it more stable than the small molecular nonionic chelates. However, the stability of GDCC was still relatively low in comparison to the macrocyclic agents. Given its comparably higher in vivo retention than that of the small molecular agents (173), GDCC is still suffering from higher risks associated with long-term deposit and release of Gd^{3+}, which hinders its further clinical translation.

Statement of Problem

Macromolecular Gd(III)-based contrast agents have shown promising potential in the more challenging diagnosis areas such as tumor detection and staging. However, they are confined by safety issues associated with inefficient eliminations. To improve the elimination efficiency while pertaining the advantages of macromolecular agents, we have developed disulfide-based biodegradable polymeric Gd(III) contrast agents with efficient elimination and relatively good tumor diagnosing efficacy. However, the

previous developed polydisulfides were based on the kinetically labile nonionic linear chelates which can possibly trigger severe side effects (81, 99). To further improve the safety profile of polydisulfide based MR contrast agents, two alternative strategies were proposed and investigated in the following chapters: 1) development of polydisulfide based non-Gd(III) MR contrast agents; 2) replacement of the linear chelates with the more stable macrocyclic chelates on the polydisulfide structure.

Manganese-based Biodegradable MR Contrast Agent

Paramagnetic manganese(II) chelates or compounds are an alternative class of MRI contrast agents (12). As an endogenous metal, the manganese-based contrast agents exhibit unique biodistribution pattern and effective contrast enhancement in the myocardium, liver, and brain (175, 176). The main limitation of the manganese-based contrast agents is their relatively low relaxivities. Because of this, an increased dose is often needed to generate sufficient contrast enhancement, which may lead to unexpected toxic side effects. Chemical modifications of manganese-based contrast agents may result in more effective nongadolinium contrast agents by improving their relaxivities and optimizing their pharmacokinetics and biodistribution.

Project Aims

Incorporation of manganese(II) into polydisulfides may result in effective manganese-based MRI contrast agents with improved contrast enhancement at a relatively low dose. In this study, two polydisulfide Mn(II) complexes were synthesized and evaluated as non-gadolinium biodegradable macromolecular MRI contrast agents. In

vivo contrast enhancement of the agents were evaluated on mice bearing MDA-MB-231 breast cancer xenografts.

The Polydisulfide Biodegradable System Based on Macrocyclic Gd(III) Chelates

Macromolecular Gd(III)-based contrast agents are effective for contrast-enhanced blood pool and cancer MRI in preclinical studies (9). However, their clinical applications are impeded by potential safety concerns associated with slow excretion and prolonged retention of these agents in the body. To improve the elimination efficiency of macromolecular MR contrast agents, we have designed and developed biodegradable polymeric Gd(III) contrast agents based on polydisulfide Gd(III) complexes. The previous polydisulfide agents were based on the less stable nonionic linear Gd(III) chelates, causing safety concerns for further clinical development. In this study, we designed and synthesized a new generation of polydisulfide Gd(III) complexes based on the more stable macrocyclic Gd(III) chelate: Gd-DOTA monoamide which has improved safety profile.

Project Aims

In this study, we have designed and synthesized two new polydisulfides based on the macrocyclic Gd chelates as biodegradable blood pool agents with high overall kinetic inertness. The work includes: 1) synthesis and characterization of the new agent; 2) demonstration of degradation mechanism in vitro; 3) evaluation of the kinetic stability in vitro; 4) evaluation of efficacy in MR blood pool imaging and cancer diagnosis; 5) pharmacokinetics study; 6) biodistribution study; 7) metabolic study of transmetallation.

References

1. Marinus T. Vlaardingerbroek JAB, A. Luiten. Magnetic resonance imaging: theory and practices: Springer; 2004.

2. Prasad PV. Magnetic resonance imaging: methods and biologic applications: Humana Press; 2005.

3. Esserman LJ, Kumar AS, Herrera AF, Leung J, Au A, Chen YY, Moore DH, Chen DF, Hellawell J, Wolverton D, Hwang ES, Hylton NM. Magnetic resonance imaging captures the biology of ductal carcinoma in situ. J Clin Oncol. 2006;24(28):4603-4610.

4. Lauffer RB. Paramagnetic metal complexes as water proton relaxation agents for NMR imaging: theory and design. Chem Rev. 1987;87(5):901-927.

5. Caravan P, Ellison JJ, McMurry TJ, Lauffer RB. Gadolinium(III) chelates as MRI contrast agents: structure, dynamics, and applications. Chem Rev. 1999;99(9):2293-2352.

6. Bellin MF, Vasile M, Morel-Precetti S. Currently used non-specific extracellular MR contrast media. Eur Radiol. 2003;13(12):2688-2698.

7. Brasch RC. Rationale and applications for macromolecular Gd-based contrast agents. Magn Reson Med. 1991;22(2):282-287.

8. Brasch R, Pham C, Shames D, Roberts T, van Dijke K, van Bruggen N, Mann J, Ostrowitzki S, Melnyk O. Assessing tumor angiogenesis using macromolecular MR imaging contrast media. J Magn Reson Imaging. 1997;7(1):68-74.

9. Barrett T, Kobayashi H, Brechbiel M, Choyke PL. Macromolecular MRI contrast agents for imaging tumor angiogenesis. Eur J Radiol. 2006;60(3):353-366.

10. Aime S, Castelli DD, Crich SG, Gianolio E, Terreno E. Pushing the sensitivity envelope of lanthanide-based magnetic resonance imaging (MRI) contrast agents for molecular imaging applications. Acc Chem Res. 2009;42(7):822-831.

11. Aime S, Caravan P. Biodistribution of gadolinium-based contrast agents, including gadolinium deposition. J Magn Reson Imaging. 2009;30(6):1259-1267.

12. Koretsky AP, Silva AC. Manganese-enhanced magnetic resonance imaging (MEMRI). NMR Biomed. 2004;17(8):527-531.

13. Bulte JW, Kraitchman DL. Iron oxide MR contrast agents for molecular and cellular imaging. NMR Biomed. 2004;17(7):484-499.

14. Itoh N, Kawakita M. Characterization of Gd^{3+} and Tb^{3+} binding sites on Ca^{2+},Mg^{2+}-adenosine triphosphatase of sarcoplasmic reticulum. J Biochem. 1984;95(3):661-669.

15. Evans C. Biochemistry of the lanthanides: Springer; 1990.

16. Chang CA, Sieving PF, Watson AD, Dewey TM, Karpishin TB, Raymond KN. Ionic versus nonionic MR imaging contrast media: operational definitions. J Magn Reson Imaging. 1992;2(1):95-98.

17. Idee JM, Port M, Raynal I, Schaefer M, Le Greneur S, Corot C. Clinical and biological consequences of transmetallation induced by contrast agents for magnetic resonance imaging: a review. Fundam Clin Pharmacol. 2006;20(6):563-576.

18. Brucher E, Tircso, G., Baranyai, Z., Kovacs, Z. and Sherry, A.D Stability and toxicity of contrast agents. In: A. Merbach LH, E. Toth, editor. The chemistry of contrast agents in medical magnetic resonance imaging: John Wiley & Sons, Ltd; 2013.

19. Husztik E, Lazar G, Parducz A. Electron microscopic study of Kupffer-cell phagocytosis blockade induced by gadolinium chloride. Br J Exp Pathol. 1980;61(6):624-630.

20. Lazar G, Jr., Lazar G, Kaszaki J, Olah J, Kiss I, Husztik E. Inhibition of anaphylactic shock by gadolinium chloride-induced Kupffer cell blockade. Agents Actions. 1994;41 Spec No:C97-98.

21. Palasz A, Czekaj P. Toxicological and cytophysiological aspects of lanthanides action. Acta Biochim Pol. 2000;47(4):1107-1114.

22. Bousquet JC, Saini S, Stark DD, Hahn PF, Nigam M, Wittenberg J, Ferrucci JT, Jr. Gd-DOTA: characterization of a new paramagnetic complex. Radiology. 1988;166(3):693-698.

23. Singh R. Coordination chemistry: Mittal Publications; 2002.

24. Port M, Idee JM, Medina C, Robic C, Sabatou M, Corot C. Efficiency, thermodynamic and kinetic stability of marketed gadolinium chelates and their possible clinical consequences: a critical review. Biometals. 2008;21(4):469-490.

25. Cacheris WP, Quay SC, Rocklage SM. The relationship between thermodynamics and the toxicity of gadolinium complexes. Magn Reson Imaging. 1990;8(4):467-481.

26. Brucher E, Sherry AD. Stability and toxicity of contrast agents. New York:

Wiley; 2001.

27. Moreau J, Guillon E, Pierrard JC, Rimbault J, Port M, Aplincourt M. Complexing mechanism of the lanthanide cations Eu^{3+}, Gd^{3+}, and Tb^{3+} with 1,4,7,10-tetrakis(carboxymethyl)-1,4,7,10-tetraazacyclododecane (dota)-characterization of three successive complexing phases: study of the thermodynamic and structural properties of the complexes by potentiometry, luminescence spectroscopy, and EXAFS. Chemistry. 2004;10(20):5218-5232.

28. Cram DJ. The design of molecular hosts, guests, and their complexes (nobel lecture). Angew Chem Int Ed Engl. 1988;27(8):1009-1020.

29. Kumar K, Jin T, Wang X, Desreux JF, Tweedle MF. Effect of ligand basicity on the formation and dissociation equilibria and kinetics of Gd3+ complexes of macrocyclic polyamino carboxylates. Inorg Chem. 1994;33(17):3823-3829.

30. Desreux JF. Nuclear magnetic resonance spectroscopy of lanthanide complexes with a tettraacetic tetraaza macrocycle. Unusual conformation properteis. Inorg Chem. 1980;19:1319-1324.

31. Desreux JF. Nuclear magnetic resonance spectroscopy of lanthanide complexes with a tetraacetic tetraaza macrocycle. Unusual conformation properties. Inorg Chem. 1980;19(5):1319-1324.

32. Fossheim R, Dugstad H, Dahl SG. Structure-stability relationships of Gd(III) ion complexes for magnetic resonance imaging. J Med Chem. 1991;34(2):819-826.

33. Kumar K. Macrocyclic polyamino carboxylate complexes of Gd(III) as magnetic resonance imaging contrast agents. J Alloys Comp. 1997;249:163-172.

34. Maiocchi A. The use of molecular descriptors in the design of gadolinium (III) chelates as MRI contrast agents. Mini Rev Med Chem. 2003;3(8):845-859.

35. Kumar K, Tweedle MF, Malley MF, Gougoutas JZ. Synthesis, Stability, and Crystal Structure Studies of Some Ca^{2+}, Cu^{2+}, and Zn^{2+} Complexes of Macrocyclic Polyamino Carboxylates. Inorg Chem. 1995;34(26):6472-6480.

36. Szilágyi E, Tóth, É, Kovács, Z, Platzek, J, Radüchel, B & Brücher, E. Equilibria and formation kinetics of some cyclen derivative complexes of lanthanides. Inorg Chim Acta. 2000;298:226-245.

37. Lukeš I, Kotek J, Vojtíšek P, Hermann P. Complexes of tetraazacycles bearing methylphosphinic/phosphonic acid pendant arms with copper(II), zinc(II) and lanthanides(III). A comparison with their acetic acid analogues. Coord Chem Rev. 2001;216–217:287-312.

38. Sherry AD, Ren J, Huskens J, Brücher E, Tóth É, Geraldes CFCG, Castro MMCA, Cacheris WP. Characterization of lanthanide(III) DOTP complexes: thermodynamics, protonation, and coordination to alkali metal ions. Inorg Chem. 1996;35(16):4604-4612.

39. Lazar I, Sherry AD, Ramasamy R, Brucher E, Kiraly R. Synthesis and complexation properties of a new macrocyclic polyaza polyphosphinate ligand, DOTEP(1,4,7,10-tetraazacyclododecane-1,4,7,10-tetrakis(methyleneethylphosphinate)). Inorg Chem. 1991;30(26):5016-5019.

40. Kim WD, Kiefer GE, Huskens J, Sherry AD. NMR studies of the lanthanide(III) complexes of 1,4,7,10-tetraazacyclododecane-1,4,7,10-tetrakis-(methanephosphonic acid mono(2‘,2‘,2‘-trifluoroethyl) ester). Inorg Chem. 1997;36(18):4128-4134.

41. Burai L, Király R, Lázár I, Brücher E. Formation and dissociation kinetics of the complexes Gd(DOTP)5− and Gd(DOTPMB)−. Eur J Inorg Chem. 2001;2001(3):813-820.

42. Forsterova M, Jandurova Z, Marques F, Gano L, Lubal P, Vanek J, Hermann P, Santos I. Chemical and biological evaluation of 153Sm and 166Ho complexes of 1,4,7,10-tetraazacyclododecane-1,4,7,10-tetrakis(methylphosphonic acid monoethylester) (H4 dotp OEt). J Inorg Biochem. 2008;102(7):1531-1540.

43. Táborskýa P. LP, Havela J., Kotekb J., Hermannb P., Lukeš I. . Thermodynamic and kinetic studies of lanthanide(III) complexes with h5do3ap (1,4,7,10-tetraazacyclododecane-1,4,7-triacetic-10-(methylphosphonic acid)), a monophosphonate analogue of h4dota. Collect Czech Chem Commun. 2005;70:1909-1942.

44. Forsterova M, Svobodova I, Lubal P, Taborsky P, Kotek J, Hermann P, Lukes I. Thermodynamic study of lanthanide(iii) complexes with bifunctional monophosphinic acid analogues of H4dota and comparative kinetic study of yttrium(iii) complexes. Dalton Trans. 2007(5):535-549.

45. Chang CA. Magnetic resonance imaging contrast agents. Design and physicochemical properties of gadodiamide. Invest Radiol. 1993;28 Suppl 1:S21-27.

46. Jackson GE, Wynchank S, Woudenberg M. Gadolinium(III) complex equilibria: the implications for Gd(III) MRI contrast agents. Magn Reson Med. 1990;16(1):57-66.

47. Sarka L, Burai L, Brucher E. The rates of the exchange reactions between $[Gd(DTPA)]^{2-}$ and the endogenous ions Cu^{2+} and Zn^{2+}: a kinetic model for the prediction of the in vivo stability of $[Gd(DTPA)]^{2-}$, used as a contrast agent in

magnetic resonance imaging. Chemistry. 2000;6(4):719-724.

48. De Haen C, Cabrini M, Akhnana L, Ratti D, Calabi L, Gozzini L. Gadobenate dimeglumine 0.5 M solution for injection (MultiHance) pharmaceutical formulation and physicochemical properties of a new magnetic resonance imaging contrast medium. J Comput Assist Tomogr. 1999;23 Suppl 1:S161-168.

49. Brücher E. Kinetic Stabilities of gadolinium(III) chelates used as MRI contrast agents. In: Krause W, editor. Contrast agents I: Springer Berlin Heidelberg; 2002. p. 103-122.

50. Tweedle MF. Physicochemical properties of gadoteridol and other magnetic resonance contrast agents. Invest Radiol. 1992;27 Suppl 1:S2-6.

51. Wedeking P, Kumar K, Tweedle MF. Dissociation of gadolinium chelates in mice: relationship to chemical characteristics. Magn Reson Imaging. 1992;10(4):641-648.

52. Harrison A, Walker CA, Pereira KA, Parker D, Royle L, Pulukkody K, Norman TJ. Hepato-biliary and renal excretion in mice of charged and neutral gadolinium complexes of cyclic tetra-aza-phosphinic and carboxylic acids. Magn Reson Imaging. 1993;11(6):761-770.

53. Kumar K, Chang CA, Tweedle MF. Equilibrium and kinetic studies of lanthanide complexes of macrocyclic polyamino carboxylates. Inorg Chem. 1993;32(5):587-593.

54. Schmitt-Willich H. Stability of linear and macrocyclic gadolinium based contrast agents. Br J Radiol. 2007;80(955):581-582; author reply 584-585.

55. Sarka L, Burai L, Kiraly R, Zekany L, Brucher E. Studies on the kinetic stabilities of the Gd(3+) complexes formed with the N-mono(methylamide), N'-mono(methylamide) and N,N''-bis(methylamide) derivatives of diethylenetriamine-N,N,N',N'',N''-pentaacetic acid. J Inorg Biochem. 2002;91(1):320-326.

56. White DH, deLearie LA, Moore DA, Wallace RA, Dunn TJ, Cacheris WP, Imura H, Choppin GR. The thermodynamics of complexation of lanthanide (III) DTPA-bisamide complexes and their implication for stability and solution structure. Invest Radiol. 1991;26 Suppl 1:S226-228; discussion S232-225.

57. Tóth É, Király R, Platzek J, Radüchel B, Brücher E. Equilibrium and kinetic studies on complexes of 10-[2,3-dihydroxy-(1-hydroxymethyl)-propyl]-1,4,7,10-tetraazacyclododecane-1,4,7-triacetate. Inorganica Chimica Acta. 1996;249(2):191-199.

58. Puttagunta NR, Gibby WA, Smith GT. Human in vivo comparative study of zinc and copper transmetallation after administration of magnetic resonance imaging contrast agents. Invest Radiol. 1996;31(12):739-742.

59. Tweedle MF, Eaton SM, Eckelman WC, Gaughan GT, Hagan JJ, Wedeking PW, Yost FJ. Comparative chemical structure and pharmacokinetics of MRI contrast agents. Invest Radiol. 1988;23 Suppl 1:S236-239.

60. Laurent S, Elst LV, Copoix F, Muller RN. Stability of MRI paramagnetic contrast media: a proton relaxometric protocol for transmetallation assessment. Invest Radiol. 2001;36(2):115-122.

61. Laurent S, Elst LV, Muller RN. Comparative study of the physicochemical properties of six clinical low molecular weight gadolinium contrast agents. Contrast Media Mol Imaging. 2006;1(3):128-137.

62. Kumar K. Marcocyclic polyamino carboxylate complexes of Gd(III) as magnetic resonance imaging contrast agents. J Alloys Comp. 1997;249:163-172.

63. Caravan P, Comuzzi C, Crooks W, McMurry TJ, Choppin GR, Woulfe SR. Thermodynamic stability and kinetic inertness of MS-325, a new blood pool agent for magnetic resonance imaging. Inorg Chem. 2001;40(9):2170-2176.

64. Tweedle MF. "Stability" of gadolinium chelates. Br J Radiol. 2007;80(955):583-584; author reply 584-585.

65. Tweedle MF, Wedeking P, Kumar K. Biodistribution of radiolabeled, formulated gadopentetate, gadoteridol, gadoterate, and gadodiamide in mice and rats. Invest Radiol. 1995;30(6):372-380.

66. Gibby WA, Gibby KA. Comparison of Gd DTPA-BMA (Omniscan) versus Gd HP-DO3A (ProHance) retention in human bone tissue by inductively coupled plasma atomic emission spectroscopy. Invest Radiol. 2004;39(3):138-142.

67. White GW, Gibby WA, Tweedle MF. Comparison of Gd(DTPA-BMA) (Omniscan) versus Gd(HP-DO3A) (ProHance) relative to gadolinium retention in human bone tissue by inductively coupled plasma mass spectroscopy. Invest Radiol. 2006;41(3):272-278.

68. Harpur ES, Worah D, Hals PA, Holtz E, Furuhama K, Nomura H. Preclinical safety assessment and pharmacokinetics of gadodiamide injection, a new magnetic resonance imaging contrast agent. Invest Radiol. 1993;28 Suppl 1:S28-43.

69. Corot C, Idee JM, Hentsch AM, Santus R, Mallet C, Goulas V, Bonnemain B, Meyer D. Structure-activity relationship of macrocyclic and linear gadolinium

chelates: investigation of transmetallation effect on the zinc-dependent metallopeptidase angiotensin-converting enzyme. J Magn Reson Imaging. 1998;8(3):695-702.

70. Wible JH, Jr., Troup CM, Hynes MR, Galen KP, MacDonald JR, Barco SJ, Wojdyla JK, Periasamy MP, Adams MD. Toxicological assessment of gadoversetamide injection (OptiMARK), a new contrast-enhancement agent for use in magnetic resonance imaging. Invest Radiol. 2001;36(7):401-412.

71. Abdou N, Napoli AM, Hynes MR, Allen JC, Jr., Wible JH, Jr. Safety assessment of gadoversetamide (OptiMARK) administered by power injector. J Magn Reson Imaging. 2004;19(1):133-140.

72. Kimura J, Ishiguchi T, Matsuda J, Ohno R, Nakamura A, Kamei S, Ohno K, Kawamura T, Murata K. Human comparative study of zinc and copper excretion via urine after administration of magnetic resonance imaging contrast agents. Radiat Med. 2005;23(5):322-326.

73. Tweedle MF, Hagan JJ, Kumar K, Mantha S, Chang CA. Reaction of gadolinium chelates with endogenously available ions. Magn Reson Imaging. 1991;9(3):409-415.

74. Caravan P, Cloutier NJ, Greenfield MT, McDermid SA, Dunham SU, Bulte JW, Amedio JC, Jr., Looby RJ, Supkowski RM, Horrocks WD, Jr., McMurry TJ, Lauffer RB. The interaction of MS-325 with human serum albumin and its effect on proton relaxation rates. J Am Chem Soc. 2002;124(12):3152-3162.

75. Lauffer RB, Parmelee DJ, Ouellet HS, Dolan RP, Sajiki H, Scott DM, Bernard PJ, Buchanan EM, Ong KY, Tyeklar Z, Midelfort KS, McMurry TJ, Walovitch RC. MS-325: a small-molecule vascular imaging agent for magnetic resonance imaging. Acad Radiol. 1996;3 Suppl 2:S356-358.

76. Parmelee DJ, Walovitch RC, Ouellet HS, Lauffer RB. Preclinical evaluation of the pharmacokinetics, biodistribution, and elimination of MS-325, a blood pool agent for magnetic resonance imaging. Invest Radiol. 1997;32(12):741-747.

77. Pascolo L, Cupelli F, Anelli PL, Lorusso V, Visigalli M, Uggeri F, Tiribelli C. Molecular mechanisms for the hepatic uptake of magnetic resonance imaging contrast agents. Biochem Biophys Res Commun. 1999;257(3):746-752.

78. Kirchin MA, Pirovano GP, Spinazzi A. Gadobenate dimeglumine (Gd-BOPTA). An overview. Invest Radiol. 1998;33(11):798-809.

79. Joffe P, Thomsen HS, Meusel M. Pharmacokinetics of gadodiamide injection in patients with severe renal insufficiency and patients undergoing hemodialysis or continuous ambulatory peritoneal dialysis. Acad Radiol. 1998;5(7):491-502.

80. Schuhmann-Giampieri G, Schmitt-Willich H, Frenzel T, Press WR, Weinmann HJ. In vivo and in vitro evaluation of Gd-DTPA-polylysine as a macromolecular contrast agent for magnetic resonance imaging. Invest Radiol. 1991;26(11):969-974.

81. Thomsen HS, Morcos SK. Nephrogenic systemic fibrosis and nonionic linear chelates. AJR Am J Roentgenol. 2007;188(6):W580; author reply W581.

82. Weinmann HJ, Laniado M, Mutzel W. Pharmacokinetics of GdDTPA/dimeglumine after intravenous injection into healthy volunteers. Physiol Chem Phys Med NMR. 1984;16(2):167-172.

83. VanWagoner M, O'Toole M, Worah D, Leese PT, Quay SC. A phase I clinical trial with gadodiamide injection, a nonionic magnetic resonance imaging enhancement agent. Invest Radiol. 1991;26(11):980-986.

84. McLachlan SJ, Eaton S, De Simone DN. Pharmacokinetic behavior of gadoteridol injection. Invest Radiol. 1992;27 Suppl 1:S12-15.

85. Van Wagoner M, Worah D. Gadodiamide injection. First human experience with the nonionic magnetic resonance imaging enhancement agent. Invest Radiol. 1993;28 Suppl 1:S44-48.

86. Swan SK, Baker JF, Free R, Tucker RM, Barron B, Barr R, Seltzer S, Gazelle GS, Maravilla KR, Barr W, Stevens GR, Lambrecht LJ, Pierro JA. Pharmacokinetics, safety, and tolerability of gadoversetamide injection (OptiMARK) in subjects with central nervous system or liver pathology and varying degrees of renal function. J Magn Reson Imaging. 1999;9(2):317-321.

87. Tombach B, Bremer C, Reimer P, Schaefer RM, Ebert W, Geens V, Heindel W. Pharmacokinetics of 1M gadobutrol in patients with chronic renal failure. Invest Radiol. 2000;35(1):35-40.

88. Baker JF, Kratz LC, Stevens GR, Wible JH, Jr. Pharmacokinetics and safety of the MRI contrast agent gadoversetamide injection (OptiMARK) in healthy pediatric subjects. Invest Radiol. 2004;39(6):334-339.

89. McMurry TJ, Parmelee DJ, Sajiki H, Scott DM, Ouellet HS, Walovitch RC, Tyeklar Z, Dumas S, Bernard P, Nadler S, Midelfort K, Greenfield M, Troughton J, Lauffer RB. The effect of a phosphodiester linking group on albumin binding, blood half-life, and relaxivity of intravascular diethylenetriaminepentaacetato aquo gadolinium(III) MRI contrast agents. J Med Chem. 2002;45(16):3465-3474.

90. Agency EM. EMEA scientific discussion document for gadofosveset trisodium. In.: European Medicines Agency; 2005.

91. Kribben A, Witzke O, Hillen U, Barkhausen J, Daul AE, Erbel R. Nephrogenic systemic fibrosis: pathogenesis, diagnosis, and therapy. J Am Coll Cardiol. 2009;53(18):1621-1628.

92. Kuo PH, Kanal E, Abu-Alfa AK, Cowper SE. Gadolinium-based MR contrast agents and nephrogenic systemic fibrosis. Radiology. 2007;242(3):647-649.

93. Marckmann P, Skov L, Rossen K, Dupont A, Damholt MB, Heaf JG, Thomsen HS. Nephrogenic systemic fibrosis: suspected causative role of gadodiamide used for contrast-enhanced magnetic resonance imaging. J Am Soc Nephrol. 2006;17(9):2359-2362.

94. Cowper SE, Robin HS, Steinberg SM, Su LD, Gupta S, LeBoit PE. Scleromyxoedema-like cutaneous diseases in renal-dialysis patients. Lancet. 2000;356(9234):1000-1001.

95. Cowper SE. Nephrogenic systemic fibrosis: a review and exploration of the role of gadolinium. Adv Dermatol. 2007;23:131-154.

96. Cowper SE, Rabach M, Girardi M. Clinical and histological findings in nephrogenic systemic fibrosis. Eur J Radiol. 2008;66(2):191-199.

97. Daram SR, Cortese CM, Bastani B. Nephrogenic fibrosing dermopathy/nephrogenic systemic fibrosis: report of a new case with literature review. Am J Kidney Dis. 2005;46(4):754-759.

98. Introcaso CE, Hivnor C, Cowper S, Werth VP. Nephrogenic fibrosing dermopathy/nephrogenic systemic fibrosis: a case series of nine patients and review of the literature. Int J Dermatol. 2007;46(5):447-452.

99. Broome DR. Nephrogenic systemic fibrosis associated with gadolinium based contrast agents: a summary of the medical literature reporting. Eur J Radiol. 2008;66(2):230-234.

100. Grobner T. Gadolinium--a specific trigger for the development of nephrogenic fibrosing dermopathy and nephrogenic systemic fibrosis? Nephrol Dial Transplant. 2006;21(4):1104-1108.

101. Muller LK, Landfester K. Natural liposomes and synthetic polymeric structures for biomedical applications. Biochem Biophys Res Commun. 2015;468(3):411-418

102. Goyen M, Shamsi K, Schoenberg SO. Vasovist-enhanced MR angiography. Eur Radiol. 2006;16 Suppl 2:B9-14.

103. Turetschek K, Floyd E, Helbich T, Roberts TP, Shames DM, Wendland MF,

Carter WO, Brasch RC. MRI assessment of microvascular characteristics in experimental breast tumors using a new blood pool contrast agent (MS-325) with correlations to histopathology. J Magn Reson Imaging. 2001;14(3):237-242.

104. Aime S, Cabella C, Colombatto S, Geninatti Crich S, Gianolio E, Maggioni F. Insights into the use of paramagnetic Gd(III) complexes in MR-molecular imaging investigations. J Magn Reson Imaging. 2002;16(4):394-406.

105. Brasch R, Turetschek K. MRI characterization of tumors and grading angiogenesis using macromolecular contrast media: status report. Eur J Radiol. 2000;34(3):148-155.

106. Louie A. Multimodality imaging probes: design and challenges. Chem Rev. 2010;110(5):3146-3195.

107. Ogan MD, Schmiedl U, Moseley ME, Grodd W, Paajanen H, Brasch RC. Albumin labeled with Gd-DTPA. An intravascular contrast-enhancing agent for magnetic resonance blood pool imaging: preparation and characterization. Invest Radiol. 1987;22(8):665-671.

108. Schmiedl U, Ogan M, Paajanen H, Marotti M, Crooks LE, Brito AC, Brasch RC. Albumin labeled with Gd-DTPA as an intravascular, blood pool-enhancing agent for MR imaging: biodistribution and imaging studies. Radiology. 1987;162(1 Pt 1):205-210.

109. Baxter AB, Lazarus SC, Brasch RC. In vitro histamine release induced by magnetic resonance imaging and iodinated contrast media. Invest Radiol. 1993;28(4):308-312.

110. Bogdanov Jr AA, Weissleder R, Brady TJ. Long-circulating blood pool imaging agents. Adv Drug Deliver Rev. 1995;16(2–3):335-348.

111. Vexler VS, Clement O, Brasch RC. A macromolecular contrast agent for magnetic resonance imaging. Effect of molecular weight on blood pharmacokinetics and enhancement patterns for polylysine-gadopentetate dimeglumine. Invest Radiol. 1994;29 Suppl 2:S62-64.

112. Wen X, Jackson EF, Price RE, Kim EE, Wu Q, Wallace S, Charnsangavej C, Gelovani JG, Li C. Synthesis and characterization of poly(L-glutamic acid) gadolinium chelate: a new biodegradable MRI contrast agent. Bioconjug Chem. 2004;15(6):1408-1415.

113. Zhang G, Zhang R, Melancon MP, Wong K, You J, Huang Q, Bankson J, Liang D, Li C. The degradation and clearance of Poly(N-hydroxypropyl-L-glutamine)-DTPA-Gd as a blood pool MRI contrast agent. Biomaterials. 2012;33(21):5376-5383.

114. Loubeyre P, Canet E, Zhao S, Benderbous S, Amiel M, Revel D. Carboxymethyl-dextran-gadolinium-DTPA as a blood-pool contrast agent for magnetic resonance angiography. Experimental study in rabbits. Invest Radiol. 1996;31(5):288-293.

115. Sirlin CB, Vera DR, Corbeil JA, Caballero MB, Buxton RB, Mattrey RF. Gadolinium-DTPA-dextran: a macromolecular MR blood pool contrast agent. Acad Radiol. 2004;11(12):1361-1369.

116. Aberg M, Hedner U, Bergentz SE. The antithrombotic effect of dextran. Scand J Haematol Suppl. 1979;34:61-68.

117. Wang SC, Wikstrom MG, White DL, Klaveness J, Holtz E, Rongved P, Moseley ME, Brasch RC. Evaluation of Gd-DTPA-labeled dextran as an intravascular MR contrast agent: imaging characteristics in normal rat tissues. Radiology. 1990;175(2):483-488.

118. Bumb A, Brechbiel MW, Choyke P. Macromolecular and dendrimer-based magnetic resonance contrast agents. Acta Radiol. 2010;51(7):751-767.

119. Mehvar R. Dextrans for targeted and sustained delivery of therapeutic and imaging agents. J Control Release. 2000;69(1):1-25.

120. Helbich TH, Gossman A, Mareski PA, Raduchel B, Roberts TP, Shames DM, Muhler M, Turetschek K, Brasch RC. A new polysaccharide macromolecular contrast agent for MR imaging: biodistribution and imaging characteristics. J Magn Reson Imaging. 2000;11(6):694-701.

121. Huang Y, Zhang X, Zhang Q, Dai X, Wu J. Evaluation of diethylenetriaminepentaacetic acid-manganese(II) complexes modified by narrow molecular weight distribution of chitosan oligosaccharides as potential magnetic resonance imaging contrast agents. Magn Reson Imaging. 2011;29(4):554-560.

122. Lebduskova P, Kotek J, Hermann P, Vander Elst L, Muller RN, Lukes I, Peters JA. A gadolinium(III) complex of a carboxylic-phosphorus acid derivative of diethylenetriamine covalently bound to inulin, a potential macromolecular MRI contrast agent. Bioconjug Chem. 2004;15(4):881-889.

123. Ladd DL, Hollister R, Peng X, Wei D, Wu G, Delecki D, Snow RA, Toner JL, Kellar K, Eck J, Desai VC, Raymond G, Kinter LB, Desser TS, Rubin DL. Polymeric gadolinium chelate magnetic resonance imaging contrast agents: design, synthesis, and properties. Bioconjug Chem. 1999;10(3):361-370.

124. Ye F, Ke T, Jeong EK, Wang X, Sun Y, Johnson M, Lu ZR. Noninvasive visualization of in vivo drug delivery of poly(L-glutamic acid) using contrast-enhanced MRI. Mol Pharm. 2006;3(5):507-515.

125. Berthezene Y, Vexler V, Kuwatsuru R, Rosenau W, Muhler A, Clement O, Price DC, Brasch RC. Differentiation of alveolitis and pulmonary fibrosis with a macromolecular MR imaging contrast agent. Radiology. 1992;185(1):97-103.

126. Bogdanov AA, Jr., Weissleder R, Frank HW, Bogdanova AV, Nossif N, Schaffer BK, Tsai E, Papisov MI, Brady TJ. A new macromolecule as a contrast agent for MR angiography: preparation, properties, and animal studies. Radiology. 1993;187(3):701-706.

127. Tomalia DA, Naylor AM, Goddard WA. Starburst Dendrimers: Molecular-Level Control of Size, Shape, Surface Chemistry, Topology, and Flexibility from Atoms to Macroscopic Matter. Angew Chem Int Ed Engl. 1990;29(2):138-175.

128. Kesharwani P, Iyer AK. Recent advances in dendrimer-based nanovectors for tumor-targeted drug and gene delivery. Drug Discov Today. 2015;20(5):536-547.

129. Longmire MR, Ogawa M, Choyke PL, Kobayashi H. Dendrimers as high relaxivity MR contrast agents. Wiley Interdiscip Rev Nanomed Nanobiotechnol. 2014;6(2):155-162.

130. Bryant LH, Jr., Brechbiel MW, Wu C, Bulte JW, Herynek V, Frank JA. Synthesis and relaxometry of high-generation (G = 5, 7, 9, and 10) PAMAM dendrimer-DOTA-gadolinium chelates. J Magn Reson Imaging. 1999;9(2):348-352.

131. Kobayashi H, Kawamoto S, Jo SK, Bryant HL, Jr., Brechbiel MW, Star RA. Macromolecular MRI contrast agents with small dendrimers: pharmacokinetic differences between sizes and cores. Bioconjug Chem. 2003;14(2):388-394.

132. Kobayashi H, Sato N, Kawamoto S, Saga T, Hiraga A, Haque TL, Ishimori T, Konishi J, Togashi K, Brechbiel MW. Comparison of the macromolecular MR contrast agents with ethylenediamine-core versus ammonia-core generation-6 polyamidoamine dendrimer. Bioconjug Chem. 2001;12(1):100-107.

133. Caruthers SD, Winter PM, Wickline SA, Lanza GM. Targeted magnetic resonance imaging contrast agents. Methods Mol Med. 2006;124:387-400.

134. Swanson SD, Kukowska-Latallo JF, Patri AK, Chen C, Ge S, Cao Z, Kotlyar A, East AT, Baker JR. Targeted gadolinium-loaded dendrimer nanoparticles for tumor-specific magnetic resonance contrast enhancement. Int J Nanomedicine. 2008;3(2):201-210.

135. Konda SD, Aref M, Wang S, Brechbiel M, Wiener EC. Specific targeting of folate-dendrimer MRI contrast agents to the high affinity folate receptor expressed in ovarian tumor xenografts. MAGMA. 2001;12(2-3):104-113.

136. Cheng Z, Thorek DL, Tsourkas A. Gadolinium-conjugated dendrimer

nanoclusters as a tumor-targeted T1 magnetic resonance imaging contrast agent. Angew Chem Int Ed Engl. 2010;49(2):346-350.

137. Bozzuto G, Molinari A. Liposomes as nanomedical devices. Int J Nanomedicine. 2015;10:975-999.

138. Fossheim SL, Fahlvik AK, Klaveness J, Muller RN. Paramagnetic liposomes as MRI contrast agents: influence of liposomal physicochemical properties on the in vitro relaxivity. Magn Reson Imaging. 1999;17(1):83-89.

139. Kabalka GW, Buonocore E, Hubner K, Davis M, Huang L. Gadolinium-labeled liposomes containing paramagnetic amphipathic agents: targeted MRI contrast agents for the liver. Magn Reson Med. 1988;8(1):89-95.

140. Tilcock C, Unger E, Cullis P, MacDougall P. Liposomal Gd-DTPA: preparation and characterization of relaxivity. Radiology. 1989;171(1):77-80.

141. Tilcock C, MacDougall P, Unger E, Cardenas D, Fajardo L. The effect of lipid composition on the relaxivity of Gd-DTPA entrapped in lipid vesicles of defined size. Biochim Biophys Acta. 1990;1022(2):181-186.

142. Mody VV, Nounou MI, Bikram M. Novel nanomedicine-based MRI contrast agents for gynecological malignancies. Adv Drug Deliv Rev. 2009;61(10):795-807.

143. Discher BM, Won YY, Ege DS, Lee JC, Bates FS, Discher DE, Hammer DA. Polymersomes: tough vesicles made from diblock copolymers. Science. 1999;284(5417):1143-1146.

144. Katz JS, Zhong S, Ricart BG, Pochan DJ, Hammer DA, Burdick JA. Modular synthesis of biodegradable diblock copolymers for designing functional polymersomes. J Am Chem Soc. 2010;132(11):3654-3655.

145. Cheng Z, Thorek DL, Tsourkas A. Porous polymersomes with encapsulated Gd-labeled dendrimers as highly efficient MRI contrast agents. Adv Funct Mater. 2009;19(23):3753-3759.

146. Cheng Z, Tsourkas A. Paramagnetic porous polymersomes. Langmuir. 2008;24(15):8169-8173.

147. Glogard C, Hovland R, Fossheim SL, Aasen AJ, Klaveness J. Synthesis and physicochemical characterisation of new amphiphilic gadolinium DO3A complexes as contrast agents for MRI. J Chem Soc, Perkin Trans 2. 2000(5):1047-1052.

148. Kielar F, Tei L, Terreno E, Botta M. Large relaxivity enhancement of

paramagnetic lipid nanoparticles by restricting the local motions of the Gd(III) chelates. J Am Chem Soc. 2010;132(23):7836-7837.

149. Tei L, Gugliotta G, Baranyai Z, Botta M. A new bifunctional Gd(III) complex of enhanced efficacy for MR-molecular imaging applications. Dalton Trans. 2009(44):9712-9714.

150. Torres S, Martins JA, Andre JP, Geraldes CF, Merbach AE, Toth E. Supramolecular assembly of an amphiphilic Gd(III) chelate: tuning the reorientational correlation time and the water exchange rate. Chemistry. 2006;12(3):940-948.

151. Turner JL, Pan D, Plummer R, Chen Z, Whittaker AK, Wooley KL. Synthesis of gadolinium-labeled shell-crosslinked nanoparticles for magnetic resonance imaging applications. Adv Funct Mater. 2005;15(8):1248-1254.

152. Winter PM. Perfluorocarbon nanoparticles: evolution of a multimodality and multifunctional imaging agent. Scientifica (Cairo). 2014;2014:746574.

153. Flacke S, Fischer S, Scott MJ, Fuhrhop RJ, Allen JS, McLean M, Winter P, Sicard GA, Gaffney PJ, Wickline SA, Lanza GM. Novel MRI contrast agent for molecular imaging of fibrin: implications for detecting vulnerable plaques. Circulation. 2001;104(11):1280-1285.

154. Winter PM, Caruthers SD, Yu X, Song SK, Chen J, Miller B, Bulte JW, Robertson JD, Gaffney PJ, Wickline SA, Lanza GM. Improved molecular imaging contrast agent for detection of human thrombus. Magn Reson Med. 2003;50(2):411-416.

155. Cyrus T, Abendschein DR, Caruthers SD, Harris TD, Glattauer V, Werkmeister JA, Ramshaw JA, Wickline SA, Lanza GM. MR three-dimensional molecular imaging of intramural biomarkers with targeted nanoparticles. J Cardiovasc Magn Reson. 2006;8(3):535-541.

156. Lanza GM, Winter PM, Caruthers SD, Hughes MS, Hu G, Schmieder AH, Wickline SA. Theragnostics for tumor and plaque angiogenesis with perfluorocarbon nanoemulsions. Angiogenesis. 2010;13(2):189-202.

157. Schmieder AH, Winter PM, Caruthers SD, Harris TD, Williams TA, Allen JS, Lacy EK, Zhang H, Scott MJ, Hu G, Robertson JD, Wickline SA, Lanza GM. Molecular MR imaging of melanoma angiogenesis with alphanubeta3-targeted paramagnetic nanoparticles. Magn Reson Med. 2005;53(3):621-627.

158. Winter P, Athey P, Kiefer G, Gulyas G, Frank K, Fuhrhop R, Robertson D, Wickline S, Lanza G. Improved paramagnetic chelate for molecular imaging with MRI. J Magn Magn Mater. 2005;293(1):540-545.

159. Huang CH, Tsourkas A. Gd-based macromolecules and nanoparticles as magnetic resonance contrast agents for molecular imaging. Curr Top Med Chem. 2013;13(4):411-421.

160. Deal KA, Motekaitis RJ, Martell AE, Welch MJ. Evaluation of the stability and animal biodistribution of gadolinium (III) benzylamine-derivatized diethylenetriaminepentaacetic acid. J Med Chem. 1996;39(16):3096-3106.

161. Ke T, Feng Y, Guo J, Parker DL, Lu ZR. Biodegradable cystamine spacer facilitates the clearance of Gd(III) chelates in poly(glutamic acid) Gd-DO3A conjugates for contrast-enhanced MR imaging. Magn Reson Imaging. 2006;24(7):931-940.

162. Lu ZR, Mohs AM, Zong Y, Feng Y. Polydisulfide Gd(III) chelates as biodegradable macromolecular magnetic resonance imaging contrast agents. Int J Nanomedicine. 2006;1(1):31-40.

163. Lu ZR, Parker DL, Goodrich KC, Wang X, Dalle JG, Buswell HR. Extracellular biodegradable macromolecular gadolinium(III) complexes for MRI. Magn Reson Med. 2004;51(1):27-34.

164. Lu ZR, Ye F, Vaidya A. Polymer platforms for drug delivery and biomedical imaging. J Control Release. 2007;122(3):269-277.

165. Lu ZR, Wang X, Parker DL, Goodrich KC, Buswell HR. Poly(l-glutamic acid) Gd(III)-DOTA conjugate with a degradable spacer for magnetic resonance imaging. Bioconjug Chem. 2003;14(4):715-719.

166. Zong Y, Guo J, Ke T, Mohs AM, Parker DL, Lu ZR. Effect of size and charge on pharmacokinetics and in vivo MRI contrast enhancement of biodegradable polydisulfide Gd(III) complexes. J Control Release. 2006;112(3):350-356.

167. Zong Y, Wang X, Jeong EK, Parker DL, Lu ZR. Structural effect on degradability and in vivo contrast enhancement of polydisulfide Gd(III) complexes as biodegradable macromolecular MRI contrast agents. Magn Reson Imaging. 2009;27(4):503-511.

168. Wang X, Feng Y, Ke T, Schabel M, Lu ZR. Pharmacokinetics and tissue retention of (Gd-DTPA)-cystamine copolymers, a biodegradable macromolecular magnetic resonance imaging contrast agent. Pharm Res. 2005;22(4):596-602.

169. Caravan P. Strategies for increasing the sensitivity of gadolinium based MRI contrast agents. Chem Soc Rev. 2006;35(6):512-523.

170. Zong Y, Wang X, Goodrich KC, Mohs AM, Parker DL, Lu ZR. Contrast-enhanced MRI with new biodegradable macromolecular Gd(III) complexes in

tumor-bearing mice. Magn Reson Med. 2005;53(4):835-842.

171. Feng Y, Zong Y, Ke T, Jeong EK, Parker DL, Lu ZR. Pharmacokinetics, biodistribution and contrast enhanced MR blood pool imaging of Gd-DTPA cystine copolymers and Gd-DTPA cystine diethyl ester copolymers in a rat model. Pharm Res. 2006;23(8):1736-1742.

172. Lu ZR, Wu X. Polydisulfide based biodegradable macromolecular magnetic resonance imaging contrast agents. Isr J Chem. 2010;50(2):220-232.

173. Wu X, Zong Y, Ye Z, Lu ZR. Stability and biodistribution of a biodegradable macromolecular MRI contrast agent Gd-DTPA cystamine copolymers (GDCC) in rats. Pharm Res. 2010;27(7):1390-1397.

174. Wu X, Jeong EK, Emerson L, Hoffman J, Parker DL, Lu ZR. Noninvasive evaluation of antiangiogenic effect in a mouse tumor model by DCE-MRI with Gd-DTPA cystamine copolymers. Mol Pharm. 2010;7(1):41-48.

175. Lee JH, Koretsky AP. Manganese enhanced magnetic resonance imaging. Curr Pharm Biotechnol. 2004;5(6):529-537.

176. Silva AC, Lee JH, Aoki I, Koretsky AP. Manganese-enhanced magnetic resonance imaging (MEMRI): methodological and practical considerations. NMR Biomed. 2004;17(8):532-543.

CHAPTER 2

POLYDISULFIDE MANGANESE(II) COMPLEXES AS NON-GADOLINIUM BIODEGRADABLE MACROMOLECULAR MRI CONTRAST AGENTS

Introduction

Magnetic resonance imaging is a clinical diagnostic imaging modality advantageous in providing images of soft tissues in high resolution with no ionizing radiation. Paramagnetic chelates and ferromagnetic nanoparticles are developed as MRI contrast agents to effectively improve tissue contrast by altering the relaxation rates of water protons in the tissue of interest. Currently, the most commonly used clinical contrast agents are stable Gd(III) chelates, including Gd-DTPA (Magnevist®), Gd-DOTA (Dotaram®), Gd(DTPA-BMA) (Omniscan®), Gd(DOTA-HP) (ProHance®) and Gd(BOPTA) (MultiHance®) (1, 2). Recently, the Gd(III)-based contrast agents have been found in association with nephrogenic systemic fibrosis (NSF), a severe disease affecting a small percentage of the patients with kidney deficiency who had a history of the exposure to Gd(III)-based contrast agents (2-4). Although the cause for NSF is still unclear, the design and development of effective non-gadolinium contrast agents with lower toxicity may alleviate the safety concerns over MRI contrast agents.

Paramagnetic manganese(II) chelates or compounds are an alternative class of MRI contrast agents. As an endogenous metal, the manganese based contrast agents exhibit unique biodistribution pattern and effective contrast enhancement in the myocardium, liver and brain (5, 6). Currently, two manganese based contrast agents, an oral formulation of $MnCl_2$ (Lumanhance) and an intravenous formulation of MnDPDP (Mangafordipir triosodium), are available for clinical application (5). The main limitation of manganese based contrast agents is their relatively low relaxivities. Because of this, an increased dose is often needed to generate sufficient contrast enhancement. However, a high dose of manganese based contrast agents may lead to unexpected toxic side effects. Chemical modifications of manganese based contrast agents may result in more effective non-gadolinium contrast agents by improving their relaxivities and optimizing their pharmacokinetics and biodistribution (7-11).

Recently, we have designed and developed polydisulfide Gd(III) chelates as biodegradable macromolecular MRI contrast agents (12-14) to address the safety issue associated with long accumulation of macromolecular contrast agents. The polydisulfide Gd(III) chelates have shown increased relaxivity, prolonged circulation and preferential tumor accumulation as compared to small molecular Gd(III) chelates (15). These biodegradable macromolecular contrast agents were degraded into oligomeric Gd(III) chelates, which can be rapidly excreted via renal filtration after imaging (16). Incorporation of Mn(II) into polydisulfides may result in effective manganese-based contrast agents with improved contrast enhancement at a relatively low dose. In this study, two polydisulfide Mn(II) complexes were synthesized and evaluated as nongadolinium biodegradable macromolecular MRI contrast agents. In vivo contrast

enhancement of the agents were evaluated in female nu/nu athymic mice bearing MDA-MB-231 breast cancer xenografts.

Experimental Section

Synthesis of Contrast Agents

The biodegradable macromolecular contrast agents, Mn-DTPA cystamine copolymers (MDCC) and Mn-EDTA cystamine copolymers (MECC), were synthesized by complexing Mn(II) with its polymeric ligand DTPA cystamine copolymers (DCC) and EDTA cystamine copolymers (ECC), respectively. The polymeric ligand DTPA cystamine copolymers were prepared by copolymerizing DTPA dianhydride (5.0 mmol, 1.79 g) and cystamine (5.0 mmol, 1.13 g) as previously reported ((12, 14)). The ligand EDTA cystamine copolymers (ECC) were obtained similarly by copolymerizing EDTA dianhydride (5.0 mmol, 1.12g) and cystamine (5.0 mmol, 1.13g). $Mn(OAc)_2$ (1.5 mmol, 0.26 g) was then complexed with DTPA cystamine copolymers (1.0 mmol, 0.51 g) or EDTA cystamine copolymers (1.0 mmol, 0.41 g) in deionized water at room temperature for 2.5 hours. The final product, Mn-DTPA cystamine copolymers and Mn-EDTA cystamine copolymers, were purified by dialysis against de-ionized water using a 10 kDa molecular-weight-cut-off membrane, and then lyophilized. The molecular weight of Mn-DTPA cystamine copolymers was determined by size exclusion chromatography (SEC) on an AKTA FPLC system with a Superose™ 6 column (GE Healthcare Life Sciences). The column was calibrated using water soluble poly[*N*-(2-hydroxylpropyl)-methacrylamide] (HPMA) standards with a series of different molecular weight (M_n = 32, 47, 80 and 148 kDa). The structures of the polymeric ligands, DTPA cystamine copolymers and EDTA cystamine copolymers, were verified using ^{1}H-NMR and FT-IR.

The manganese content in the copolymers was measured by inductively coupled plasma atomic emission spectroscopy (ICP-OES). The yield is approximately 45% for both Mn-DTPA cystamine copolymers and Mn-EDTA cystamine copolymers after purification.

Kinetic Stability

Calcium can replace Mn(II) from manganese complexes *in vivo* due to their structure similarity, causing the release of Mn^{2+}. The kinetic stability of Mn-DTPA cystamine copolymers and Mn-EDTA cystamine copolymers in the presence of Ca^{2+} was investigated *in vitro* by ultrafiltration as recently reported (17). Briefly, Mn-DTPA cystamine copolymers (0.71 mM-Mn) or Mn-EDTA cystamine copolymers (0.71 mM-Mn) were incubated with $CaCl_2$ (2 mM) in aqueous solution at physiological pH under room temperature for 1 hr. The solution was then transferred to the sample reservoir of a centrifugal filter (Amicon Ultra®, 3000 Da molecular weight cut-off), and centrifuged at 4000 rpm and 25 ºC for 20 min. The released Mn^{2+} was filtered through the membrane, and thus separated from the polymer bound Mn(II). The concentration of Mn(II) and Ca(II) in the pre-filtered solutions and the filtrates were determined by ICP-OES. Aqueous solutions of the polymers (0.71 mM-Mn) or $CaCl_2$ (2 mM) were used as controls. The experiments were repeated in triplicate. The degree of transmetallation was calculated as the ratio percentage of the concentration of the released Mn^{2+} in filtrate over the Mn(II) concentration before ultrafiltration.

In Vitro Degradation

The degradation of Mn-DTPA cystamine copolymers and Mn-EDTA cystamine copolymers was evaluated by *in vitro* incubation with cysteine. The polydisulfide Mn(II) complexes (0.71 mM-Mn) were incubated with cysteine (15 μM) in PBS buffer at physiological pH. Samples were collected before and at 15, 30, 60, 120, 360 min and 24 hr during incubation. The molecular weight of the samples were determined using SEC (AKTA FPLC system with a Superose™ 6 column, GE Healthcare Life Sciences). The column was calibrated using water soluble poly[*N*-(2-hydroxylpropyl)methacrylamide] (HPMA) standards with a series of different molecular weight (M_n = 32, 47, 80 and 148 kDa).

Relaxivity Measurement

The T_1 relaxivity of the contrast agents was determined using a Siemens Trio 3T MRI scanner. T_1 relaxation time of the aqueous solution of each contrast agent at different concentrations (0.2, 0.4, 0.6 and 0.8 mM) was measured using a saturation-recovery pulse sequence at room temperature. Data acquisition was completed at a fixed echo time (TE=11 ms) and different repetition times (TR=100, 200, 400, 800, 1600 and 3200 ms). The net magnetization (M) of each sample was measured using the software Osirix (http://www.osirix-viewer.com). T_1 was derived from the nonlinear regression equation $M = M_0(1 - e^{-TR/T_1})$ by fitting with the MATLAB software. Relaxivity was calculated as the slope of the plot of $1/T_1$ versus the concentration of Mn(II). Similarly, the T_2 relaxivity was determined using the Bruker minispec relaxometer (1.5T, 60Hz). The Mn(II) content of each sample was confirmed by ICP-OES after the MR scanning.

Animal Tumor Model

Female athymic nu/nu mice (4-6 weeks old) weighted 18-22 g were purchased from the National Cancer Institute (Frederick, MD). The animals were cared following an approved protocol and the guidelines of the local Institutional Animal Care and Use Committee. The mice were subcutaneously implanted in both flanks with 2×10^6 MDA-MB-231 cells in a mixture of 50 μL culture medium and 50 μL Matrigel. The MRI study was performed when the tumor size reached 0.5-1.0 cm in diameter in 3~4 weeks.

Contrast Enhanced MR Imaging

The contrast enhancement of polydisulfide Mn(II) complexes was investigated in female nu/nu athymic mice with MDA-MB-231 breast cancer xenografts. The mice were anaesthetized by i.p. injection of a mixture of ketamine (80 mg/kg) and xylazine (12 mg/kg). A wrist coil was used for image acquisition. The MR images were acquired on a Siemens Trio 3T MR scanner with a 3D FLASH pulse sequence (TE = 2.74 ms, TR = 7.73 ms, flip angle = 25°, slice thickness = 0.5 mm, 128×256×48 matrix size, 120 mm field of view, 0.39×0.39×0.5 mm^3 spatial resolution, 3 averages) and a 2D spin-echo sequence (TE=8.9 ms, TR=400 ms, flip angle=90°, slice thickness = 2.00 mm, 128×256 matrix size, 120 mm field of view, 0.25×0.25×2 mm^3 spatial resolution, 3 averages). Three tumor bearing mice were used for each contrast agent. The contrast agents were administered to the anesthetized mice at a dose of 0.05 mmol-Mn/kg via tail vein injection. Images were acquired before administration and at 2, 5, 10, 15, 30, 60 minutes post injection. The anesthetized mice were kept warm using a warming pad during and between image acquisitions. Signal intensity of the regions of interest (ROIs) was

obtained using the Osirix software. Contrast to noise ratio (CNR) in the tumor was calculated using the equation $CNR=(S-S_0)/\sigma_n$, where S (post injection) and S_0 (thigh muscle) denote the signal within the ROIs, and σ_n are the standard deviation of random background noise. Statistical analysis was performed using a two-way ANOVA with Bonferroni's, assuming statistical significance at $p < 0.05$.

Results

Synthesis of Polydisulfide Manganese(II) Complexes

The synthesis of Mn-DTPA cystamine copolymers and Mn-EDTA cystamine copolymers is described in Figure 2.1. DTPA cystamine copolymers: ^{1}H-NMR (300 MHz, D_2O, 25°C): 2.60-2.8 (t, 4H), 2.75-3.0 (s, 4H), 3.05-3.10 (t, 4H), 3.10-3.18 (s, 4H), 3.18-3.30 (s, 4H), 3.35-3.45 (t, 4H), 3.55-3.66 (s, 2H); FR-IR: 2720-3800 cm^{-1} (ν_{O-H}), 1480-2000 cm^{-1} ($\nu_{C=O}$), 1200-1480 cm^{-1} (δ_{O-H}, ν_{C-O} and ν_{C-N}). The Mn(II) content in Mn-DTPA cystamine copolymers was 9.84% (w/w). FR-IR: 2640-3600 cm^{-1} (ν_{O-H}), 1480-1760 cm^{-1} ($\nu_{C=O}$), 1200-1480 cm^{-1} (δ_{O-H}, ν_{C-O} and ν_{C-N}). EDTA cystamine copolymers: ^{1}H-NMR (300 MHz, D_2O, 25°C): 2.65-2.8 (t, 4H), 3.0-3.2 (s, 4H), 3.35-3.50 (s, 8H), 3.55-3.70 (s, 4H); FT-IR: 2800-3680 cm^{-1} (ν_{O-H}), 1440-1880 cm^{-1} ($\nu_{C=O}$), 1200-1480 cm^{-1} (δ_{O-H}, ν_{C-O} and ν_{C-N}). The Mn(II) content in Mn-EDTA cystamine copolymers was 10.14% (w/w). FT-IR: 2640-3600 cm^{-1} (ν_{O-H}), 1440-1720 cm^{-1} ($\nu_{C=O}$), 1200-1480 cm^{-1} (δ_{O-H}, ν_{C-O} and ν_{C-N}).The number average molecular weight (M_n) and weight average molecular weight (M_w) were 45.7 kD and 64.3 kD kDa for DTPA cystamine copolymers (polydispersity, PD = 1.4), and 156 and 255.3 kDa (PD = 1.6) for EDTA cystamine copolymers, as determined by SEC. The number average molecular weight and weight

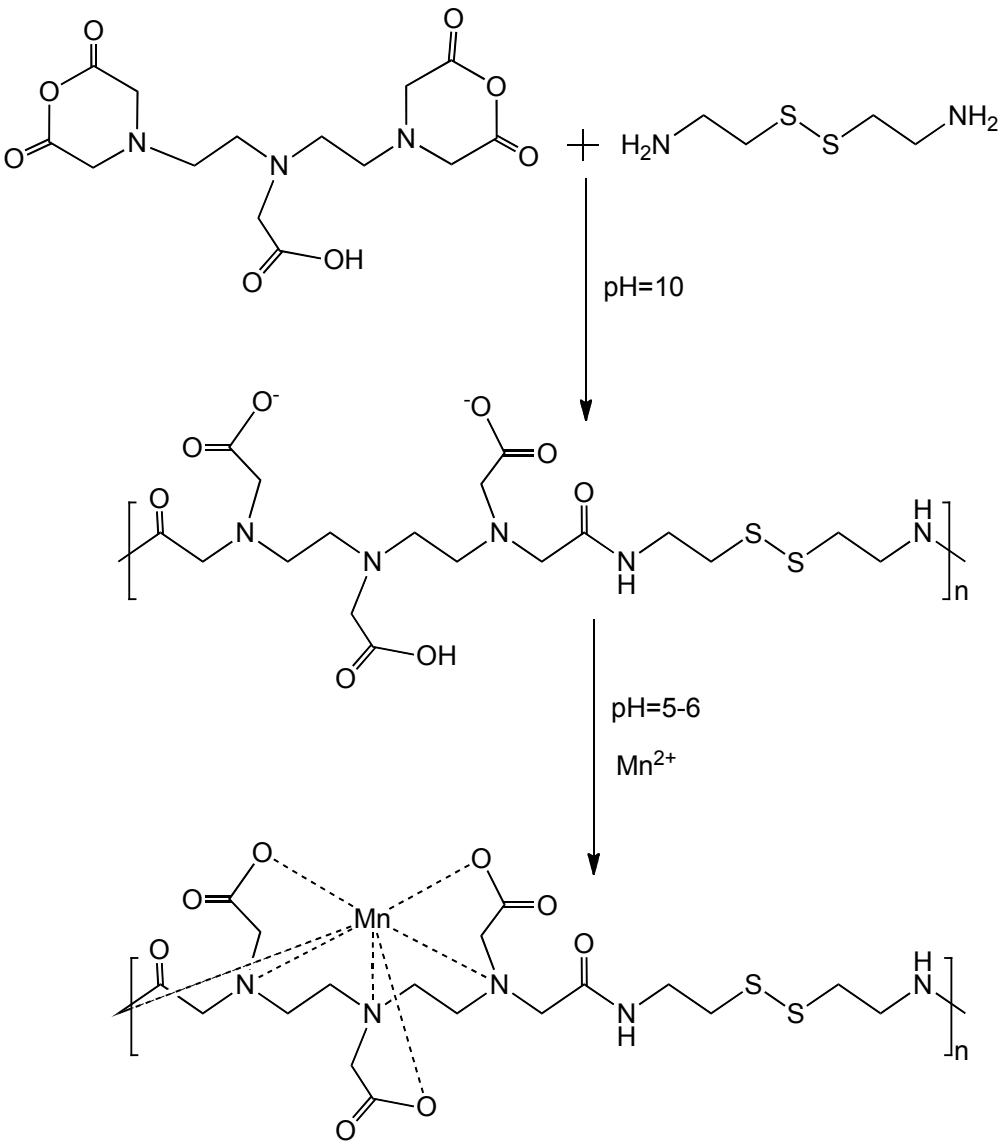

Figure 2.1. Synthesis of Mn-DTPA cystamine copolymers and Mn-EDTA cystamine copolymers.

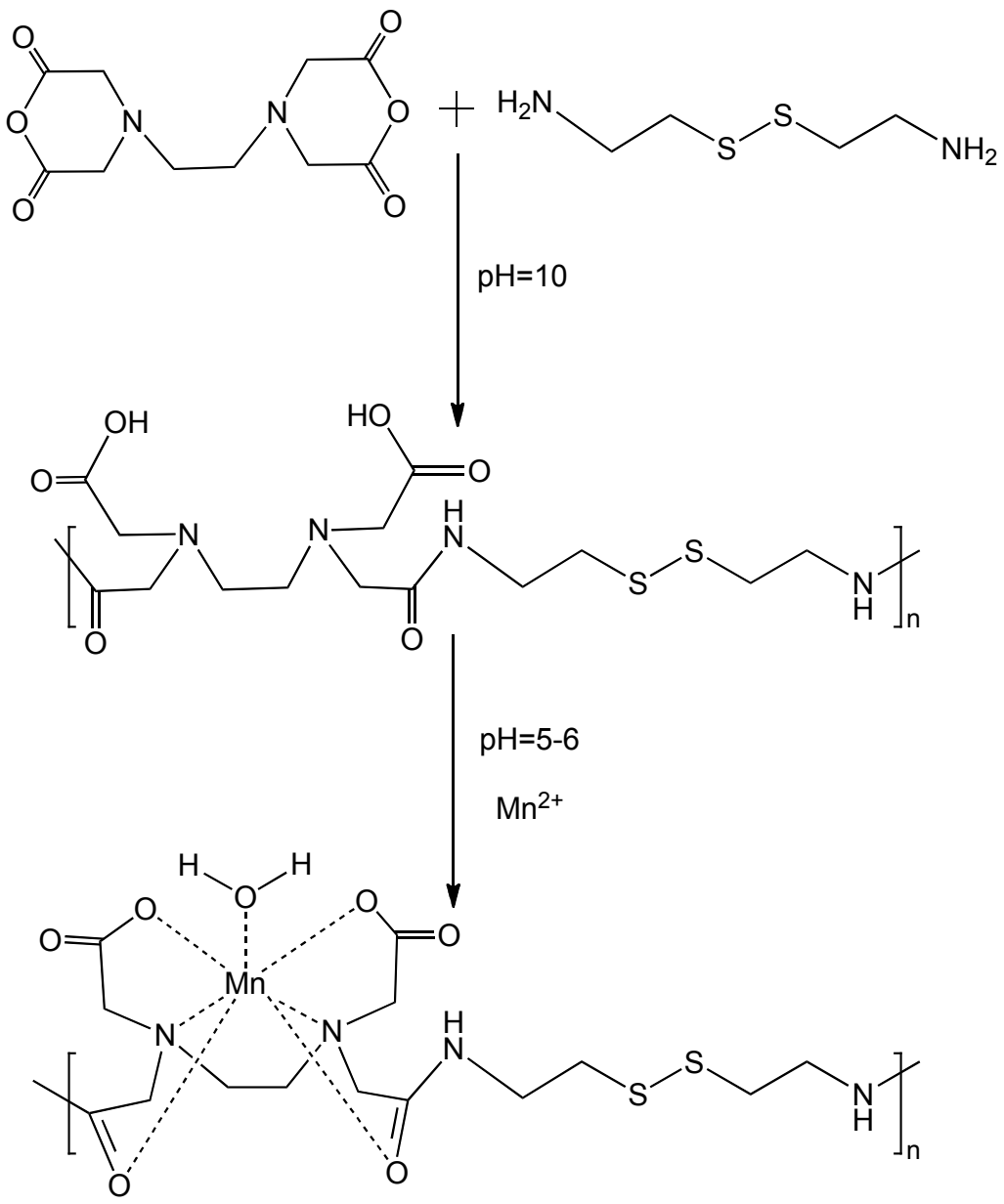

Figure 2.1. Continued.

average molecular weight were 30.50 and 37.35 kDa for Mn-DTPA cystamine copolymers (PD=1.2), and 61.80 and 126.37 kDa (PD = 2.0) for Mn-EDTA cystamine copolymers.

Kinetic Stability

Transmetallation, the replacement of Mn(II) ions in the chelates by endogenous metal ions, is considered as a main cause of in vivo kinetic instability for MR contrast agents based on paramagnetic metal chelates (2,3). Ca(II) ions have the same charge and similar size as Mn(II) ions, and are abundantly present in human plasma. As a result, plasma Ca(II) ions are considered as the main cause of *in vivo* transmetallation of Mn(II) complexes. Ultrafiltration was effective to separate the released and bound Mn(II) species. In the control studies, 88.5±4.6% free Ca^{2+} ions in $CaCl_2$ aqueous solution was filtered through via ultrafiltration, while the bound Mn(II) ions of both polymeric chelates did not filter through the membrane. Only 0.82± 1.1% Mn(II) was measured in the filtrate for Mn-DTPA cystamine copolymers, and 1.03±0.10 % for Mn-EDTA cystamine copolymers. Figure 2.2 shows that in the presence of $CaCl_2$, more Mn(II) (12.2±0.02%) was released from Mn-DTPA cystamine copolymers than that from Mn-EDTA cystamine copolymers (3.36±0.08%). The result indicates that Mn-EDTA cystamine copolymers were kinetically more stable than Mn-DTPA cystamine copolymers against transmetallation with Ca^{2+} ions.

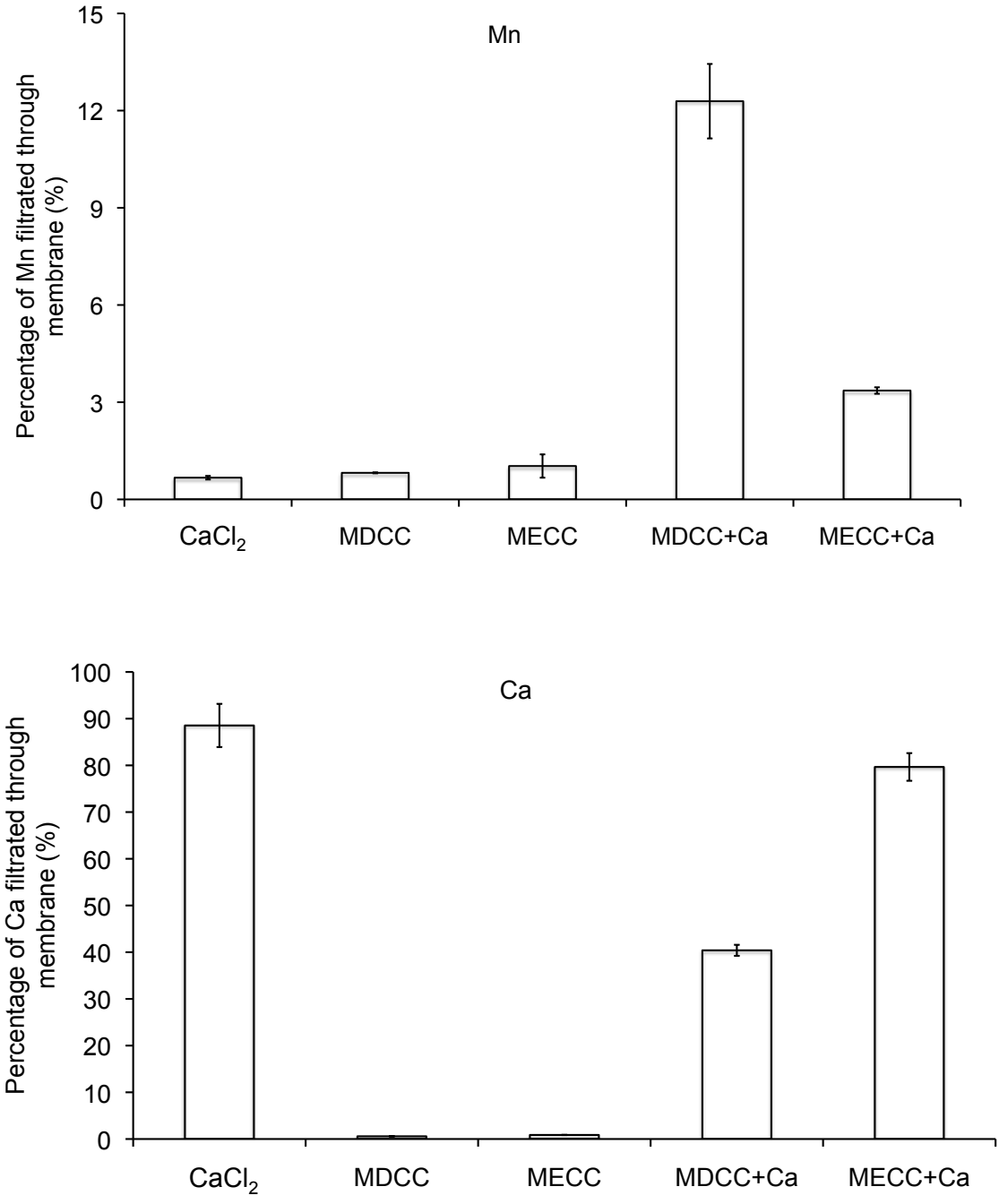

Figure 2.2. Transmetallation of Mn-DTPA cystamine copolymer (MDCC), Mn-EDTA cystamine Copolymer (MECC) with Ca2+.

In Vitro Degradation

The degradation of polydisulfides Mn(II) chelates were verified by *in vitro* incubation studies. The Mn(II) chelates were incubated in 15 μM cysteine aqueous solution (the plasma concentration of free thiols) at physiological pH. Gradual decrease of molecular weight was observed for both Mn-DTPA cystamine copolymers and Mn-EDTA cystamine copolymers, Figure 2.3. It appears that Mn-EDTA cystamine copolymers degraded more rapidly than Mn-DTPA cystamine copolymers. The number average molecular weights (M_n) were 30.50, 29.34, 25.60, 23.57, 21.35, 18.64 and 13.50 kDa for Mn-DTPA cystamine copolymers, and were 61.80, 56.45, 49.75, 45.36, 38.62, 32.64 and 22.57 kDa for Mn-EDTA cystamine copolymers before and at 15, 30, 60, 120, 360 and 24 hours post incubation with cysteine. Mn-DTPA cystamine copolymers were negatively charged and charge repulsion might inhibit the attack of the negatively charged cysteine at physiological pH to the disulfide bonds. In comparison, Mn-EDTA cystamine copolymers were neutral polymers and cysteine could readily react with the disulfide bonds. Consequently the neutral Mn-EDTA cystamine copolymers had a faster degradation rate than Mn-DTPA cystamine copolymers in the presence of cysteine, similar to previously reported polydisulfide Gd(III) complexes (9).

Relaxivity

Figure 2.4 shows the MR images of the aqueous solutions of Mn-DTPA cystamine copolymers, Mn-EDTA cystamine copolymers and $MnCl_2$ at different Mn(II) concentrations acquired using the inversion-recovery sequence at 3T and the plot of $1/T_1$ versus Mn(II) concentration. The signal brightness at the same Mn(II) concentration was

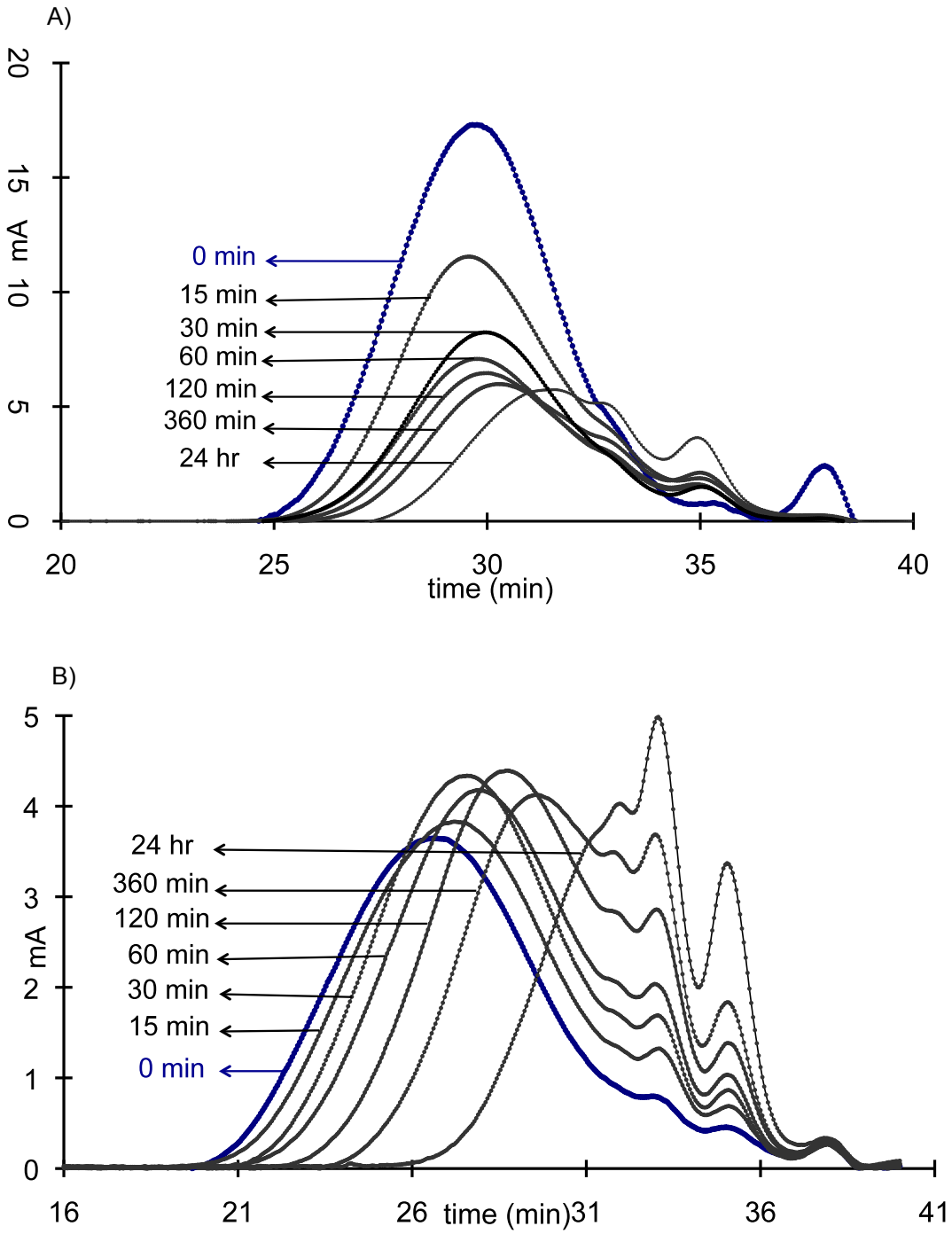

Figure 2.3. The molecular weight distribution before (blue line) and at 15, 30, 60, 120, 360 and 24 hrs post incubation of the Mn-DTPA cystamine copolymer (A) and Mn-EDTA cystamine copolymer (B) against plasma concentration of cysteine (15 μM)

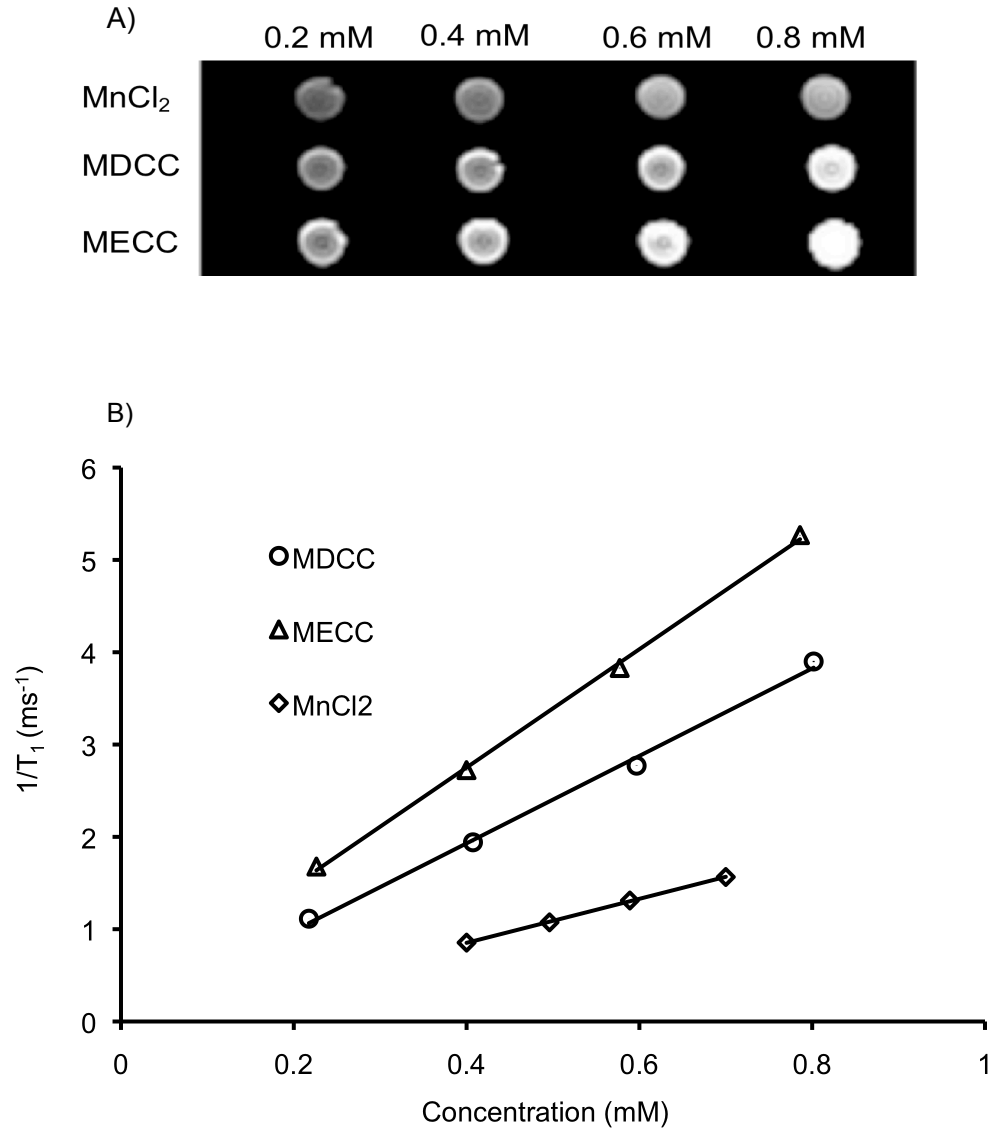

Figure 2.4. (A) MR imaging of aqueous solutions of $MnCl_2$, Mn-DTPA cystamine copolymer (MDCC) and Mn-EDTA cystamine copolymer (MECC) at concentrations of 0.2, 0.4, 0.6 and 0.8 mM. (B) $1/T_1$ versus concentration plot of $MnCl_2$, MDCC and MECC for the calculation of the longitudinal relaxation rate (R_1).

in the order of Mn-EDTA cystamine copolymers > Mn-DTPA cystamine copolymers > $MnCl_2$. The longitudinal relaxivity (r_1) was 2.4, 4.74 and 6.41 $mM^{-1}s^{-1}$ per Mn(II) for $MnCl_2$, Mn-DTPA cystamine copolymers and Mn-EDTA cystamine copolymers, respectively. The r_2 was 10.38 and 9.72 $mM^{-1}s^{-1}$ for Mn-DTPA cystamine copolymer and Mn-EDTA cystamine copolymer.

In Vivo MR Imaging

Figure 2.5 shows the T_1-weighted coronal MR images of mice bearing MDA-MB-231 human breast carcinoma xenografts before and after intravenous injection of $MnCl_2$, Mn-DTPA cystamine copolymers and Mn-EDTA cystamine copolymers. The agents resulted in similar *in vivo* enhancement pattern, where significant enhancement was observed in the liver, blood pool, myocardium and bladder. The strong and prolonged liver enhancement was observed for all three agents. The polydisulfide Mn(II) complexes resulted in significant blood pool enhancement at 2 minutes post injection and the blood signal decreased afterwards. The $MnCl_2$ control resulted in little blood pool enhancement, but significant enhancement in the myocardium during the experiment. Contrast enhancement in the urinary bladder increased for Mn-DTPA cystamine copolymers at 20 minutes post injection and for Mn-EDTA cystamine copolymers at 5 minutes post injection. No signal enhancement was observed in the bladder for $MnCl_2$ during the period of experiment. The results indicate that the polydisulfide Mn(II) complexes are degraded and excreted via renal filtration. EDTA cystamine copolymers excreted more rapidly due to its rapid in vivo degradation even though the agent had a high molecular weight.

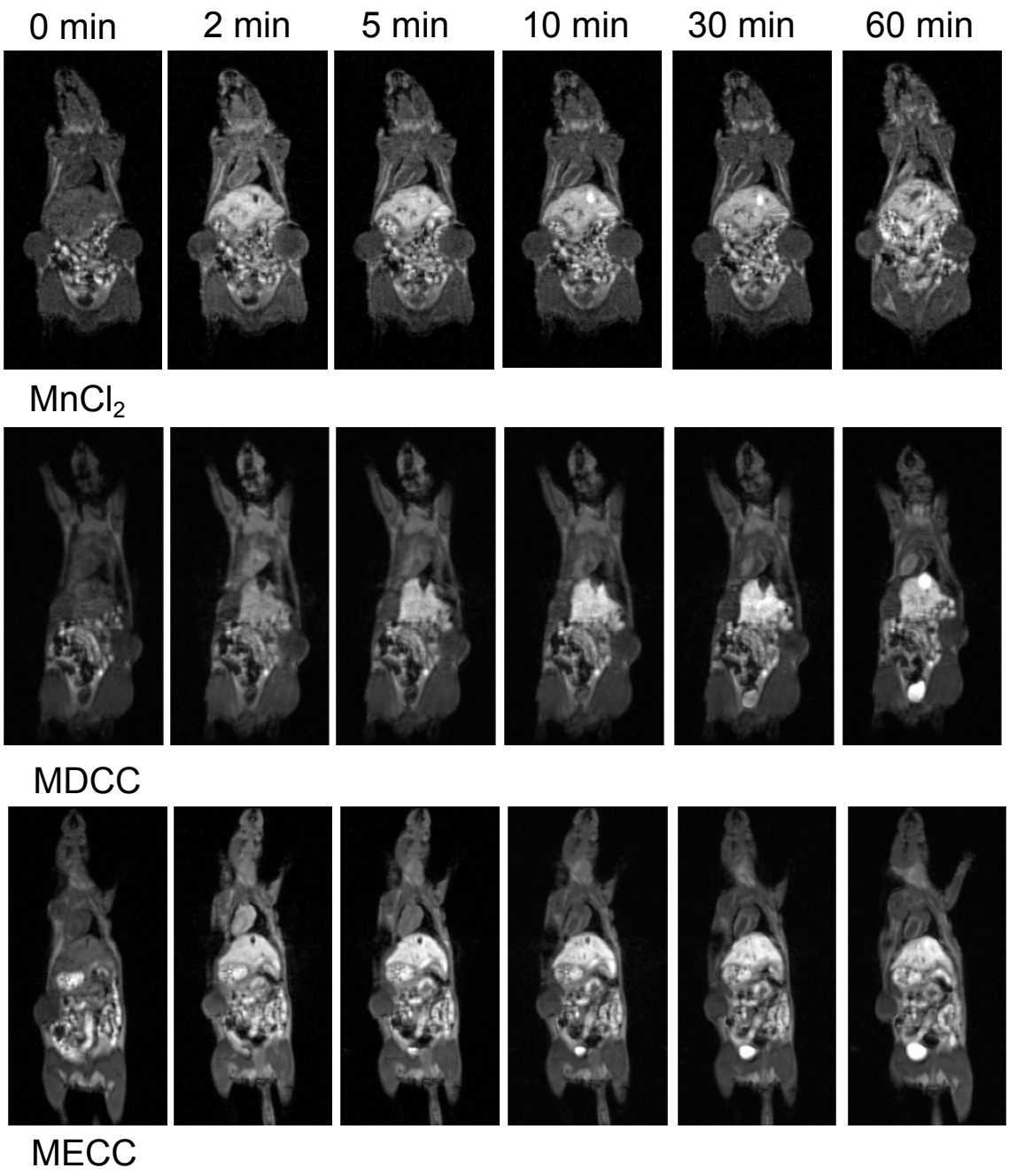

Figure 2.5. 3D coronal images before (0 min) and at 2, 5, 10, 30 and 60 minutes post injection of $MnCl_2$, Mn-DTPA cystamine copolymers (MDCC), and Mn-EDTA cystamine copolymers (MECC) at a dose of 0.05 mmol-Mn(II)/kg.

Figure 2.6 shows the axial T_1-weighted 2D spin-echo MR images of the tumor before and at different time points after injection of the agents. Slight enhancement was observed in the tumor with $MnCl_2$ and Mn-DTPA cystamine copolymers. Mn-EDTA cystamine copolymers resulted in more significant tumor enhancement than Mn-DTPA cystamine copolymers. Quantitative analysis of the contrast-to-noise ratio in the tumor periphery (Figure 2.7) showed that Mn-EDTA cystamine copolymers resulted in more significant tumor enhancement than Mn-DTPA cystamine copolymers and $MnCl_2$ for at least 1 hour.

Discussion

In this study, we aim to develop Mn(II) based biodegradable macromolecular contrast agent as an alternative for Gd(III)-based contrast agents. Two types of

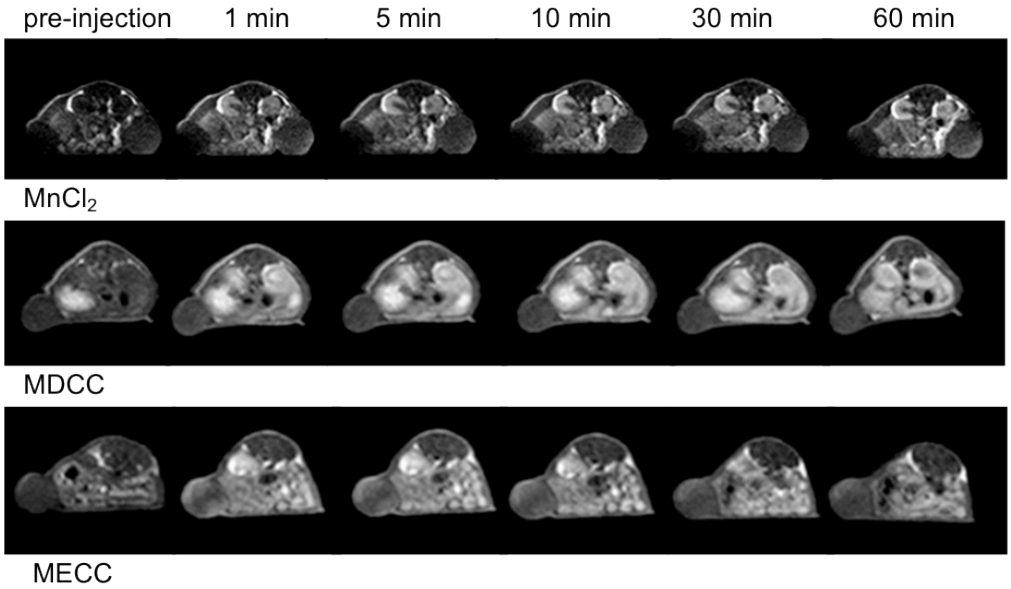

Figure 2.6. 2D spin echo image of the tumor before and 2, 5, 10, 30 and 60 minute after intravenous injection of $MnCl_2$, Mn-DTPA cystamine copolymers (MDCC) and Mn-EDTA cystamine copolymers (MECC) at a dose of 0.05 mmol-Mn/kg.

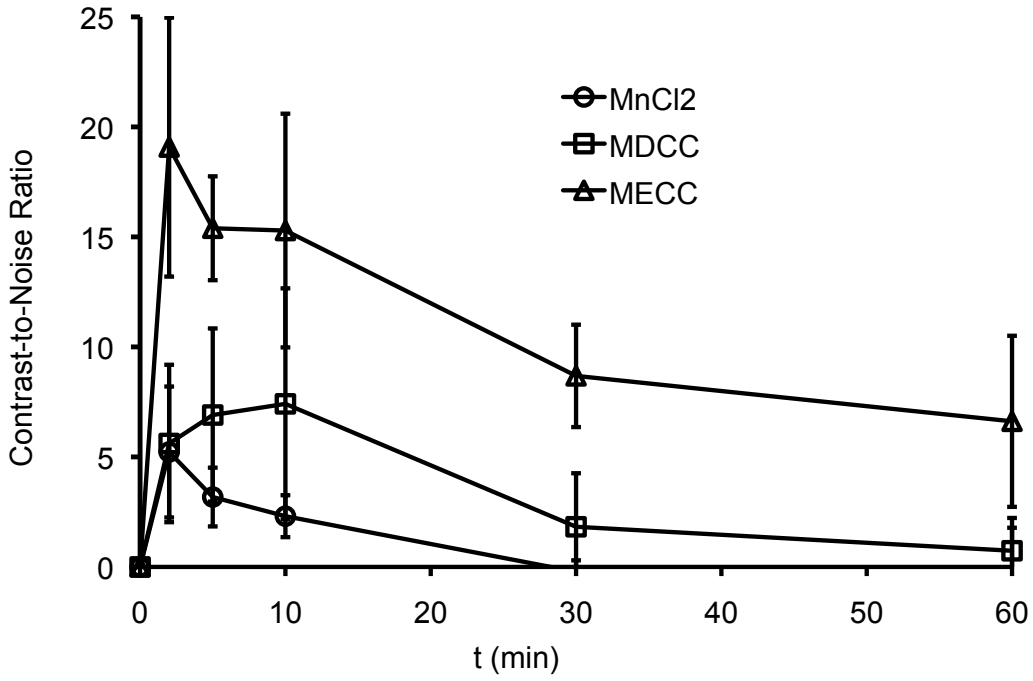

Figure 2.7. Contrast-to-Noise Ratio (CNR) of tumor periphery before and at 2, 5, 10, 20, 30 and 60 minutes post tail vein injection of $MnCl_2$ (circle), Mn-DTPA cystamine copolymers (square), Mn-EDTA cystamine copolymers (triangle) at a dose of 0.05 mmol-Mn/kg.

polydisulfide Mn(II) complexes, Mn-DTPA cystamine copolymer and Mn-EDTAcystamine copolymer, were synthesized and evaluated. The polymeric ligands were synthesized based on reported protocol, followed by Mn(II) complexation. After chelation, both polydisufide Mn(II)-DTPA and Mn(II)-EDTA showed decreased molecular weight and change in IR spectrum. The hydrodynamic volume of Mn(II) complexes appeared smaller because the polymer became nonionic after chelation. From the IR spectrum, red shift was observed with vibration peak of C=O (from 1480-2000 to 1480-1760 for DTPA based Mn(II) chelates, and 1440-1880 to 1440-1720 for EDTA based Mn(II) chelates). In addition, significant bond weakening of the vibration of C-O

and C-N (1200-1480) were observed for both Mn(II)-EDTA cystamine copolymer and Mn(II)-DTPA cystamine copolymer, indicating the contribution of the carbonyl oxygen, carboxylic oxygen and tertiary nitrogen for Mn(II) complexation.

The polydisulfide Mn(II) complexes, Mn-DTPA cystamine copolymers and Mn-EDTA cystamine copolymers, have shown some interesting features as compared to $MnCl_2$ as MRI contrast agents. The T_1 relaxivity of the polydisulfide Mn(II) complexes was increased as compared to that of $MnCl_2$ due to the increase of molecular size. The macromolecular agents had large size and hydrodynamic volume, which significantly prolonged their rotational tumbling time, resulting in relaxivity increase. Although free Mn^{2+} might have more water molecules in the inner coordination sphere, the results in this study imply that the structure and size of the agents had a stronger impact on the relaxivity of the contrast agents than a large number of water molecules in the inner sphere (18). Recent studies have shown that the water exchange rate of manganese complexes was significantly faster than that of the gadolinium chelates, compensating the lower intrinsic paramagnetism of manganese (19). Consequently, the r_1 relaxivity of the polydisulfide Mn(II) complexes was comparable to that of polydisulfide gadolinium(III) complexes, Gd-DTPA cystamine copolymers (GDCC) at 3T (20).

Mn-EDTA cystamine copolymers (6.41 $mM^{-1}s^{-1}$) had higher r_1 relaxivity than Mn-DTPA cystamine copolymers (4.74 $mM^{-1}s^{-1}$). Although the former had higher molecular weight, the size of polydisulfides might not be the main cause of difference in relaxivity of the agents based on our previous observation on the polydisulfide Gd(III) complexes (15, 21). The high relaxivity of Mn-EDTA cystamine copolymers might be attributed to the low coordination number of EDTA bisamides in the copolymers, which

might result in more rapid water exchange of the chelates. The chelating groups are 6 and 8 for the EDTA bisamide and DTPA bisamide in the polydisulfides, respectively. The coordination number of Mn(II) ions was up to 7 (22, 23), larger than the number of chelating groups in EDTA bisamide. One coordination site from Mn(II) was available for water complexation in Mn-EDTA cystamine copolymers, while there was no free coordination site from the Mn(II) complex in Mn-DTPA cystamine copolymers. The availability of inner sphere water binding could be the main reason for higher relaxivity of Mn-EDTA cystamine copolymers. Similar relaxivity difference between Mn-DTPA based chelates and Mn-EDTA based chelates were also observed in other Mn(II) based contrast agents (7, 24)

In comparison with Gd(III) chelates (log $K_{Gd\text{-}DTPA}$=17.35, log $K_{Gd\text{-}DOTA}$=22.46), Mn(II) chelates (log $K_{Mn\text{-}EDTA}$=13.9, log $K_{Mn\text{-}DTPA}$=15.2) are less stable, generating more concerns on transmetallation and *in vivo* metal release. Ca^{2+} is structurally similar to Mn^{2+}, and is viewed as the major cause of *in vivo* transmetallation for Mn(II) chelates (25, 26). Although the thermodynamic stability of Mn-DTPA chelates (log $K_{Mn\text{-}DTPA}$= 13.5) are one to two magnitude higher than the Mn-EDTA chelates (log $K_{Mn\text{-}EDTA}$=14.31-15.6), our kinetic stability study showed that Mn(II)-EDTA cystamine copolymers were more stable against Ca^{2+} transmetallation than Mn(II)-DTPA cystamine copolymers. After 1 hr incubation with Ca^{2+} under plasma concentration, less Mn^{2+} was released from Mn(II)-EDTA cystamine copolymers (3.36±0.08 %) than that from the Mn(II)-DTPA cystamine copolymers (12.2±0.02 %). The kinetic stability of metal chelates is generally affected by complicated factors. In our case, the higher kinetic lability of Mn(II)-DTPA based polydisulfide may be attributed to its more extended conformation in solution due

to the negative charges on the polymer, exposing higher extent of the chelates to the surrounded Zn^{2+} in solution (28). In addition, the negative charges on the subunits of MDCC can also facilitate the approach of Zn^{2+} to the chelates through ionic interactions. In comparison, MECC is a neutral polymer with a more compacted conformation, which can create additional steric hindrance against Zn^{2+} transmetallation in solution. The difference of kinetic stability against Zn(II) transmetallation between MDCC and MECC might not be as significant in vivo as that from in vitro experiments, since plasma Zn(II) is often presented in a protein-bound form instead of free ions in vivo.

The degradability of MDCC and MECC were confirmed via in vitro incubation study using plasma thiol concentration of cysteine, an endogenous free thiol. During the incubation, no nitrogen protection was used to eliminate the impact of air on the oxidation of cysteine, which will gradually lose its reduction capacity through formation of the disulfide derivative of cystine during the incubation. As a result, more efficient degradation may be expected in vivo where plasma concentration of free thiols is in a more steady range.

Polydisulfide Mn(II) complexes resulted in less contrast enhancement in the blood pool as compared to polydisulfide Gd(III) complexes reported in our previous studies (12). Significant blood pool enhancement was observed in the first two minutes for the manganese based agents and then quickly disappeared, even for Mn-EDTA cystamine copolymers of high molecular weight. In contrast, Gd-DTPA cystamine copolymers with similar r_1 relaxivity and molecular weight resulted in more prolonged blood pool contrast enhancement (12). Polydisulfide Mn(II) complexes also resulted in strong and prolonged contrast enhancement in the liver, while Gd-DTPA cystamine copolymers had much less

contrast enhancement in the liver. Strong liver enhancement of polydisulfide Mn(II) complexes indicated liver affinity and high liver accumulation of the agents. The liver accumulation of Mn(II) based contrast agent may be attributed to favorable hepatic uptake of Mn(II). High and rapid liver accumulation of the agents could significantly reduce their concentration in the blood, consequently low blood pool enhancement.

Mn-EDTA cystamine copolymers resulted in more prominent tumor enhancement than $MnCl_2$ and Mn-DTPA cystamine copolymers in T_1 weighted 2D spin-echo MR images. However, the polydisulfide Mn(II) chelates generated less tumor enhancement than polydisulfide Gd(III) complexes (15, 21). This could be attributed to the relatively low stability and high liver accumulation of the Mn(II) complexes. Between the tested Mn(II) based agents, Mn-EDTA cystamine copolymers had larger molecular weight, higher relaxivity and stability against transmetallation with Ca^{2+}, and resulted in more significant tumor contrast enhancement. The polydisulfide Mn(II) complexes also facilitated the excretion of the agents via renal filtration, as evidenced by strong bladder enhancement at 60 minutes after the injection, while little $MnCl_2$ was excreted via renal filtration.

The design and development of Mn(II) based MRI contrast agents have recently attracted a significant amount of attention because of the better safety profiles of residual Mn(II) ions (34, 35). We have shown in this study that polydisulfide Mn(II) complexes had better relaxivity, pharmacokinetics, clearance and in vivo enhancement than $MnCl_2$. In comparison to some recently reported dendritic agents and colloidal systems (7, 9, 10), our polydisufide based Mn(II) contrast agents, especially MECC, showed relatively higher relaxivity possibly due to the relatively large hydrodynamic volume of the

polydisulfides and the existence of inner sphere water binding site of the Mn-EDTA chelate. However, the main limitation of currently available Mn(II) complexes is their low complexation stability, including both thermodynamic and kinetic stabilities. Further studies are needed to design new Mn(II) chelates with high thermodynamic and kinetic stability in order to develop novel Mn(II) based contrast agents and to expand their application in MR imaging of other tissues and organs. The magnetic properties of Mn(II) based agents are also different from that of Gd(III)-based contrast agents. Mn(II) complexes often have much higher T_2 relaxivity, which can significantly reduce the signal in T_1-weighted imaging. This could be overcome by designing better imaging sequence to reduce T_2 effect in T1-weighted MRI in the future studies.

Conclusion

In conclusion, two polydisulfide Mn(II) complexes were synthesized as gadolinium free biodegradable macromolecular MRI contrast agents. The macromolecular Mn(II) complexes readily degraded in the presence of endogenous free thiols. Both polydisulfide Mn(II) complexes had similar r_1 relaxivity as polydisulfide Gd(III) complexes, higher than that of $MnCl_2$. Mn-EDTA cystamine copolymers showed higher kinetic stability than Mn-DTPA cystamine copolymers against transmetallation with Ca^{2+} ions. Similar to other reported Mn(II) chelates, polydisulfide Mn(II) complexes resulted in prominent contrast enhancement in the liver and myocardium. Macromolecular Mn(II) complexes have a potential to be developed as effective contrast agents for MR imaging.

References

1. Caravan P, Ellison JJ, McMurry TJ, Lauffer RB. Gadolinium(III) chelates as MRI contrast agents: structure, dynamics, and applications. Chem Rev. 1999;99(9):2293-2352.

2. Aime S, Caravan P. Biodistribution of gadolinium-based contrast agents, including gadolinium deposition. J Magn Reson Imaging. 2009;30(6):1259-1267.

3. Kribben A, Witzke O, Hillen U, Barkhausen J, Daul AE, Erbel R. Nephrogenic systemic fibrosis: pathogenesis, diagnosis, and therapy. J Am Coll Cardiol. 2009;53(18):1621-1628.

4. Kuo PH. Gadolinium-containing MRI contrast agents: important variations on a theme for NSF. J Am Coll Radiol. 2008;5(1):29-35.

5. Lee JH, Koretsky AP. Manganese enhanced magnetic resonance imaging. Curr Pharm Biotechnol. 2004;5(6):529-537.

6. Silva AC, Lee JH, Aoki I, Koretsky AP. Manganese-enhanced magnetic resonance imaging (MEMRI): methodological and practical considerations. NMR Biomed. 2004;17(8):532-543.

7. Bertin A, Steibel J, Michou-Gallani AI, Gallani JL, Felder-Flesch D. Development of a dendritic manganese-enhanced magnetic resonance imaging (MEMRI) contrast agent: synthesis, toxicity (in vitro) and relaxivity (in vitro, in vivo) studies. Bioconjug Chem. 2009;20(4):760-767.

8. Kobayashi H, Brechbiel MW. Dendrimer-based nanosized MRI contrast agents. Curr Pharm Biotechnol. 2004;5(6):539-549.

9. Pan D, Caruthers SD, Hu G, Senpan A, Scott MJ, Gaffney PJ, Wickline SA, Lanza GM. Ligand-directed nanobialys as theranostic agent for drug delivery and manganese-based magnetic resonance imaging of vascular targets. J Am Chem Soc. 2008;130(29):9186-9187.

10. Pan D, Senpan A, Caruthers SD, Williams TA, Scott MJ, Gaffney PJ, Wickline SA, Lanza GM. Sensitive and efficient detection of thrombus with fibrin-specific manganese nanocolloids. Chem Commun (Camb). 2009(22):3234-3236.

11. Tan M, Ye Z, Jeong EK, Wu X, Parker DL, Lu ZR. Synthesis and evaluation of nanoglobular macrocyclic Mn(II) chelate conjugates as non-gadolinium(III) MRI contrast agents. Bioconjug Chem;22(5):931-937.

12. Lu ZR, Mohs AM, Zong Y, Feng Y. Polydisulfide Gd(III) chelates as biodegradable macromolecular magnetic resonance imaging contrast agents. Int J

Nanomedicine. 2006;1(1):31-40.

13. Lu ZR, Wu X. Polydisulfide based biodegradable macromolecular magnetic resonance imaging contrast agents. Isr J Chem;50(2):220-232.

14. Lu ZR, Parker DL, Goodrich KC, Wang X, Dalle JG, Buswell HR. Extracellular biodegradable macromolecular gadolinium(III) complexes for MRI. Magn Reson Med. 2004;51(1):27-34.

15. Zong Y, Guo J, Ke T, Mohs AM, Parker DL, Lu ZR. Effect of size and charge on pharmacokinetics and in vivo MRI contrast enhancement of biodegradable polydisulfide Gd(III) complexes. J Control Release. 2006;112(3):350-356.

16. Feng Y, Zong Y, Ke T, Jeong EK, Parker DL, Lu ZR. Pharmacokinetics, biodistribution and contrast enhanced MR blood pool imaging of Gd-DTPA cystine copolymers and Gd-DTPA cystine diethyl ester copolymers in a rat model. Pharm Res. 2006;23(8):1736-1742.

17. Wu X, Jeong EK, Emerson L, Hoffman J, Parker DL, Lu ZR. Noninvasive evaluation of antiangiogenic effect in a mouse tumor model by DCE-MRI with Gd-DTPA cystamine copolymers. Mol Pharm. 2010;7(1):41-48.

18. Lauffer RB. Paramagnetic metal complexes as water proton relaxation agents for NMR imaging: theory and design. Chem Rev. 1987;87(5):901-927.

19. Zetter MS, Dodgen HW, Hunt JP. Measurement of the water exchange rate of bound water in the manganese(II)-adenosine triphosphate complex by oxygen-17 nuclear magnetic resonance. Biochemistry. 1973;12(4):778-782.

20. Koenig SH, Brown RD, 3rd. Relaxation of solvent protons by paramagnetic ions and its dependence on magnetic field and chemical environment: implications for NMR imaging. Magn Reson Med. 1984;1(4):478-495.

21. Zong Y, Wang X, Jeong EK, Parker DL, Lu ZR. Structural effect on degradability and in vivo contrast enhancement of polydisulfide Gd(III) complexes as biodegradable macromolecular MRI contrast agents. Magn Reson Imaging. 2009;27(4):503-511.

22. Bianchi A, Calabi L, Giorgi C, Pietro Losi, Palma Mariani, Daniela Palano, Paola Paoli, Rossi P, Valtancoli B. Thermodynamic and structural aspects of manganese(II) complexes with polyaminopolycarboxylic ligands based upon 1,4,7,10-tetraazacyclododecane (cyclen). Crystal structure of dimeric [MnL]2·2CH3OH containing the new ligand 1,4,7,10-tetraazacyclododecane-1,4-diacetate. J Chem Soc Dalton. 2001(6):917-922.

23. Aime S, Anelli L, Botta M, Brocchetta M, Canton S, Fedeli F, Gianolio E,

Terreno E. Relaxometric evaluation of novel manganese(II) complexes for application as contrast agents in magnetic resonance imaging. J Biol Inorg Chem. 2002;7(1-2):58-67.

24. Troughton JS. Synthesis and evaluation of a high relaxivity manganese(II)-based MRI contrast agent. Inorg Chem. 2009;43(20):6313-6323.

25. Pan D, Caruthers SD, Senpan A, Schmieder AH, Wickline SA, Lanza GM. Revisiting an old friend: manganese-based MRI contrast agents. Wiley Interdiscip Rev Nanomed Nanobiotechnol. 2010.

26. Tan M, Wu X, Jeong EK, Chen Q, Parker DL, Lu ZR. An effective targeted nanoglobular manganese(II) chelate conjugate for magnetic resonance molecular imaging of tumor extracellular matrix. Mol Pharm. 2010;7(4):936-943.

CHAPTER 3

SYNTHESIS AND EVALUATION OF A POLYDISULFIDE WITH GD-DOTA MONOAMIDE SIDE CHAINS AS A BIODEGRADABLE MACROMOLECULAR CONTRAST AGENT FOR MR BLOOD POOL IMAGING

Introduction

Magnetic resonance imaging (MRI) is a clinical diagnostic modality without ionization radiation and provides both morphological and functional information (1, 2). In comparison with other clinical imaging modalities, MRI is advantageous in visualizing soft tissues with high spatial resolution. In order to provide more accurate diagnostic imaging, contrast agents are often used to enhance the image contrast between the tissue of interest and its surrounding tissues. Over the past 30 years, various paramagnetic compounds have been investigated as MRI contrast agents (3-6). Among these compounds, stable Gd(III) chelates are most commonly used in clinical practice (7). The small molecular Gd(III)-based clinical agents with short blood half-lives have relatively low relaxivities, rapidly extravasate from vasculature and excrete through renal glomerular filtration (8,9). These drawbacks limit their applications in clinical blood pool MRI, including both MR angiography and cancer imaging (10,11).

Two types of blood pool imaging agents, the small Gd(III) chelates that reversibly bind to plasma proteins such as MS-325 and macromolecular Gd(III) complexes, have been developed to address the limitations of clinical agents (12–16). Although MS-325 is effective for MR angiography, it is not as effective as polymeric Gd(III) chelates for evaluating tumor vascularity (11,17–19). Macromolecular Gd agents, such as polylysine Gd(III) chelate conjugates, polysaccharide Gd(III) chelate conjugates, Gadomer 17, PAMAM dendrimer Gd(III) chelate conjugates (20–23), are generally prepared by conjugating stable Gd(III) chelates to biocompatible polymers (24,25). These macromolecular agents have high relaxivities (in the range of 7~25 mM−1s−1 at 1.5T) (15,20–23), about 2–4 folds higher than their small molecular counterparts such as Gd-DTPA and Gd-DOTA (generally in the range of 3~5 mM−1s−1 at 1.5T) (3,26) due to slower molecular rotational correlation time. They also exhibit prolonged blood circulation and limited extravasation (25,27). Preclinical studies have shown that these macromolecular agents are effective for MR angiography, cancer imaging and characterization of tumor vascularity (28,29). Although macromolecular Gd(III) complexes have demonstrated some advantageous features over small molecular Gd(III) chelates, including both protein binding and non-binding agents, in preclinical studies, the clinical application of macromolecular Gd(III) based contrast agents has been impeded by the safety concerns associated with their slow excretion, which can lead to significantly higher tissue deposition of Gd(III) complexes than the small molecular agents (8), and consequently increase the probability of toxic Gd(III) ion release, causing chronic adverse effects such as the recently reported nephrogenic systemic fibrosis (8,30,31).

In order to alleviate the safety concerns of macromolecular contrast agents, we have recently developed extracellular degradable polydisulfides based polymeric MR contrast agents to accelerate the clearance of Gd chelates and minimize the tissue accumulation of Gd after the MRI examinations (29, 32, 33). These agents were prepared by copolymerization of DTPA anhydride with disulfide-contained monomers, followed by complexation with Gd(III). The disulfide bonds in the polymeric backbone was readily cleaved by in vivo plasma free thiols through disulfide-thiol exchange reaction. Pharmacokinetic studies revealed that the polydisulfide Gd chelates act as macromolecular contrast agents initially after administration, and are gradually reduced into excretive oligomeric and small Gd chelates in plasma, which are readily eliminated via renal filtration with a Gd(III) tissue retention comparable to clinical Gd(III) based MRI contrast agents. Preclinical studies showed that the polydisulfide Gd-DTPA complexes had better efficacy for contrast enhanced vascular and tumor imaging and characterization of tumor vascularity than small molecular Gd(III)-based contrast agents (34, 35). However, linear chelates, Gd-DTPA and its derivatives, exhibit relatively low kinetic stability, which may result in the release of free Gd(III) ions in vivo via transmetallation with endogenous metal ions (30, 31, 36, 37).

Chelate structure plays an essential role in the overall stability of Gd complexes, including the thermodynamic stability and the kinetic inertness (8, 36-38). The current clinically available Gd-based contrast agents are prepared from the derivatives of two types of ligands, the linear ligands, diethylenetriaminepentaacetic acid (DTPA) amd its derivatives, and the macrocyclic ligand, 1,4,7,10-tetraazacyclododecome-1,4,7,10-tetraacetic acid (DOTA) and its derivatives. The macrocyclic Gd(III) complexes exhibit

much higher kinetic stability than the linear Gd(III) chelates and no transmetallation in the presence of endogenous metal ions (39-41). The polydisulfides Gd-DTPA complexes had similar kinetic stability as the linear Gd(III) agent MultiHance®, higher than that of Omniscan®, but lower than that of the macrocyclic agent ProHance® (42). Previously, we investigated two biodegradable macromolecular contrast agents based on the more stable macrocyclic chelates, poly(*L*-glutamic acid)-cystamine-(Gd-DOTA monoamide) conjugate and the PAMAM-cystamine-(Gd-DOTA monoamide) conjugate (43, 44). Both systems showed good tumor diagnosis capacity as well as improved elimination in comparison to their non-degradable counterparts. However, limitations were also observed for these agents. The poly(*L*-glutamic acid) conjugates eliminated much slower than the polydisulfide GDCC due to the steric hindrance of randomly coiled structure of the polymer backbone on the reduction of the disulfide spacer (43, 45). The PAMAM conjugate had efficient degradation, but dendrimer became highly toxicity after the disulfide cleavage (44). Therefore, we hypothesized that the combination of macrocyclic chelates Gd(III) and polydisulfides can produce safe and effective biodegradable macromolecular blood pool agents with a clinical potential.

In this study, we have designed and synthesized a new generation of polydisulfides based on the macrocyclic Gd chelates to imrpove their kinetic stability. Herein, we report the synthesis of a polydisulfide with Gd-DOTA monoamide side chains, the copolymers of (N6-lysyl)lysine Gd-DOTA monoamide and 3-(2-carboxyethyldisulfanyl)propanoic acid (GODC), as a new biodegradable macromolecular MRI contrast agent. We characterized the kinetics stability of G(III) chelates in the agents and in vitro and in vivo degradation of the polymers. We evaluated the effectiveness of

GODC for contrast enhanced MR vascular imaging and tumor imaging in a mouse beast cancer model.

Experimental Section

Materials

Fmoc-lys(ivDDe)-OH was purchased from Chem-Impex International (Wood Dale, IL). 2-chlorotrityl chloride resin, 1-hydroxybenzotriazole (HOBT), 2-(1H-benzotriazole-1-yl)-1,1,3,3-tetramethyluronium hexafluorophosphate (HBTU) and benzotriazol-1-yl-oxytripyrrolidinophosphonium hexafluorophosphate (PyBOP) were purchased from Nova Biochem (Darmstadt, Germany). 1,4,7,10-Tetraazacyclododecane-1, 4,7-*tris*-*tert*-butyl acetate-10-acetic acid [DOTA-*tris*(*t*-Bu)] was purchased from TCI America (Portland, OR). *N,N*-Diisopropylethylamine (DIPEA), piperidine, hydrazine and trifluoroacetic acid (TFA) were purchased from Alfa Aesar (Ward Hill, MA). *N,N*-Dimethylformamide anhydrous (DMF), dichloromethane (DCM), methanol, ethyl ether and phosphate buffer saline (PBS) were purchased from Fisher Scientific (Pittsburgh, PA). Fmoc-lys(Fmoc)-OH, the Kaiser test kit, ethylenediamine dihydrochloride, 1,2-ethanedithiol (EDT), triisopropylsilane (TIS), Xylenol orange, dithiobis(succinimidylpropioniate) (DSP) and $Gd(OAc)_3$ were purchased from Sigma-Aldrich, Inc. (Louis, MO). All reagents were used without further purification unless otherwise stated. The synthetic product was verified and characterized using high performance liquid chromatography (HPLC, Agilent), the matrix-assisted laser desorption/ionization time-of-flight (MALDI-TOF) mass spectra (Bruker Autoflex III), ^{1}H-NMR (300 MHz Varian Gemini NMR spectrometer) and Fourier transform infrared

(FT-IR, Varian Inc.). The MALDI-TOF mass spectrum was acquired on a Voyager DE-STR spectrometer (PerSpeptive BioSystems) in linear mode with R-cyano-4-hydroxycinnamic acid as a matrix. The polymer conjugates were purified by ultrafiltration with Millipore's Amicon Ultra-15 centrifugal filter of 3 kDa molecular weight cut-offs against de-ionized water. The Gd(III) and Zn(II) content was measured by inductively coupled plasma-optical emission spectroscopy (ICP-OES Optima 3100XL, Perkin-Elmer, Norwalk, CT).

Synthesis of (N_6-Lysyl)lysine-DOTA

(N_6-Lysyl)lysine-DOTA was synthesized following a solid phase peptide chemistry approach. Fmoc-lys(ivDDe)-OH (0.52 g, 0.91 mmol) was first loaded to the 2-chlorotrityl chloride resin (1.15 g, 1.50 mmol, swelled in dichloromethane) with 800 µl DIPEA in 10 ml DMF and shaken for 2 hrs. The reaction media was then filtered out, followed by blocking the un-reacted active sites on the resin using 10 ml of methanol with 400 µl DIPEA (20 min x 2). The resin was washed with DCM and DMF to exclude the excess reactants. A Kaiser test was carried out with a small amount of resin samples, and showed negative result (yellow color), indicating no detection of primary amines. The resin was then reacted with 10 ml 20% of piperidine/DMF to remove the Fmoc group. DCM and DMF were used to wash out the remaining piperidine. After the reaction, Kaiser test of the resin showed positive result (blue color), indicating the removal of the Fmoc group. DOTA-tris(t-Bu) ester (1.04 g, 0.91 mmol) was then reacted to the resin with HOBT (0.37 g, 0.91 mmol), HBTU (1.03 g, 0.91 mmol) and 300 µl DIPEA in 10 ml DMF. The reaction media was shaken for 2 hrs, washed with DCM and

DMF. The next step was carried out when Kaiser test showed negative results, indicating complete reaction of the primary amine. The resin was then reacted with 10 ml 2% hydrazine/DMF to remove the ivDDe group. After removal of the ivDDe group (positive Kaiser test), Fmoc-lys (Fmoc)-OH (1.60 g, 0.91 mmol) was loaded to the resin with PyBOP (1.41 g, 0.91 mmol), HOBT (0.37 g, 0.91 mmol) and 500 μl DIPEA in 10 ml DMF. The reaction was carried out for 50 minutes. The Fmoc group was then removed using 10 ml 20% piperidine/DMF. After removal of the Fmoc, the resin was washed with DCM, dried. A mixture of trifluoroacetic acid (TFA), 1,2-ethanedithiol (EDT), water, TIS (95:2.5:2.5:2, 15 ml) was used to remove the tert-butyl groups and separate the final product from the resin. The reaction media was filtered out, and the raw product of (N_6-Lysyl)lysine-DOTA was precipitated in ethyl ether. The precipitate was recrystallized in DMSO and DIPEA (5:1). DIPEA also served as a base to remove TFA from the (N_6-lysyl)lysine DOTA monoamide. HPLC was used to verify the purity of the final product and showed good purity of the monomer after the recrystallization. The resulted DOTA monoamide was then characterized by ^{1}H-NMR and MALDI-TOF mass spectrometry. The yield of the monomer was 62%. ^{1}H-NMR (300 MHz, D_2O, 25°C): 1.20-1.35 (m, 4H), 1.40-1.50 (m, 2H), 1.55-1.85 (m, 6H), 2.85-2.95 (t, 2H), 2.98-3.50 (m, 19H), 3.60-4.05 (m, 8H), 4.15-4.25 (t, 1H). MALDI-TOF MS: 661.02 ($M+H^+$), 683.19 ($M+Na^+$) (measured); 660.76 (calculated).

Synthesis of (N_6-Lysyl)lysine-DOTA monoamide and 3-(2-carboxyethyldisulfanyl)-propionic Acid Copolymers (GODC)

The polymerization was performed by slowly adding the DMF solution of dithiobis(succinimidylpropionate) (DSP) (0.2 g, 0.45 mmol) portion by portion to the concentrated aqueous solution of (N_6-Lysyl)lysine-DOTA monoamide (0.4 g, 0. 45 mmol in 0.5 ml DI water) while stirring. The reaction was stirred at room temperature for 4 hours after adding the DSP solution. The product was purified through ultrafiltration using a filter with a molecular weight cut-off of 3,000 Da to remove low molecular weight oligomers, and then lyophilized to give the colorless polymeric ligand. The yield of the purified product was 10%. The apparent number- and weight-average molecular weights of the copolymers were determined using size exclusion chromatography on an AKTA FPLC system with a Superose™ 12 column (GE Healthcare Life Sciences). The column was calibrated using water soluble poly[*N*-(2-hydroxylpropyl)methacrylamide] (HPMA) standards with number average molecular weight of 14, 23, 32 and 47 kDa. Polymers with molecular weight lower than 10 kD cannot be separated effectively using this column. The polymeric ligand was characterized by ^{1}H-NMR and FT-IR. ^{1}H-NMR (300 MHz, D_2O, 25°C): 1.05-1.20 (m, 4nH), 1.20-1.40 (s, 4nH), 1.40-1.68 (m, 4nH), 2.25-2.65 (m, 8nH), 2.70-3.14 (m, 16nH), 3.15-3.45 (s, 8nH), 3.50-3.75 (d, 4nH), 3.76-4.20 (s, 2nH). FT-IR: 2800-3680 cm^{-1} (ν_{O-H}), 1440-1800 cm^{-1} ($\nu_{C=O}$), 1100-1240 cm^{-1} (δ_{O-H}, ν_{C-O} and ν_{C-N}).

Complexation with Gd(III)

The polymeric ligand was complexed with two folds excess of $Gd(OAc)_3$ at pH 6 for 48 hrs at room temperature. The resulting solution was purified via dialysis against water using a membrane with molecular weight cut-off of 8,000 Da, and lyophilized to give a final white product, (N_6-Lysyl)lysine-Gd-DOTA monoamide 3-(2-carboxyethyl-disulfanyl)-propionic acid copolymer (GODC). Size exclusion chromatography was used to determine the apparent molecular weights of the complexed polymer. Xylenol orange was used to detect the presence of free Gd(III) ions. No color change was observed with Xylenol orange in the polymer solution after dialysis, indicating complete removal of the excess of $Gd(OAc)_3$. The Gd(III) content of the polymer was determined using inductive coupled atomic emission spectrometry (ICP-OES, PerkinElmers®). The size of GODC in aqueous solution was determined using dynamic light scattering (DLS). The experiment was performed using a Brookhaven BI-200SM goniometer and BI-9000AT digital correlator equipped with a He-Ne laser (λ =633 nm) at room temperature. GODC in de-ionized water (1.33 mg/ml) was filtered through a 0.22 μm filter and measured at a scattering angle of 90. A Nanosphere™ polystyrene size standard (diameter=102 nm $\pm$ 3 nm) (Thermo Scientific, Waltham, MA) was analyzed in line to confirm accuracy. All measurements were performed 3-5 times.

Relaxivity Measurement

The T_1 relaxivity of GODC was determined using a Bruker Minispec® Relaxometer (1.5T, 60 Hz) at 37°C. Different concentrations of GODC (0.2, 0.4, 0.6 and 0.8 mM of Gd) were prepared, and their T_1 values were obtained using an inversion-

recovery pulse sequence from the relaxometer. The longitudinal relaxivity (r_1) was calculated as the slope of the plot of $1/T_1$ versus the concentration of Gd(III). Similarly, the T_2 relaxivity was determined using a Carr-Purcell-Meiboom-Gill (CPMG) spin echo method. The Gd(III) content of each sample was confirmed by ICP-OES after the MR measurement.

Degradation of the Polydisulfide

In vitro degradation study of GODC polymer was carried out via incubation of GODC (0. 42 mM-Gd) with cysteine at plasma thiol concentration (15 μM) (46, 47) to mimic the in vivo conditions. The polydisulfide with 0.42 mM of Gd(III) were incubated with 15 μM *L*-cysteine in PBS buffer at pH 7.4 and 37°C for 24 hours. The change of apparent molecular weight of GODC during the incubation was determined using size exclusion chromatography (Superose® 12 column, AKTA® FPLC). The column was calibrated using water soluble poly[*N*-(2-hydroxylpropyl)methacrylamide] (HPMA) standards with a series of different molecular weight (M_n = 14, 23, 32 and 47 kDa).

The degradation mechanism of the polydisulfide was also investigated both *in vitro* and *in vivo*. For *in vitro* experiment, GODC was incubated with an excess of *L*-cysteine (1.5 mM) in PBS solution at 37°C for 60 minutes. The reaction mixture was analyzed by MALDI-TOF mass spectrometry. For *in vivo* experiment, GODC was administered to mice at a dose of 0.1 mmol-Gd/kg via a tail vein, and urine samples were collected 30 minutes after the injection and analyzed by MALDI-TOF mass spectrometry.

Kinetic Inertness

The kinetic inertness of polydisulfide Gd-DOTA against transmetallation_was evaluated in vitro in comparison with our previously reported Gd-DTPA cystamine copolymers (GDCC) (48). GODC (0.42 mM-Gd) or GDCC (0.42 mM-Gd) was incubated with $ZnCl_2$ at the plasma Zn^{2+} concentration (50 μM) in PBS buffer at pH=7.4 and 37°C for 2 hrs. Samples were collected before and at 30, 60 and 120 minutes of incubation. The polymer bound Gd(III) and released Gd(III) ions were separated using a PD-10 column (GE Health Science). The concentration of polymer bound Gd(III) was measured by ICP-OES (Perkin-Elmers). The kinetic stability was determined as the percentage of bound Gd(III) in polymers post-incubation to that before-incubation. GODC and GDCC incubated with Zn^{2+} free PBS buffer were used as negative controls.

Mouse Tumor Model

Female BALB/c mice weighing 18-22 g were purchased from Charles River (Wilmington, MA, USA). The animals were cared following an approved protocol and the guidelines of the Animal Resource Center of Case Western Reserve University. Mouse breast cancer 4T1 cells (5×10^4 cells suspended in 50 μl Matrigel) were injected into the inguinal mammary fat pads of mice. The MRI study was performed when tumor size reached 0.5-1.0 cm in diameter in 2 weeks.

In Vivo MRI Study

The contrast enhancement of GODC was preliminarily evaluated in mice using the clinical agent Magnevist® as a control. The tumor bearing mice were anaesthetized

with 2.5% ~ 3.5% of isoflurane in oxygen initially, and maintained at 1.5%-2.5% during the experiment. The temperature, respiration and electrocardiograms (ECGs) of the mice were monitored during image acquisitions. The animals were kept warm at 34°C using an air conditioning system controlled through a temperature module. The contrast agent was intravenously administered to anesthetized mouse via tail vein at a dose of 0.1 mmol-Gd/kg. MR images were acquired before administration and at different time points post injection for up to 30 minutes on a Siemens 1.5T clinical scanner with a 3D FLASH pulse sequence (211 FOV, 1.1 mm slice thickness, 14.0 ms TR, 3.09 ms TE, 25° flip angle, 2 averages, 64×256 matrix size, 32 slices per slab) and a 2D spin-echo sequence (19.1 ms TE, 465 ms TR, 25° flip angle, 0.8 mm slice thickness, 100×256 matrix size, 211 mm FOV, 2 averages). Three tumor-bearing mice were used for each contrast agent. Signal intensity of the regions of interest (ROI) was measured using the Osirix software. Signal increase of the tumor periphery was calculated using the ratio of the signal post-contrast to that of pre-contrast within the ROI at different time points post injection. Statistical analysis was performed using a two-way ANOVA with Bonferroni's, assuming statistical significance at $p < 0.05$.

Results

Synthesis of (N_6-Lysyl)lysine-DOTA-Gd Monoamide and 3-(2-carboxy-ethyldisulfanyl)propanoic Acid Copolymers (GODC)

The monomer containing Gd-DOTA, (N_6-Lysyl)lysine-DOTA-Gd, was first synthesized using solid phase chemistry, Figure 3.1. The new biodegradable

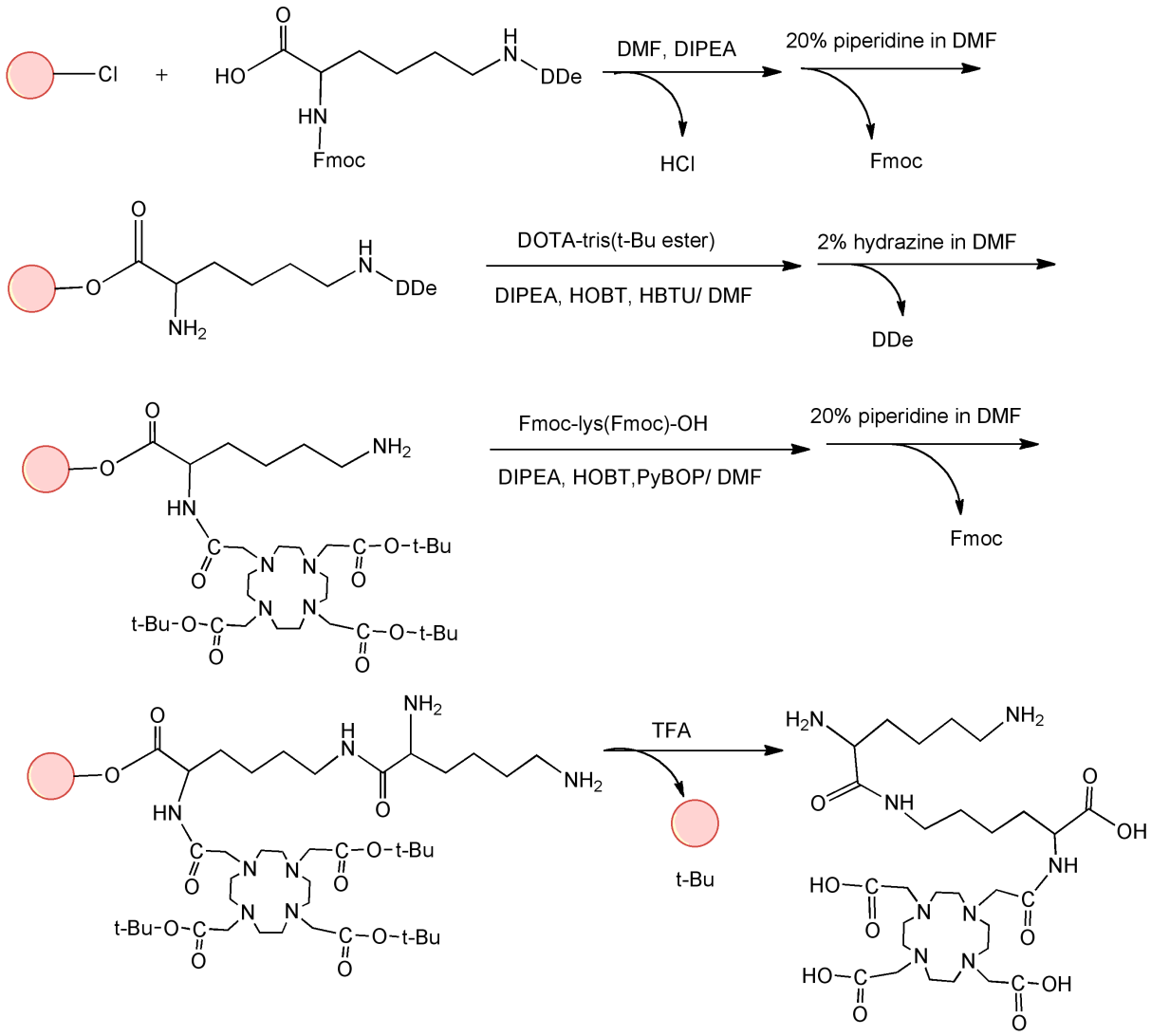

Figure 3.1. Synthetic scheme of (N_6-lysyl)lysine DOTA monoamide.

macromolecular MRI contrast agent, (N_6-Lysyl)lysine Gd-DOTA monoamide and 3-(2-carboxyethyldisulfanyl)propanoic acid copolymers (GODC), was synthesized by condensation polymerization of the Gd-DOTA monoamide and dithiobis(succinimidyl-propionate) (Figure 3.2). The polymeric ligand, (N_6-Lysyl)lysine DOTA monoamide and 3-(2-carboxyethyldisulfanyl)propanoic acid copolymers, was characterized using ^{1}H-NMR and FT-IR. The apparent number average and weight average molecular weights of the polymeric ligand were 20.7 and 25.8 kDa. After complexation, the final product GODC were purified against deioniazed water using dialysis membrane with higher molecular weight cutoff to further narrow down the polydispersity. The resulting number average and weight average molecular weight of GODC were 24.2 and 26.4 kDa, respectively. The Gd(III) content in the agent was 15.08% (w/w) as determined by ICP-OES. The calculated Gd content was 15.63% (w/w). The efficiency of complexation was 96.5%. The DLS measurement showed the hydrodynamic effective diameter of GODC to be around 5-7 nm. The r_1 and r_2 relaxivities of GODC were 8.25 $mM^{-1}s^{-1}$ (Figure 3.3a) and 10.08 $mM^{-1}s^{-1}$ (Figure 3.3b) at 1.5 T. The T_1 relaxivity (r_1) of GODC increased approximatly 2 folds compared to the r_1 of Gd(DO3A-HP) (ProHance®, 4.1 $mM^{-1}s^{-1}$ at 1.5T, 20°C) (26).

Degradability of GODC

The polydisulfide structure of GODC was designed so that the polymers could be readily degraded and excreted via renal filtration in vivo through the disulfide-thiol exchange reaction (32). The degradability of GODC was demonstrated via the incubation study with *L*-cysteine, the most abundant free thiols in plasma (46). Figure 3.4

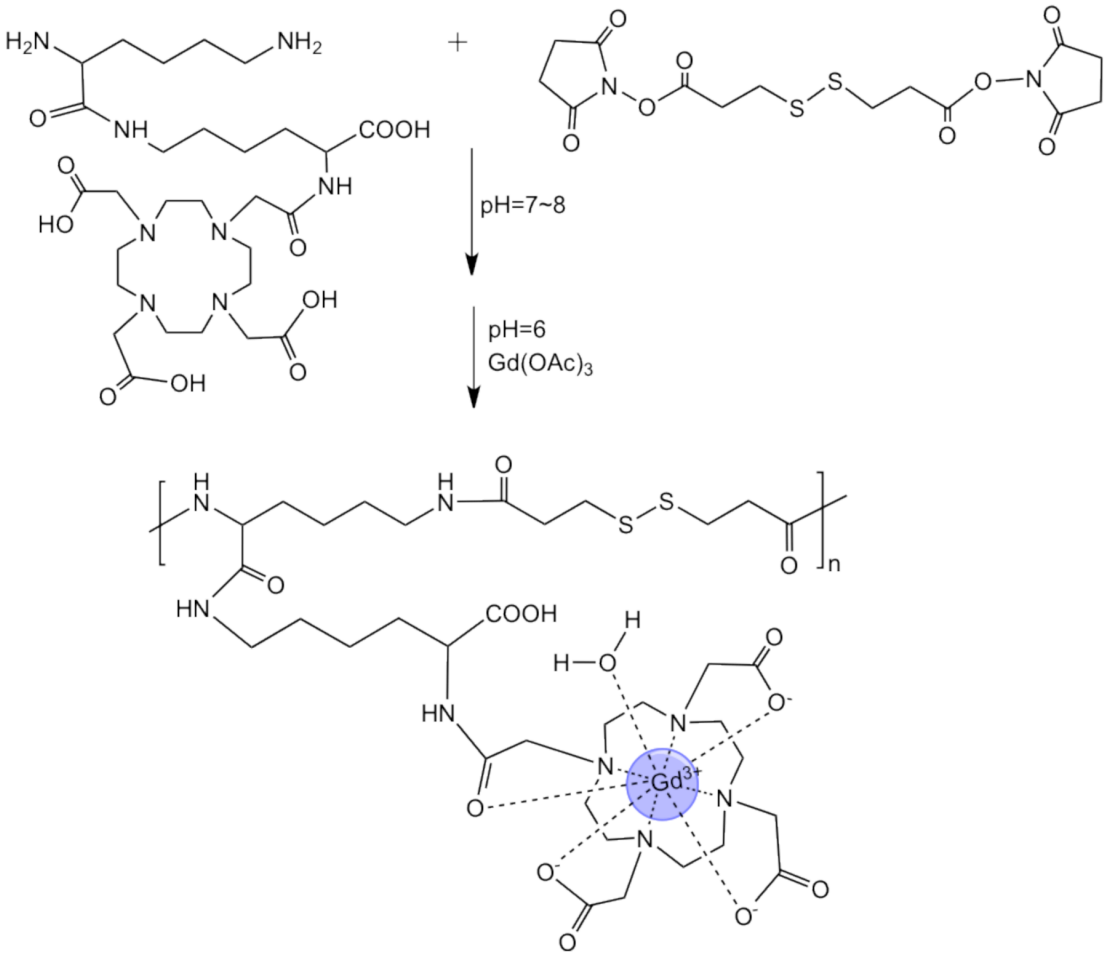

Figure 3.2. Synthetic scheme of (N_6-lysyl)lysine-(Gd-DOTA) monoamide 3-(2-carboxyethyldisulfanyl)propionic acid copolymer (GODC).

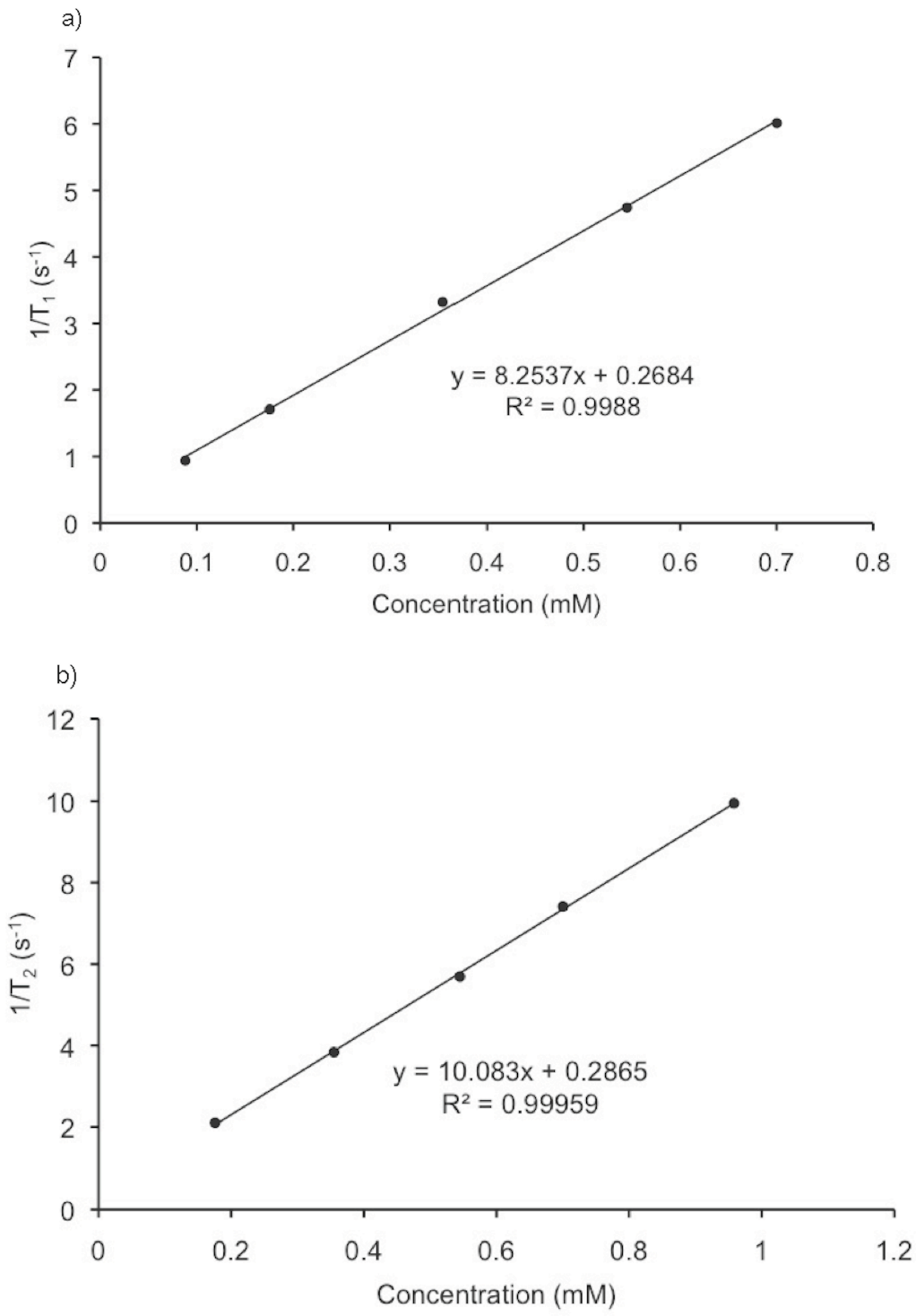

Figure 3.3. The relaxation rate $1/T_1$ (a) and $1/T_2$ (b) versus concentration plot of (N_6-lysyl)lysine-(Gd-DOTA) monoamide dithiobispropionic acid copolymer (GODC).

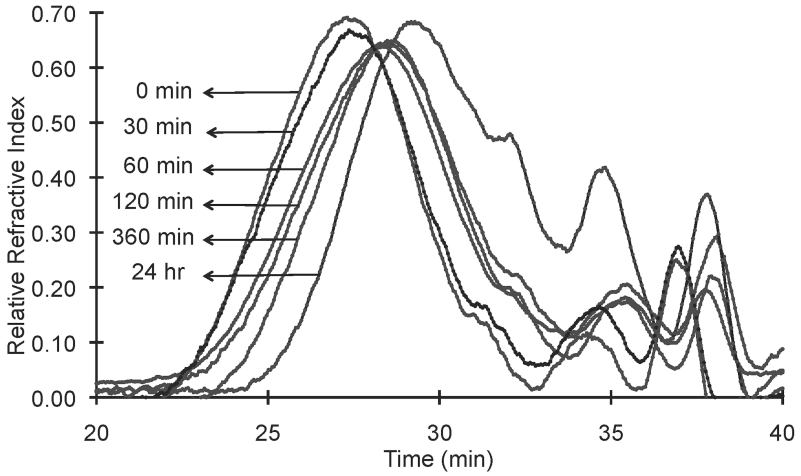

Figure 3.4. The apparent molecular weight distribution before (0 min) and in the incubation of GODC against cysteine (15 μM) at plasma concentration for 30, 60, 120, 360 min and 24 hrs at 37ºC.

shows that the number average molecular weight of GODC decreased from 24.2 kDa before incubation to 23 kDa, 22.1 kDa, 19.7 kDa, 18.6 and 13.1 kDa at 30, 60, 120, 240 min, and 24 hrs in the incubation. In terms of degree of polymerization, the average chelates per chain reduced from 25 to 12 after 24 hrs of in vitro incubation.

The degradation mechanism was demonstrated both in vitro and in vivo. In vitro experiments revealed that the polydisulfides can be reduced to their smallest repeating units via disulfide-thiol exchange reaction when sufficient amount of free thiols was provided (Figure 3.5). Figure 3.6a showed the MALDI-TOF mass spectrum of the 60-minutes-incubation mixture of GODC and excess of *L*-cysteine. The peaks of in vitro degradation products were compound I (m/z=978.3, M^+; m/z=1000.8, $M+Na^+$; m/z=1022.4, $M+2Na^+$), the smallest building block of the polymer. In vivo analysis of metabolites in urine samples also illustrated similar route of degradation. Similar degradation products [m/z=1000 ($I+Na^+$)] and the other degradation product of cysteine, compound II [m/z=1212 ($M+H^+$)], were also identifed by MALDI-TOF mass

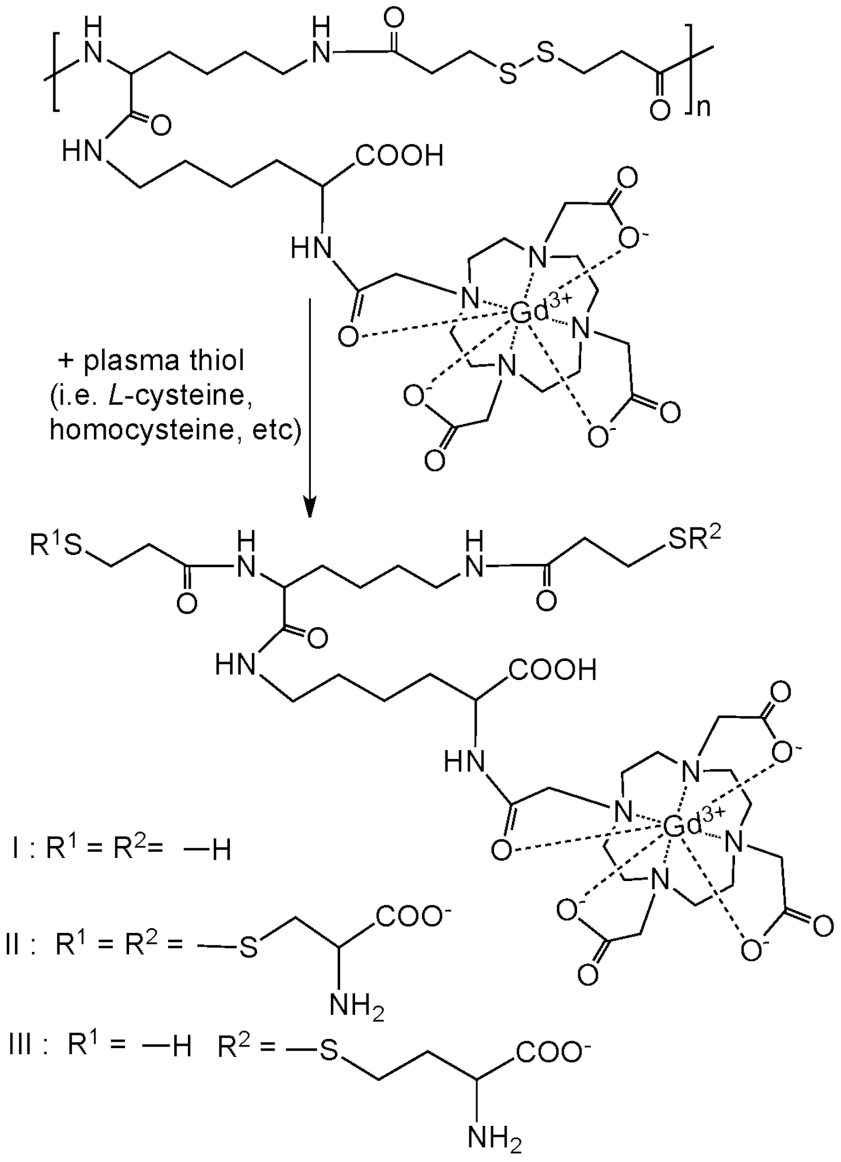

Figure 3.5. Complete degradation products of GODC with *L*-cysteine.

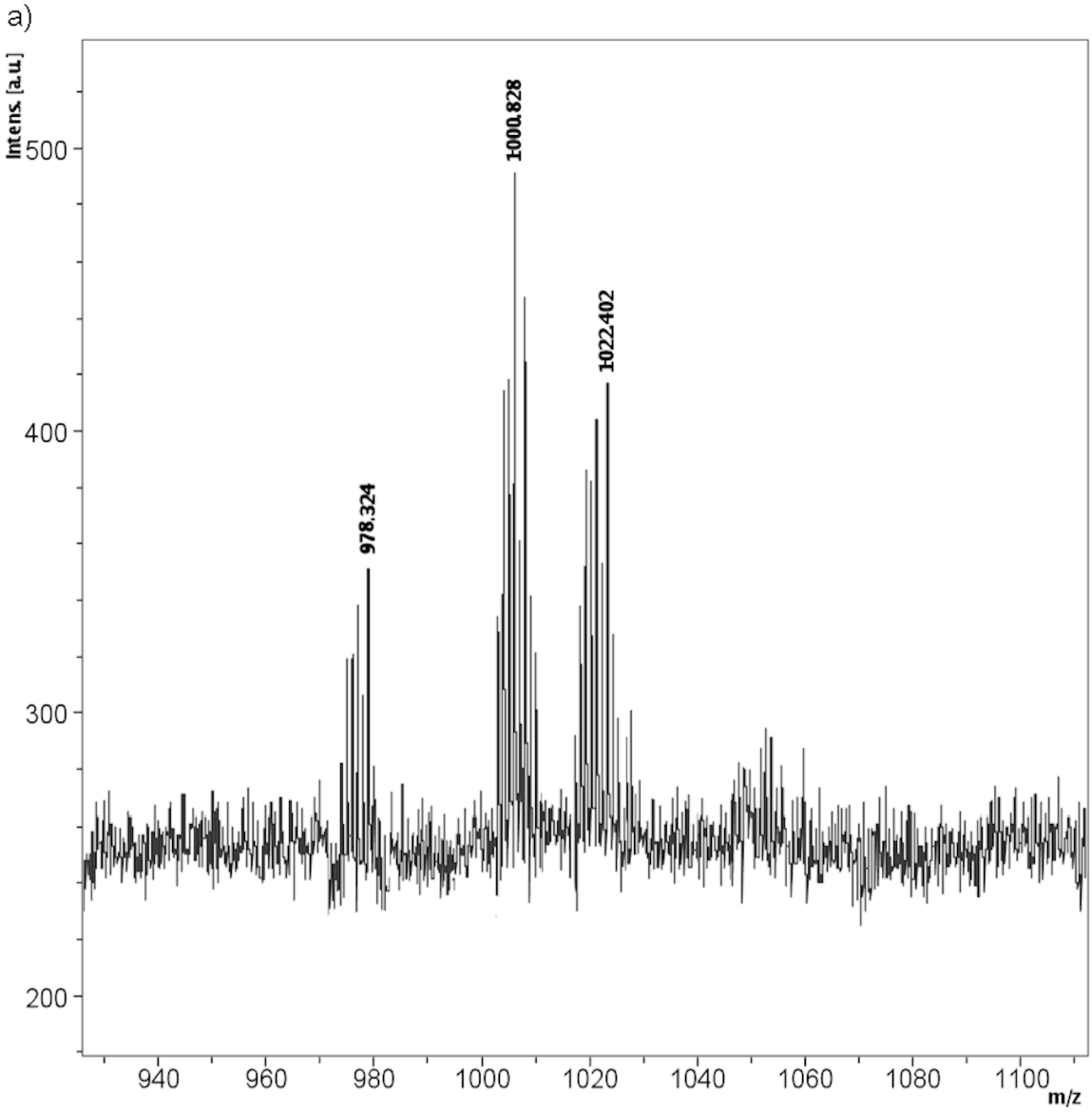

Figure 3.6. The MALDI-TOF mass spectrum of degradation products (a) collected 60 minutes post incubation of GODC with an excess of *L*-cysteine (1.5 mM), and mouse urine samples (b) collected 30 minutes after the injection of GODC.

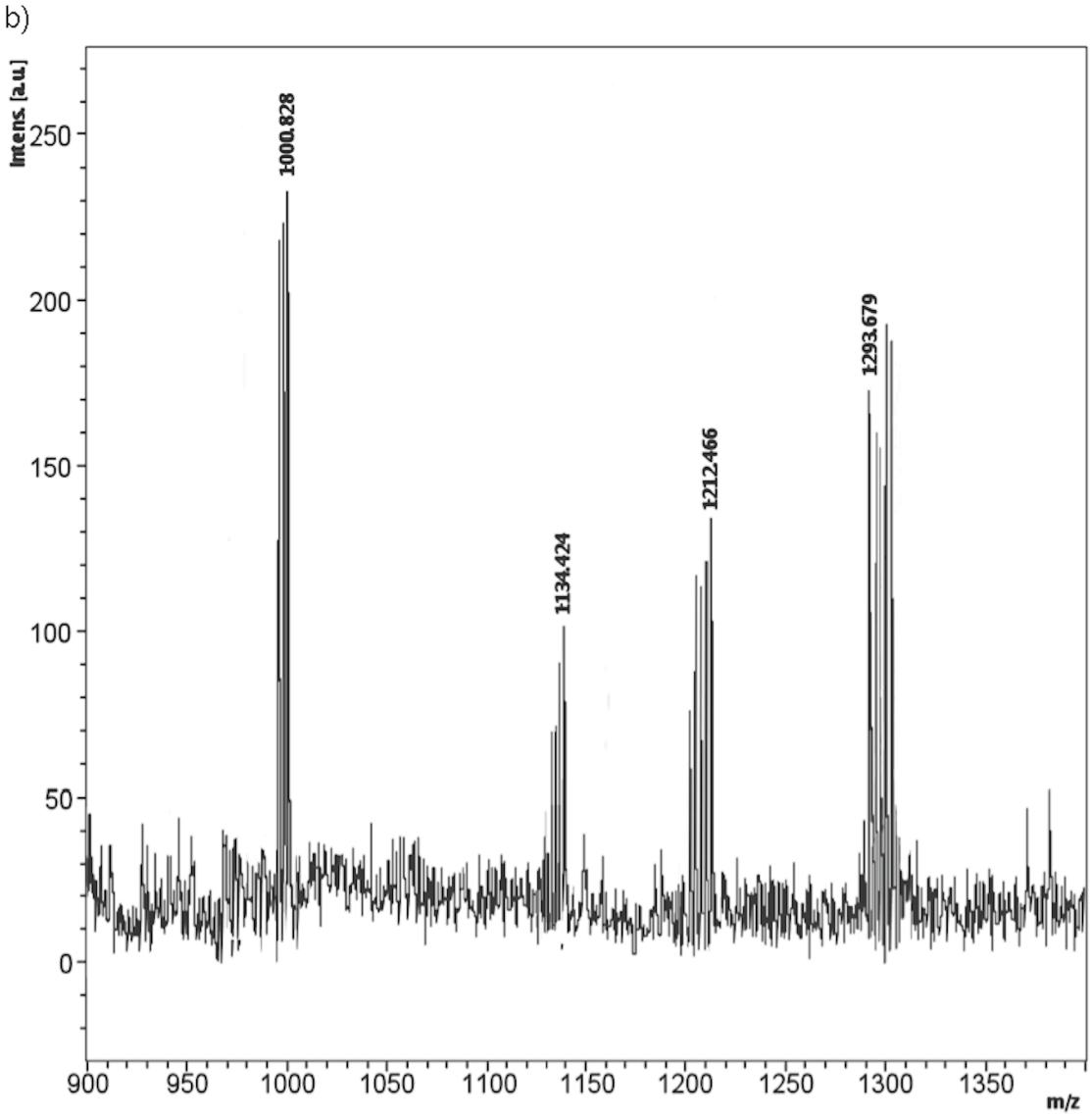

Figure 3.6. Continued.

spectrometry in urine samples collected 8 hours after intravenous injection of GODC (Figure 3.6b). The major metabolites in the urine samples had the mass of 1000.8 ($I+Na^+$), 1134.4 (compound I-homocysteine+Na^+), 1212.5 ($II+H^+$) and 1293.7 (unkown).

Kinetic Inertness of GODC

The new macrocyclic Gd chelate based polydisulfide, GODC, demonstrated much higher kinetic inertness against transmetallation than that of the linear Gd chelates based polydisulfides, GDCC. Figure 3.7 reveals gradual loss of polymer bound Gd with GDCC from the initial 100 % to 92% at 30 min, 88 % at 90 min and 82 % at 120 min during in

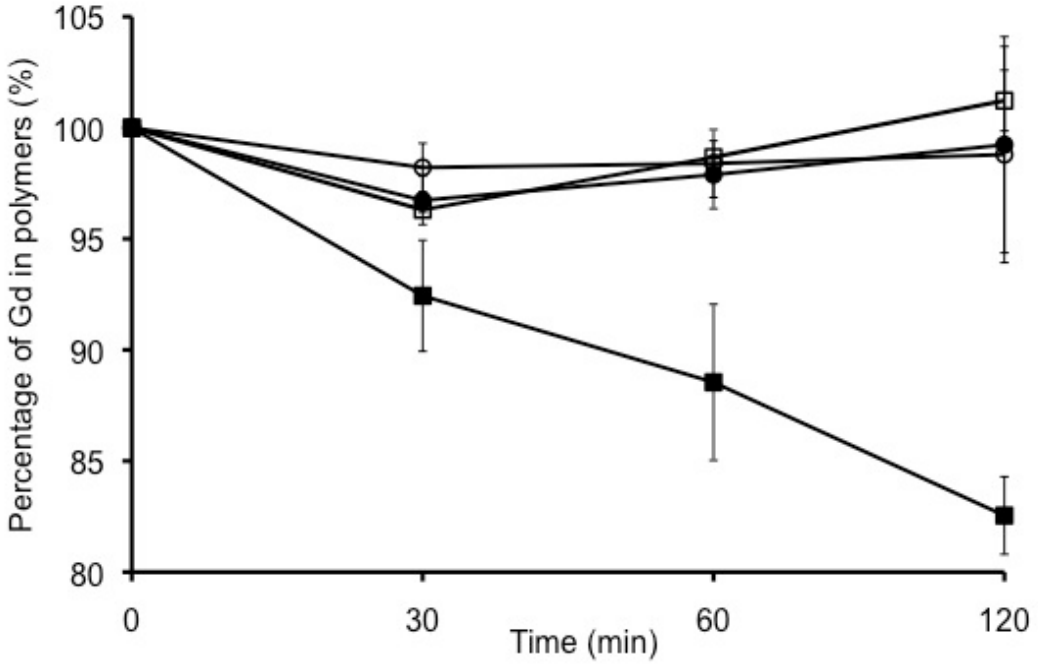

Figure 3.7. The Gd(III) content in GDCC (square) and GODC (circle) before and in the incubation in PBS buffer with $ZnCl_2$ (50 μM, filled) and without $ZnCl_2$ (open) for 30, 60, and 120 min.

vitro incubation with Zn^{2+}, whereas neglegible loss of Gd was observed with GODC. The Gd content remained similar over time for the control samples of GDCC and GODC, as well as the incubated samples of GODC, indicating good kinetic stability of the macrocyclic Gd based polydisulfides.

In Vivo MR Imaging

Figure 3.8 shows the T_1-weighted 3D maximum intensity projection MR images of mice bearing orthotopic 4T1 mouse malignant tumor before and after intravenous injection of GODC and Magnevist®. Significant and prolonged blood pool contrast enhancement was observed with GODC in comparison with Magnevist®, indicating the relatively prolonged blood circulation of GODC. The blood pool enhancement was gradually descreased, but still visible at 30 minutes post injection. Contrast enhancement inside the urinary bladder was observed at 3 minutes post injection of Magnevist®, and at 10 minutes post injection of GODC, indicating relatively fast excretion of GODC. Figure 3.9a shows the axial T_1-weighted 2D spin-echo MR images and signal intensity ratio of the tumor before and at different time points after injection of the agents. GODC resulted in more significant enhancement in the tumor periphery of mice than that of Magnevist®. Quantitative analysis of the signal intensity in the tumor periphery showed that GODC produced stronger signal enhancement in the tumor than Magnevist® for at least 30 minutes (Figure 3.9b).

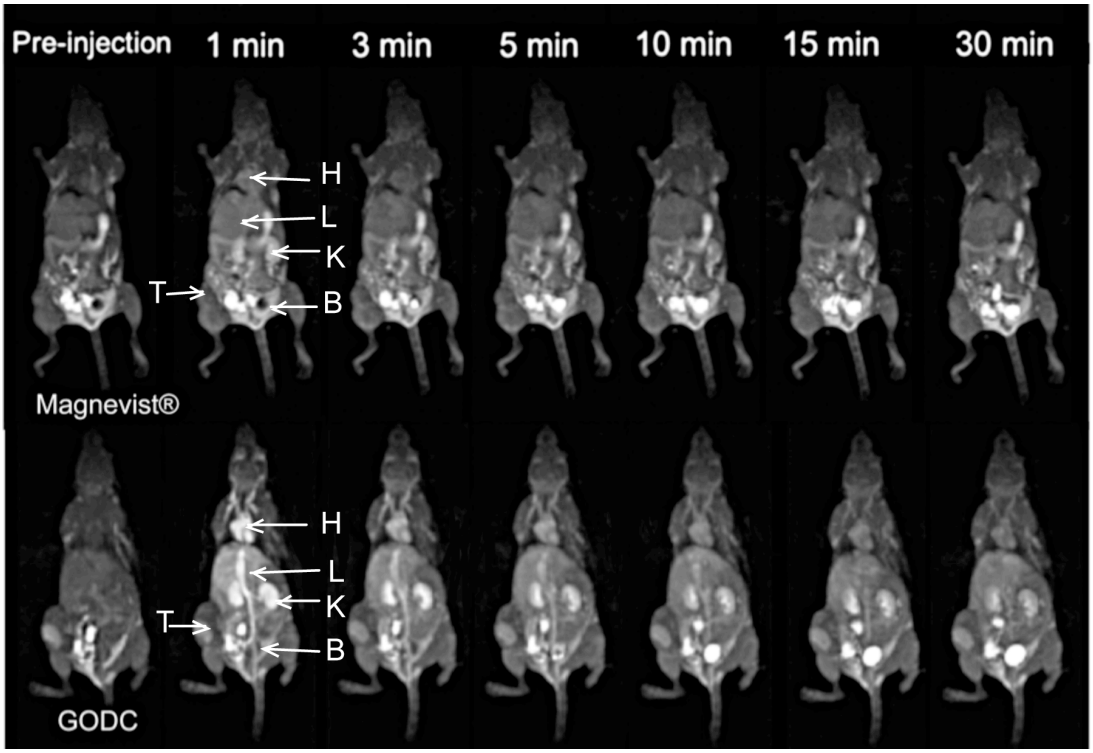

Figure 3.8. Three-dimensional maximum intensity projection images (coronal view) of mice bearing 4T1 breast tumor xenografts before and at 1, 3, 5, 10, 15 and 30 minutes post injection of Magnevist® and GODC at a dose of 0.1 mmol-Gd/kg. The major organs were pointed out as H (heart), L (liver), K (kidney), B (bladder) and T (tumor).

9(a)

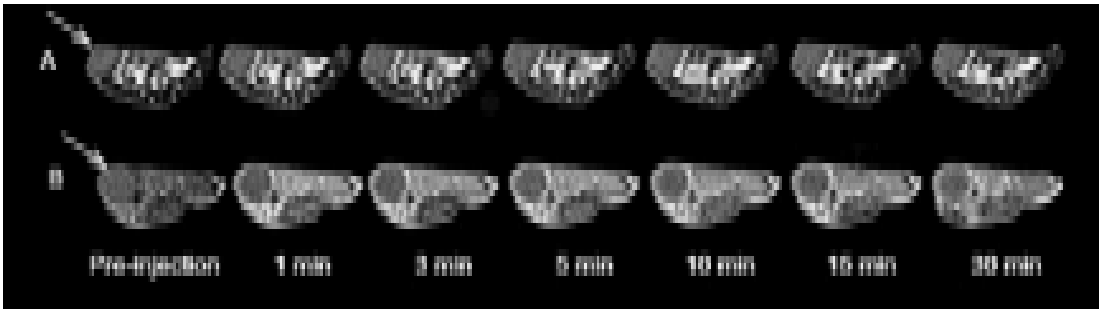

9(b)

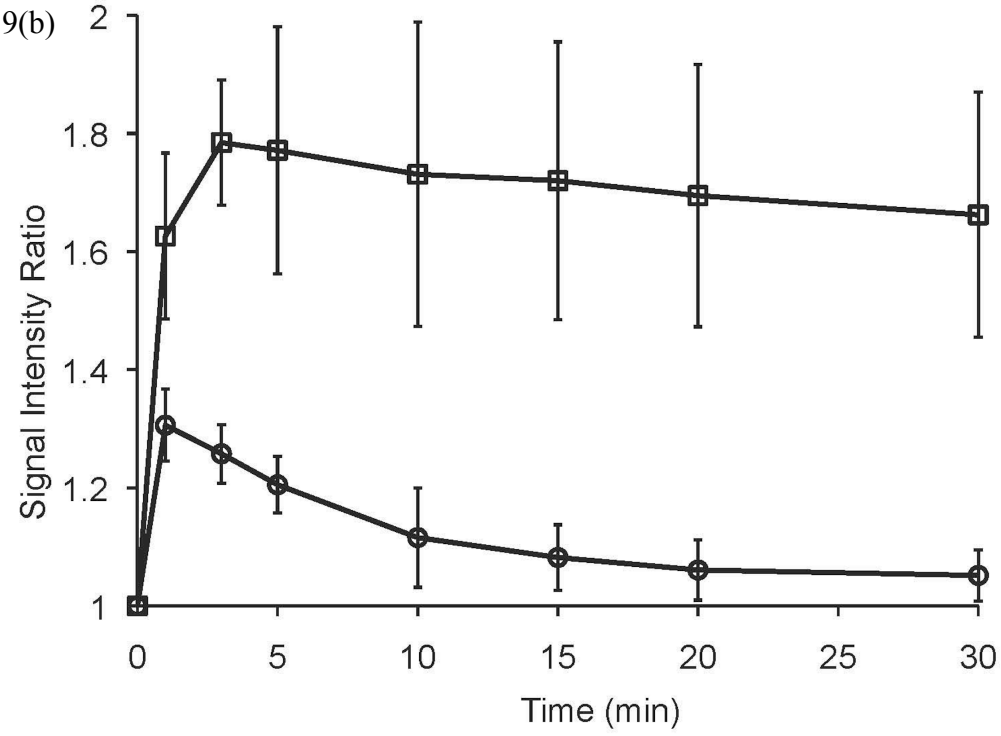

Figure 3.9**.** a) Axial 2D spin echo images of mice bearing 4T1 breast tumor xenografts before and at 1, 3, 5, 10, 15 and 30 minutes post injection of Magnevist® (A) and GODC (B) at a dose of 0.1 mmol-Gd/kg. b) Signal intensity ratio of tumor periphery of mice bearing malignant breast cancer before and at different time points after administration of Magnevist® (circle) and GODC (square).

Discussion

A polydisulfide with macrocyclic Gd(III) chelate side chains, 2,2',2"-(10-(2-((1-carboxy-5-(2,6-diaminohexanamido)pentyl)amino)-2-oxoethyl) Gd-DOTA monoamide and 3-(2-carboxyethyldisulfanyl)propanoic acid copolymers (GODC), was synthesized asa new generation of disulfide based biodegradable macromolecular MRI contrast agent with improved kinetic inertness against the previously reported DTPA based agents (32, 35). The monomer (N_6-Lysyl)lysine DOTA monoamide had an unsymmetrical structure as shown in Figure 3.1. In consequence, the condensation polymerization of the monomers could result in polymer chains with random arrangement of the (N_6-Lysyl)lysine Gd-DOTA monoamide. The final product of GODC could have three possible arrangements of the lysine based Gd-DOTA monoamide in the polymer chains: two α-amines of separate Gd-DOTA monoamide molecules connected to the same DSP molecule, two ε-amines connected to the same DSP, and one α-amine and one ε-amine connected to DSP. The polymerization might also result in cyclized products. High concentrations of monomers (0.8 g/ml of DI water) were used in the polymerization reaction to minimize the cyclization. Differences in monomer arrangement in the polymer chains should not affect the degradability and magnetic properties of GODC as a biodegradable macromolecular MRI contrast agent. Despite molecular weight, the actual size of GODC in solution was measured using dynamic light scattering. The hydrodynamic diameter of GODC in solution was around 5-7 nm, right above the renal filtration threshold without degradation. To demonstrate the indispensability of degradation, we have also compared the pharmacokinetics and long-term tissue retention of the degradable polydisulfides Gd-DTPA agents with their non-degradable counterparts

of similar molecular weight (M_n= 25 kDa, PD=1.4) in our previous study (49). The result showed significantly longer blood circulation and higher tissue retention of the non-degradable agents, indicating a need of degradation for polymers with similar structure.

GODC was hypothesized to be degraded by extracellular free thiols through the thiol-disulfide exchange reaction. In vitro preliminary study was performed via incubation of GODC with *L*-cysteine at plasma concentration to demonstrate the mechanism and process of degradation. *L*-cysteine was chosen because it is the most abundant species among various types of small-molecular plasma thiols, including glutathione, homocysteine and cysteinylglycine (46). The in vitro incubation study showed that GODC was gradually reduced into oliogomers in the presence of cysteine at plasma-thiol concentration (15 μM), and can be completely degraded into the smallest repeating units when given sufficient cysteine. Besides cysteine, serum albumin is another abundant source of plasma thiols. Although it is of high concentration in plasma, it has been found that serum albumin plays little part in the reduction process of the polydisulfides in vivo (48). The high steric hindrance of both the protein and polymers greatly constrained the exchange reaction between the thiol in serum albumin and the polydisulfides. In addition to the in vitro incubation study, the mechanism of in vivo degradation was also validated through mass spectrometric analysis of the urine sample after injection of GODC. Similar peaks, including the smallest building block of GODC and the cysteine reduced products, were identified in the mass spectrum of both complete in vitro degradation products and the urine metabolites, indicating similar route of degradation in vitro and in vivo. Moreover, the discovery of reduction products other than cysteine metabolites in the urine samples (e.g the homocysteine metabolites with

peaks at m/z=1134.4) further verified the degradation mechanism, and more importantly, provided a more complicated insight of the in vivo metabolism pathway.

The in vitro degradation rate of GODC appeared slower than that of our previous reported GDCC (50), which is mainly a result of polymer charge. In physiological pH, GODC was negatively charged due to the extra carboxylic groups on the side chain, whereas GDCC was a neutral polymer. Since cysteine was also negatively charged at physiological pH, the negative charges around the disulfide bonds in GODC inhibited the approach of the cysteine due to charge repulsion, resulting in slower degradation. Similar results were also observed with other negatively charged polydisulfides, e.g. Gd-DTPA cystine copolymers (50). The in vitro degradation rate of GODC appeared significantly slower in comparison to in vivo degradation, which was indirectly demonstrated with rapid bladder enhancement in the mouse MR study. This difference of degradation rate can be attributed to various reasons since the in vivo degradation pathway is much more complicated. One explanation might be the difference of thiol concentration, which was fixed during the in vitro study, but was constantly replenished by the liver in vivo. In addition, if taking account of the impact of air on cysteine oxidation during the in vitro incubation study, the cysteine concentration might be gradually decreased through formation of cystine, leading to slower degradation than that from in vivo condition. Given the complicated nature of the in vivo metabolism environment for GODC, the in vitro degradation study was only a preliminary proof-of-concept study that can hardly be considered a good simulation of in vivo degradation. Further studies of pharmacokinetics, biodistribution, metabolite analysis and etc will be carried out to look deeper into the route of in vivo fate of the new polydisulfides Gd-DOTA.

Similar to our previously reported polydisulfides Gd-DTPA, the newly developed Gd- GODC exhibited significantly higher relaxivities than Gd-DOTA and Gd(DO3A-HP) (ProHance®) (29, 35). The T_1 relaxivity of GODC was approximately two times higher than that of Gd-DOTA and Gd(DO3A-HP) at 1.5 T. The significant increase of T_1 relaxivity of GODC might be attributed to its relatively large molecular size and hydrodynamic volume. However, the relaxivity of GODC was lower in comparison to some dendrimer based Gd-DOTA contrast agents with similar molecular weight, such as the Gadomer 17 and PAMAM dendrimetic Gd conjugates (15, 22, 23). The relatively flexible hydrophilic backbone of the linear GODC polymer chains might partly compromise the slower-rotational-tumbling effect of macromolecules, resulting in limited increase of relaxivity. In comparison, the dendrimer based Gd chelates had more rigid structures, and thus was less restrained on the relaxivity enhancement.

As expected, the macrocyclic-chelate-polydisulfide GODC showed higher kinetic inertness than GDCC, the linear-chelate-polydisulfides. Since endogenous Zn(II) were the major metal species causing in vivo transmetallation of Gd(III)-based contrast agents, the preliminary stability study was carried out through in vitro incubation of the polydisulfides with Zn^{2+} to assess and compare the stability of GODC and GDCC. Little release of free Gd(III) ions from GODC were observed in the presence of Zn^{2+}, a consistent result as reported with other macrocyclic Gd(III) chelates (8, 31, 42). To the contrary, GDCC experienced gradual loss of Gd(III) over time during the incubation, showing lower kinetic inertness. High kinetic inertness of the new Gd(III)-based MRI contrast agent was critical to allow complete excretion of the agent from the body and minimize the potential toxic side effects associated with prolonged retention of Gd(III)-

based agents.

GODC was effective for contrast enhanced blood pool imaging, generating strong contrast enhancement in the heart, vasculature and the tumor periphery. In comparison to GDCC with similar molecular weight (34, 35), GODC appeared to produce longer blood pool enhancement, possibly due to its relatively slow degradation. Although characterized with slower degradation, the MR study revealed that GODC could still be readily excreted via renal filtration after in vivo degradation. Strong bladder enhancement was observed as early as 10 minutes post injection, indicating the excretion of degraded Gd(III) chelates. In comparison, the clinical agent Magnevist® resulted in shorter and weaker enhancement in the blood pool. The prolonged blood pool enhancement of GODC is mainly a result of its large hydrodynamic volume, which limited vascular extravasation, extented blood circulation and concentrated blood pool signals. In addition, the increased of relaxivity also contributed in the notable enhancement of blood pool signals during the MR examination. Stronger enhancement was generated in the tumor periphery using GODC in comparison with Magnetive®. However, little signal difference was observed in the tumor core between GODC and Magnevist®, which can be attributed to the high pressure in the necrotic tumor core that hindered the penetration of both agents. Overall, the new macrocyclic chelate based biodegradable macromolecular MR contrast agent GODC is more effective for contrast enhanced blood pool and tumor MRI than the small molecular clinical agent Magnevist®.

Conclusion

A new polydisulfide Gd-DOTA complex, GODC, was synthesized and evaluated as a biodegradable macromolecular MRI contrast agent (51). GODC demonstrated high kinetic stability against transmetallation with endogenous ions. It was readily reduced by endogenous thiols into smaller Gd(III) chelates or oligomers that could be easily excreted via renal filtration. GODC is a safe and effective biodegradable macromolecular MRI contrast agent promising for further development in clinical MR cardiovascular and cancer imaging

References

1. Barrett T, Brechbiel M, Bernardo M, Choyke PL. MRI of tumor angiogenesis. J Magn Reson Imaging. 2007;26(2):235-249.

2. Padhani AR. Dynamic contrast-enhanced MRI in clinical oncology: current status and future directions. J Magn Reson Imaging. 2002;16(4):407-422.

3. Lauffer RB. Paramagnetic metal complexes as water proton relaxation agents for NMR imaging: theory and design. Chem Rev. 1987;87(5):901-927.

4. Koretsky AP, Silva AC. Manganese-enhanced magnetic resonance imaging (MEMRI). NMR Biomed. 2004;17(8):527-531.

5. Hermann P, Kotek J, Kubicek V, Lukes I. Gadolinium(III) complexes as MRI contrast agents: ligand design and properties of the complexes. Dalton Trans. 2008(23):3027-3047.

6. Caravan P, Ellison JJ, McMurry TJ, Lauffer RB. Gadolinium(III) chelates as MRI contrast agents: structure, dynamics, and applications. Chem Rev. 1999;99(9):2293-2352.

7. Aime S, Cabella C, Colombatto S, Geninatti Crich S, Gianolio E, Maggioni F. Insights into the use of paramagnetic Gd(III) complexes in MR-molecular imaging investigations. J Magn Reson Imaging. 2002;16(4):394-406.

8. Aime S, Caravan P. Biodistribution of gadolinium-based contrast agents, including gadolinium deposition. J Magn Reson Imaging. 2009;30(6):1259-1267.

9. Bellin MF, Vasile M, Morel-Precetti S. Currently used non-specific extracellular MR contrast media. Eur Radiol. 2003;13(12):2688-2698.

10. Schalla S, Higgins CB, Saeed M. Contrast agents for cardiovascular magnetic resonance imaging. Current status and future directions. Drugs R D. 2002;3(5):285-302.

11. Turetschek K, Floyd E, Helbich T, Roberts TP, Shames DM, Wendland MF, Carter WO, Brasch RC. MRI assessment of microvascular characteristics in experimental breast tumors using a new blood pool contrast agent (MS-325) with correlations to histopathology. J Magn Reson Imaging. 2001;14(3):237-242.

12. Brasch RC. Rationale and applications for macromolecular Gd-based contrast agents. Magn Reson Med. 1991;22(2):282-287.

13. Goyen M, Shamsi K, Schoenberg SO. Vasovist-enhanced MR angiography. Eur Radiol. 2006;16 Suppl 2:B9-14.

14. Brasch R, Turetschek K. MRI characterization of tumors and grading angiogenesis using macromolecular contrast media: status report. Eur J Radiol. 2000;34(3):148-155.

15. Bumb A, Brechbiel MW, Choyke P. Macromolecular and dendrimer-based magnetic resonance contrast agents. Acta Radiol. 2010;51(7):751-767.

16. Lauffer RB, Parmelee DJ, Ouellet HS, Dolan RP, Sajiki H, Scott DM, Bernard PJ, Buchanan EM, Ong KY, Tyeklar Z, Midelfort KS, McMurry TJ, Walovitch RC. MS-325: a small-molecule vascular imaging agent for magnetic resonance imaging. Acad Radiol. 1996;3 Suppl 2:S356-358.

17. Barrett T, Kobayashi H, Brechbiel M, Choyke PL. Macromolecular MRI contrast agents for imaging tumor angiogenesis. Eur J Radiol. 2006;60(3):353-366.

18. Perreault P, Edelman MA, Baum RA, Yucel EK, Weisskoff RM, Shamsi K, Mohler ER, 3rd. MR angiography with gadofosveset trisodium for peripheral vascular disease: phase II trial. Radiology. 2003;229(3):811-820.

19. Shamsi K, Yucel EK, Chamberlin P. A summary of safety of gadofosveset (MS-325) at 0.03 mmol/kg body weight dose: Phase II and Phase III clinical trials data. Invest Radiol. 2006;41(11):822-830.

20. Schuhmann-Giampieri G, Schmitt-Willich H, Frenzel T, Press WR, Weinmann HJ. In vivo and in vitro evaluation of Gd-DTPA-polylysine as a macromolecular contrast agent for magnetic resonance imaging. Invest Radiol. 1991;26(11):969-974.

21. Helbich TH, Gossman A, Mareski PA, Raduchel B, Roberts TP, Shames DM, Muhler M, Turetschek K, Brasch RC. A new polysaccharide macromolecular contrast agent for MR imaging: biodistribution and imaging characteristics. J Magn Reson Imaging. 2000;11(6):694-701.

22. Bryant LH, Jr., Brechbiel MW, Wu C, Bulte JW, Herynek V, Frank JA. Synthesis and relaxometry of high-generation (G = 5, 7, 9, and 10) PAMAM dendrimer-DOTA-gadolinium chelates. J Magn Reson Imaging. 1999;9(2):348-352.

23. Misselwitz B, Schmitt-Willich H, Ebert W, Frenzel T, Weinmann HJ. Pharmacokinetics of Gadomer-17, a new dendritic magnetic resonance contrast agent. MAGMA. 2001;12(2-3):128-134.

24. Ladd DL, Hollister R, Peng X, Wei D, Wu G, Delecki D, Snow RA, Toner JL, Kellar K, Eck J, Desai VC, Raymond G, Kinter LB, Desser TS, Rubin DL. Polymeric gadolinium chelate magnetic resonance imaging contrast agents: design, synthesis, and properties. Bioconjug Chem. 1999;10(3):361-370.

25. Caravan P. Strategies for increasing the sensitivity of gadolinium based MRI contrast agents. Chem Soc Rev. 2006;35(6):512-523.

26. Rohrer M, Bauer H, Mintorovitch J, Requardt M, Weinmann HJ. Comparison of magnetic properties of MRI contrast media solutions at different magnetic field strengths. Invest Radiol. 2005;40(11):715-724.

27. Aime S, Castelli DD, Crich SG, Gianolio E, Terreno E. Pushing the sensitivity envelope of lanthanide-based magnetic resonance imaging (MRI) contrast agents for molecular imaging applications. Acc Chem Res. 2009;42(7):822-831.

28. Brasch R, Pham C, Shames D, Roberts T, van Dijke K, van Bruggen N, Mann J, Ostrowitzki S, Melnyk O. Assessing tumor angiogenesis using macromolecular MR imaging contrast media. J Magn Reson Imaging. 1997;7(1):68-74.

29. Lu ZR, Ye F, Vaidya A. Polymer platforms for drug delivery and biomedical imaging. J Control Release. 2007;122(3):269-277.

30. Sieber MA, Lengsfeld P, Frenzel T, Golfier S, Schmitt-Willich H, Siegmund F, Walter J, Weinmann HJ, Pietsch H. Preclinical investigation to compare different gadolinium-based contrast agents regarding their propensity to release gadolinium in vivo and to trigger nephrogenic systemic fibrosis-like lesions. Eur Radiol. 2008;18(10):2164-2173.

31. Thomsen HS, Morcos SK. Nephrogenic systemic fibrosis and nonionic linear chelates. AJR Am J Roentgenol. 2007;188(6):W580; author reply W581.

32. Lu ZR, Mohs AM, Zong Y, Feng Y. Polydisulfide Gd(III) chelates as biodegradable macromolecular magnetic resonance imaging contrast agents. Int J Nanomedicine. 2006;1(1):31-40.

33. Zong Y, Wang X, Goodrich KC, Mohs AM, Parker DL, Lu ZR. Contrast-enhanced MRI with new biodegradable macromolecular Gd(III) complexes in tumor-bearing mice. Magn Reson Med. 2005;53(4):835-842.

34. Zong Y, Guo J, Ke T, Mohs AM, Parker DL, Lu ZR. Effect of size and charge on pharmacokinetics and in vivo MRI contrast enhancement of biodegradable polydisulfide Gd(III) complexes. J Control Release. 2006;112(3):350-356.

35. Lu ZR, Wu X. Polydisulfide Based Biodegradable Macromolecular Magnetic Resonance Imaging Contrast Agents. Isr J Chem. 2010;50(2):220-232.

36. Ersoy H, Rybicki FJ. Biochemical safety profiles of gadolinium-based extracellular contrast agents and nephrogenic systemic fibrosis. J Magn Reson Imaging. 2007;26(5):1190-1197.

37. Morcos SK. Extracellular gadolinium contrast agents: differences in stability. Eur J Radiol. 2008;66(2):175-179.

38. Cacheris WP, Quay SC, Rocklage SM. The relationship between thermodynamics and the toxicity of gadolinium complexes. Magn Reson Imaging. 1990;8(4):467-481.

39. Laurent S, Elst LV, Copoix F, Muller RN. Stability of MRI paramagnetic contrast media: a proton relaxometric protocol for transmetallation assessment. Invest Radiol. 2001;36(2):115-122.

40. Puttagunta NR, Gibby WA, Smith GT. Human in vivo comparative study of zinc and copper transmetallation after administration of magnetic resonance imaging contrast agents. Invest Radiol. 1996;31(12):739-742.

41. White GW, Gibby WA, Tweedle MF. Comparison of Gd(DTPA-BMA) (Omniscan) versus Gd(HP-DO3A) (ProHance) relative to gadolinium retention in human bone tissue by inductively coupled plasma mass spectroscopy. Invest Radiol. 2006;41(3):272-278.

42. Wu X, Zong Y, Ye Z, Lu ZR. Stability and biodistribution of a biodegradable macromolecular MRI contrast agent Gd-DTPA cystamine copolymers (GDCC) in rats. Pharm Res. 2010;27(7):1390-1397.

43. Lu ZR, Wang X, Parker DL, Goodrich KC, Buswell HR. Poly(l-glutamic acid) Gd(III)-DOTA conjugate with a degradable spacer for magnetic resonance imaging. Bioconjug Chem. 2003;14(4):715-719.

44. Xu R, Wang Y, Wang X, Jeong EK, Parker DL, Lu ZR. In Vivo evaluation of a PAMAM-cystamine-(Gd-DO3A) conjugate as a biodegradable macromolecular MRI contrast agent. Exp Biol Med (Maywood). 2007;232(8):1081-1089.

45. Wang X, Feng Y, Ke T, Schabel M, Lu ZR. Pharmacokinetics and tissue retention of (Gd-DTPA)-cystamine copolymers, a biodegradable macromolecular magnetic resonance imaging contrast agent. Pharm Res. 2005;22(4):596-602.

46. Andersson A, Lindgren A, Hultberg B. Effect of thiol oxidation and thiol export from erythrocytes on determination of redox status of homocysteine and other thiols in plasma from healthy subjects and patients with cerebral infarction. Clin Chem. 1995;41(3):361-366.

47. Deneke SM. Thiol-based antioxidants. Curr Top Cell Regul. 2000;36:151-180.

48. Lu ZR, Parker DL, Goodrich KC, Wang X, Dalle JG, Buswell HR. Extracellular biodegradable macromolecular gadolinium(III) complexes for MRI. Magn Reson Med. 2004;51(1):27-34.

49. Zong Y, Wang X, Jeong EK, Parker DL, Lu ZR. Structural effect on degradability and in vivo contrast enhancement of polydisulfide Gd(III) complexes as biodegradable macromolecular MRI contrast agents. Magn Reson Imaging. 2009;27(4):503-511.

CHAPTER 4

A NEUTRAL POLYDISULFIDE CONTAINING GD(III) DOTA MONOAMIDE AS A REDOX- SENSITIVE BIODEGRADABLE MACROMOLECULAR MRI CONTRAST AGENT

Introduction

Gadolinium chelates with high thermodynamic stability are predominantly used as clinical MRI contrast agents for the diagnosis of life-threatening diseases, including cancer and cardiovascular diseases (1,2). However, most of the clinical Gd(III) contrast agents are nonspecific small molecules with relatively low relaxivities and rapid vascular extravasation rates (3). In order to overcome these limitations, macromolecular Gd(III) have been developed with improved relaxivities, specificity, and stability. Macromolecular Gd(III) MRI contrast agents are normally synthesized through the covalent incorporation of small molecular Gd(III) chelates into biocompatible macromolecules such as proteins, dendrimers, and natural and syntetic polymers (7-9). This allows the agents to have significantly improved physical chemical and biological properties, including a two- to fourfold relaxivity increase due to the reduced molecular tumbling of Gd(III) chelates (10, 11). Additionally, macromolecular MRI agents have been shown to have an enhanced tumor accumulation by the enhanced permeability and

retention (EPR) effect, as well as a prolonged blood pool circulation (12, 13).While macromolecular agents have been successful in preclinical studies, their translation into clinical application has been hindered owing to safety concerns arising from the ineffective excretion, which can cause the release and long-term deposition of the toxic Gd^{3+} ions (14, 15).

To facilitate the rapid excretion of Gd(III) chelates, environmentally labile chemical bonds have been incorporated into polymeric systems. These bonds allow for the breakdown of polymer backbones or the release of Gd(III) chelates from macromolecules (16,17). Examples of these cleavable bonds include acid labile bonds (18,19), redox-sensitive bonds (20–22) and enzymatically degradable bonds (23–25). These biodegradable macromolecular contrast agents have maintained the advantages of macromolecular contrast agents for blood pool and tumor imaging and shown minimal long-term tissue accumulation. Previously, we have designed and synthesized redox-sensitive polydisulfide Gd-DTPA complexes as extracellular degradable macromolecular contrast agents (7,26–28). These complexes have a backbone consisting of disulfide bonds, which are environmentally labile in vivo. The disulfide bonds are graduallreduced by the plasma thiols to produce monomeric or oligomeric Gd(III) complexes, which are rapidly excreted via renal filtration (29). The polydisulfide contrast agents produced significant tumor contrast enhancement. However, it was found that these Gd-DTPA complexes exhibit low kinetic inertness and release toxic Gd(III) ions by transmetallation with endogenous metal ions, mainly Zn(II) ions (30). Agents with low kinetic stability are likely to cause nephrogenic systemic fibrosis (NSF) in a small portion of the patients with compromised renal function (31,32). Macrocyclic Gd(III) chelates have shown high

kinetic stability with no transmetallation with endogenous metal ions and appeared safe from NSF (31–33).

A new generation of polydisulfides containing macrocyclic Gd(III) chelates have been designed and synthesized to further improve the kinetic stability of the Gd(III) chelates in redox-sensitive biodegradable macromolecular MRI contrast agents. (N6-lysyl) lysine-(Gd-DOTA) monoamide and 3-(2-carboxyethyldisulfanyl) propanoic acid copolymers (GODC) demonstrated high kinetic inertness and superior image enhancement (21). GODC has a free carboxylic group on each monomer unit, and is anionic under physiological pH. This has a significant impact on its in vivo properties, including pharmacokinetics and biodistribution.

In this study, we synthesized a neutral macrocyclic Gd(III) chelate containing polydisulfide N1-lysylethylenediamine Gd-DOTA monoamide and dithiobispropionic acid copolymers (GOLS). This agent is a neutral, redox-sensitive, and biodegradable macromolecular contrast agent that was prepared by the condensation copolymerization of N1-lysylethylenediamine DOTA monoamide and dithiobis(succinimidylpropionate), followed by complexation with $Gd(OAc)_3$. In addition to analyzing the physiochemical properties, the chelation stability, pharmacokinetics, and biodistribution of different polydisulfide Gd(III) complexes were analyzed in vivo. These studies were performed in comparison to the clinical contrast agent Gd(HP-DO3A) and a previously reported polydisulfide Gd-DTPA complex, GDCC (27), in a mouse model. The effectiveness of GOLS for contrast-enhanced blood pool and tumor MRI was also evaluated.

Experimental Section

Materials

2-(1H-benzotriazole-1-yl)-1,1,3,3-tetramethyluronium hexafluorophosphate (HBTU) and benzotriazol-1-yl-oxytripyrrolidino-phosphonium hexafluorophosphate (PyBOP) were purchased from Nova Biochem (Darmstadt, Germany). 1,4,7,10-Tetraazacyclododecane-1, 4,7-*tris*-*tert*-butyl acetate-10-acetic acid [DOTA-*tris*(*t*-Bu)] was purchased from TCI America (Portland, OR). *N,N*-Diisopropylethylamine (DIPEA) and trifluoroacetic acid (TFA) were purchased from Alfa Aesar (Ward Hill, MA, USA). Lysine methyl ester dihydrochloride, di-tert-butyl dicarbonate (Boc_2O), sodium bicarbonate, ethylenediamine, 3,3´-dithiobis[sulfosuccinimidylpropionate] (DTTSP) and $Gd(OAc)_3$ were purchased from Sigma-Aldrich, Inc. (Louis, MO, USA). GODC was synthesized as previously described (21). All reagents were used without further purification unless otherwise stated.

Synthesis of N^1-lysylethylenediamine DOTA Monoamide

N^{ε}-Boc-N^{α}-Boc-L-lysine methyl ester (34) and N^{ε}-Boc-N^{α}-Boc-L-lysine N-(2-aminoethyl) amide (35) were synthesized based on reported methods. N^{ε}-Boc-N^{α}-Boc-L-lysine N-(2-aminoethyl) amide (2.6 g, 6.8 mmol) and DOTA-tris(t-Bu) (3.2 g, 5.7 mmol) was dissolved in DMF (8 mL). The coupling agent, PyBOP (3.5 g, 6.8 mmol), as well as HBTU (1.3 g, 6.8 mmol) and DIPEA (1.2 mL, 6.8 mmol), were added to the mixture. The reaction solution was stirred at room temperature overnight. After the reaction, EtOAc (80 mL) was added, followed by removal of the solvent via rotary evaporation. The residue was purified through preparative silica TLC (EtOAc:DCM = 2:3). The product

was obtained as colorless crystalline compound (yield = 56%). The purified product was de-protected by mixing with TFA (10 mL) and stirred overnight at room temperature. The desired compound N^1-lysylethylenediamine Gd-DOTA monoamide was precipitated out in ether to give a colorless compound (yield = 92%). 1H NMR (300 Hz, D_2O): 1.6 (m, 3H), 1.9 (m, 3H), 2.1 (m, 3H), 3.1 (m, 5H), 3.4 (m, 18H), 4.0 (m, 7H). MALDI-TOF-MS: m/z = 574.4 (M^+).

Synthesis of N^1-lysylethylenediamine Gd-DOTA Monoamide and Dithiobispropionic Acid Copolymer (OLS) and Its Gd(III) Complex (GOLS)

GOLS was synthesized using a method similar to one previously reported (28). Briefly, the polymerization was carried out by slowly adding 3,3' -dithiobis[sulfosuccinimidylpropionate] (DTTSP) (0.6 g, 1.1 mmol) portion by portion to the concentrated aqueous solution of N^1-lysylethylenediamine DOTA monoamide (0.8 g, 1.1 mmol in 0.7 mL de-ionized water) while stirring. The mixture was stirred at room temperature for 4 h after the addition of DTTSP. The product was purified via dialysis against de-ionized water using dialysis membrane with a molecular weight cut-off of 6000–8000 Da, and freeze-dried to yield the white polymer ligand (OLS). The yield of the reaction was 16% after purification. Gd(III) complexation was then carried out by stirring the mixture of the polymeric ligand OLS and twofold excess of $Gd(OAc)_3$ in de-ionized water for 48 h at pH 6 and room temperature. The polymeric Gd(III) complex was purified through size exclusion chromatography using a Sephadex® G-50 column. Xylenol orange was added as an indicator to monitor the complexation and purification.

The final product GOLS was obtained after lyophilization as white solid. The purity and apparent molecular weight of OLS and GOLS were determined using size exclusion chromatography on an AKTA FPLC system with a Superose™ 12 column (GE Healthcare Life Sciences). The column was calibrated using water soluble poly[N-(2-hydroxylpropyl)methacrylamide] (HPMA) standards with a series of different molecular weights (Mn = 14, 23, 32 and 47 kDa). The Gd(III) content of GOLS was determined using inductive coupled plasma–optical emission spectrometry (ICP-OES, Perkin-Elmer). The hydrodynamic size of GOLS in solution was determined using dynamic light scattering (DLS). The DLS experiment was carried out using a Brookhaven BI- 200SM goniometer and BI-9000AT digital correlator equipped with a He–Ne laser (λ = 633 nm) at room temperature. The aqueous solution of GOLS (1.33 mg/mL) was filtered through a 0.22 μm filter, and then measured at a scattering angle of 90. A Nanosphere™ polystyrene size standard (diameter = 102 nm ± 3 nm) (Thermo Scientific, Waltham, MA, USA) was analyzed in line to confirm accuracy.

Relaxivity Measurement

The T1 relaxivity of GOLS was determined on a Bruker minispec® relaxometer (1.5 T, 60 Hz) at 37 °C, and a Bruker 7.0 T MR BioSpec small animal scanner. GOLS solutions containing a gradient of 0.2, 0.4, 0.6 and 0.8mMof Gd(III) were prepared. At 1.5 T, the T1 values of these solutions were measured with the relaxometer using an inversion–recovery pulse sequence. Similarly, Bruker's inversion recovery sequence with an echo planar (EPI) readout was used to determine the T1 values at 7.0 T. The longitudinal relaxivity (r1) was calculated from the slope of the 1/T1 versus Gd(III)

concentration plot. The transverse relaxivity (r2) was measured similarly; the T2 values were determined using a Carr–Purcell–Meiboom–Gill (CPMG) spin echo sequence at 1.5 T. Additionally, Bruker's standard multi-slice–multi-echo (MSME) sequence was used to measure the T2 values at 7.0 T (TE = variable, TR = 2000 ms, flip angle = 180°, slice thickness = 1 mm, slice number = 5, averages = 2, matrix = 128 × 64, field of view = 3 cm × 3 cm, resolution = 0.0234 × 0.3 mm). The Gd(III) content of the sample was re-confirmed using ICP-OES after the relaxivity measurement.

In Vitro Degradation of GOLS

GOLS (0. 42 mM-Gd) and cysteine (15 μM) were incubated together in PBS buffer (pH=7.4) at room temperature for 6 hours. The change of molecular weight of GOLS over time during the incubation was monitored using size exclusion chromatography on an AKTA® FPLC system with a Superose® 12 column.

In Vitro Kinetic Stability of GOLS

GOLS (0.42 mM-Gd) was incubated with $ZnCl_2$ (50 μM) in PBS buffer at physiological pH under 37°C for 2 hrs. Samples before and at 30, 60 and 120 minutes of incubation were collected, then went through the PD-10 column (GE Health Science) to separate the polymer bound and free Gd(III) species. The Gd(III) content in polymer after separation was determined using ICP-OES (Perkin-Elmers). The percentage of polymer bound Gd(III) post-incubation versus pre-incubation was calculated. The value was compared with that of our previously reported linear-chelates-based polymeric agent, Gd-DTPA cystamine copolymers (GDCC, 0.42 mM Gd). In addition, GOLS and GDCC

incubated with Zn^{2+} free PBS buffer were used as negative controls.

MRI Experiment

Female BALB/c mice weighing 18-22 g were purchased from Charles River (Wilmington, MA, USA). The animals were cared for under an animal protocol approved by the IACUC of Case Western Reserve University. 4T1 mouse breast cancer cells (5 x 10^4 cells) were inoculated into the inguinal mammary fat pads of each mouse, generating an orthotopic mouse model of malignant breast cancer. Contrast-enhanced MR examinations were performed when the tumor size reached 0.5-1.0 cm in diameter, as measured by a caliper. Anaesthetization of the tumor bearing mice was initially conducted using 2.5%-3.5% of isoflurane in oxygen, and then maintained with 1.5%-2.5% of isoflurane during the MR examination. The animals were kept warm at 34°C using a temperature-controlling air conditioning system. Parameters such as temperature, respiration and electrocardiograms (ECGs) of the mice were monitored during image acquisition to ensure steady physical conditions. The contrast agent was intravenously administered via tail vein at the standard clinical dose of 0.1 mmol-Gd kg^{-1}. A clinical agent Gd(HP-DO3A) (Bracco, Milan, Italy) was delivered at the same dose, as a control. MR diagnosis was performed before and at 1, 5, 10, 15 and 20 minutes post injection using a Bruker 7.0 T MR Biospec small animal scanner. A 3D FLASH pulse sequence (TE=2.6, TR=8.5, flip angle=25°, slice thickness=1 mm, slice number=32, average=3, matrix=100×512, field of view=10 cm × 3 cm, resolution=0.195 mm × 0.3 mm) and a 2D spin echo sequence (TE=8.06 ms, TR=500 ms, flip angle=90°, slice thickness=1.2 mm, slice number=16, average=2, matrix=128×128, FOV=3cm × 3 cm, resolution=0.234 mm

× 0.234 mm) were used to acquire the MR images. Three animals were used for each contrast agent.

MR Data Analysis

MR image analysis was performed using Bruker BioSpec Topspin software. Regions of interest (ROIs) were set in the heart (signal from blood), tumor and thigh muscle. Contrast to noise ratios (CNR) were calculated at each time point and averaged from different mice (n =3) for the organ/tissue. The CNR in the tumor was calculated using the following equation: $CNR= (St - Sm)/(\sigma n)$, where St and Sm denote the signal in tumor and thigh muscle and σn is the standard deviation of noise estimated from the background air. The CNR in the blood was calculated using the same equation, where St and Sm denote the signal in blood and thigh muscle. The p values were calculated using Student's two-tailed t-test, assuming statistical significance at $p < 0.05$.

Biodistribution Study

The biodistribution of GOLS was determined at 2-day and 10-day post injection in comparison with GODC, GDCC and Gd(HP-DO3A). At each time point, a group of BALB/c (male and female) were used for each agent. The contrast agent was administered at a dose of 0.1 mmol Gd/kg^{-1} via tail vain injection. The animals were sacrificed with an overdose of isoflurane, and the tissue samples (heart, spleen, lung, muscle, femur, skin, brain, liver and kidney) were collected and weighed. All the samples were dried in the 50°C oven for 3 days before dissolving in 1.0 ml of concentrated nitric acid (70%). The samples were then ten-fold diluted with de-ionized water, followed by

centrifugation at 4000 rpm for 25 min. The supernatant was collected for the determination of Gd content using ICP-OES.

In Vivo Chelation Stability

The *in vivo* chelation stability of GOLS was determined in BALB/c mice in comparison with GODC, GDCC and Gd(HP-DO3A). A total of 16 mice (male and female) were randomly divided into four groups (n=4 each) for the four contrast agents. The mice were anesthetized with 1.5-2.5% of isoflurane in oxygen, and administered with the contrast agents at a dose of 0.1 mmol-Gd kg^{-1} via tail vein injection. The mice were immediately placed into metabolic cages after the injection. Urine samples were collected during the period of 8 hrs preinjection and 0-8, 8-16, 16-24, and 24-48 hrs post injection from the metabolic cages. The urine samples were appropriately diluted using de-ionized water, then filtered to collect the filtrate. The contents of Gd(III), Zn(II), Cu (II) and Ca(II) in the filtrate of the urine samples were determined by ICP-OES.

Results

Synthesis of N^1-lysylethylenediamine Gd-DOTA Monoamide
and Dithiobispropionic Acid Copolymers (GOLS)

The DOTA containing monomer, N^1-lysylethylenediamine DOTA monoamide, was first synthesized through the carboxyl-amine coupling reactions (Figure 4.1). The neutral biodegradable macromolecular MRI contrast agent, N^1-lysylethylenediamine Gd-DOTA monoamide and dithiobispropionic acid copolymers (GOLS), was synthesized through condensation polymerization of the DOTA monoamide and 3,3′-

dithiobis[sulfosuccinimidylpropionate] (DTTSP) (Figure 4.2). The structure of the monomer N^1-lysylethylenediamine Gd-DOTA monoamide was verified using ^{1}H-NMR and MALDI-TOF mass spectrometry. The number average and weight average molecular weight of the polymeric ligand OLS was 18.4 and 29.3 kDa, respectively. After complexation, the final product of GOLS were purified and fractionated through size exclusion chromatography using a Sephadex® G-50 column. GOLS with number average and weight average molecular weight of GODC of 23.0 and 24.6 kDa were collected for *in vivo* animal studies. The hydrodynamic diameter of the GOLDS was around 3 nm as determined by DLS. The Gd(III) content in the agent was 16.1% (w/w) as determined by ICP-OES, corresponding to a complexation efficiency of 94.7% as compared with the calculated Gd content (17.0%, w/w). The longitudinal (r_1) and transverse relaxivity (r_2) of GOLS were 7.20 $mM^{-1}s^{-1}$ and 9.70 $mM^{-1}s^{-1}$ respectively at 1.5 T, 37^{o}C, approximately twice that of Gd(HP-DO3A) (ProHance®, 4.1 $mM^{-1}s^{-1}$ at 1.5T, 37°C). Similarly, the longitudinal and traverse relaxivities of GOLS at 7.0 T were r_1 = 6.62 $mM^{-1}s^{-1}$ and r_2 = 8.92 $mM^{-1}s^{-1}$.

Degradability of GOLS

The polydisulfide structure of GOLS was designed so that the polymers could be readily degraded and excreted via renal filtration *in vivo* through the disulfide-thiol exchange reaction. The degradability of GOLS was firstly demonstrated via an *in vitro* incubation study with *L*-cysteine, the most abundant free thiols in plasma. As thown in Figure 4.3, the number average molecular weight of GODC changed from 23.0 kDa

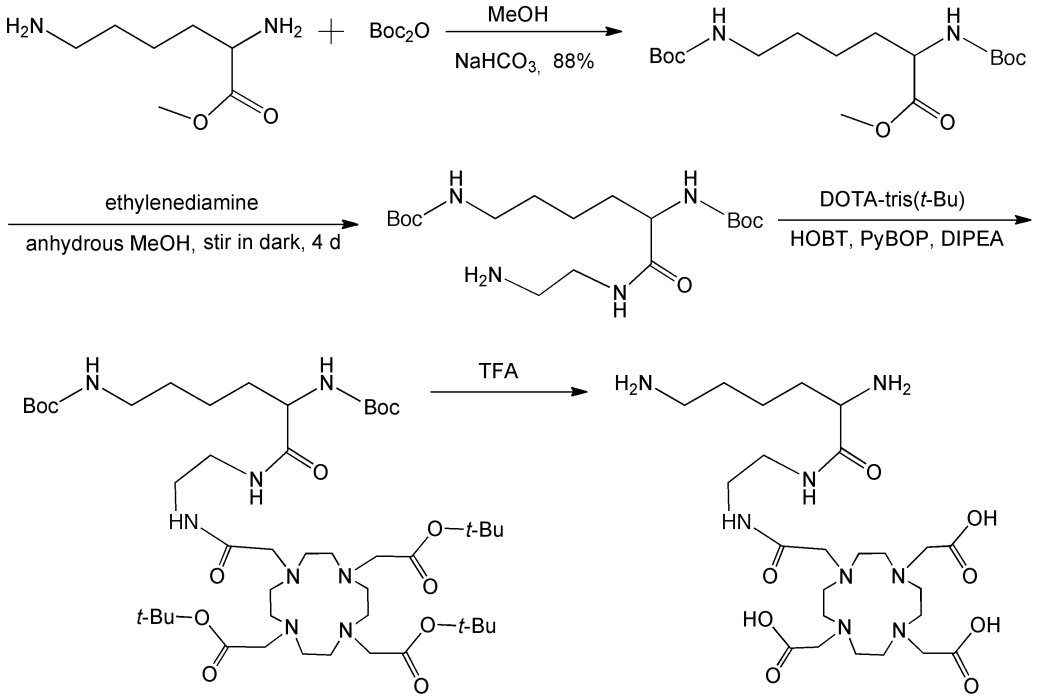

Figure 4.1. Synthetic scheme of N^1-lysylethylenediamine Gd-DOTA monoamide.

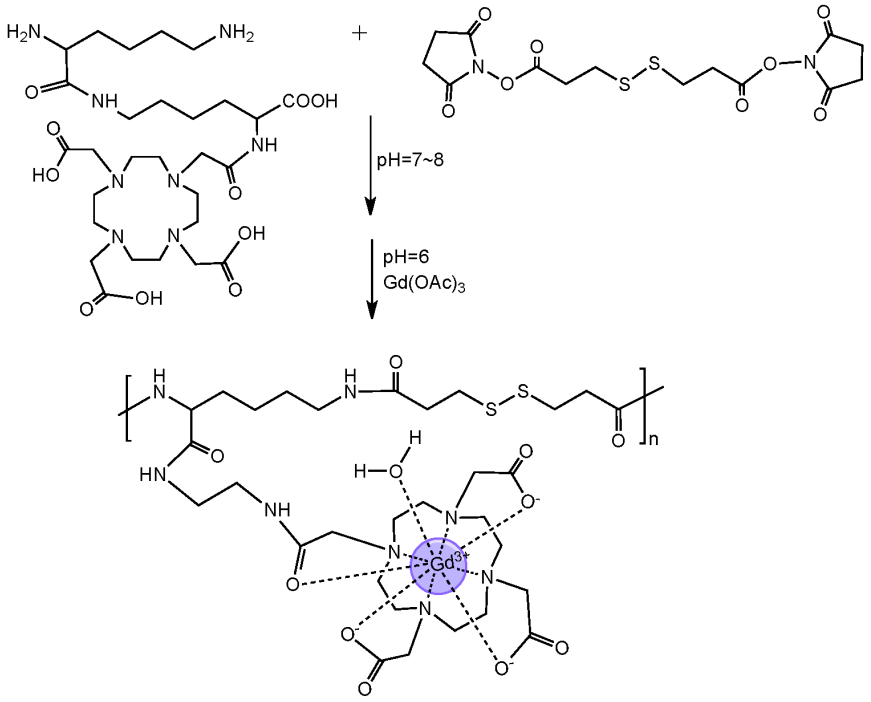

Figure 4.2. Synthetic scheme of N^1-lysylethylenediamine Gd-DOTA monoamide and dithiobispropionic acid copolymers (GOLS).

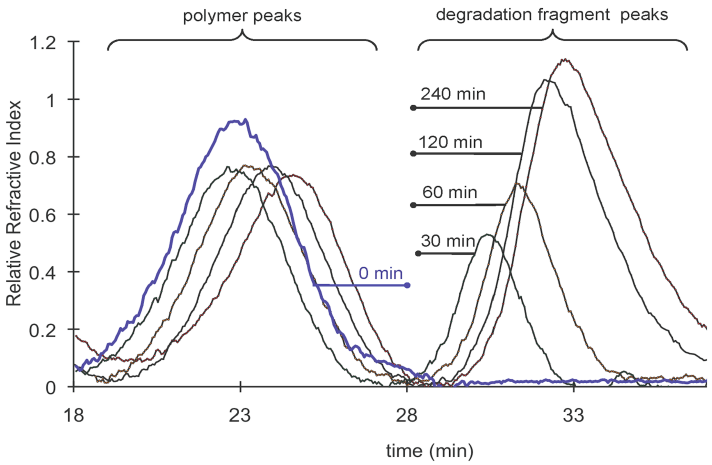

Figure 4.3. The apparent molecular weight (MW) distribution of GOLS (0.42 mM Gd) before (0 min) and after incubation with L-cysteine (15 μM) in PBS buffer for 30, 60, 120, and 240 min at 37 °C. The apparent molecular weight distribution was measured by size exclusion chromatograms. Before incubation (0 min), only the polymer peak of 23.0 kDa (peak at 23 min) was observed. With incubation time of 30, 60, 120, and 240 min, the MW of the polymer decreased to 23.0 kDa (peak at 22 min), 22.5 kDa (peak at 23 min), 21.2 kDa (peak at 24 min), and 19.0 kDa (peak at 25 min), with an increase of their corresponding small molecular fractions (peaks from 30 to 40 min).

before incubation to 23.0 kDa, 22.5 kDa, 21.2 kDa and 19.0 at 30, 60, 120 and 240 min during the incubation. Consequently, an increase of small molecular fractions (peaks from 30-40 min) were observed over time, indicating the process of degradation via incubation with free thiols.

In Vitro Chelation Stability of GOLS

The kinetic stability of GOLS against endogenous transmetallation was evaluated *in vitro* through incubation studies with $ZnCl_2$ at plasma concentrations at physiological conditions mimicking the *in vivo* environment. Zn(II) was the major metal species involved in the transmetallation of Gd(III)-based contrast agents in vivo. As shown in Figure 4.4, a gradual loss of Gd(III) in polymer was observed with GDCC from the initial

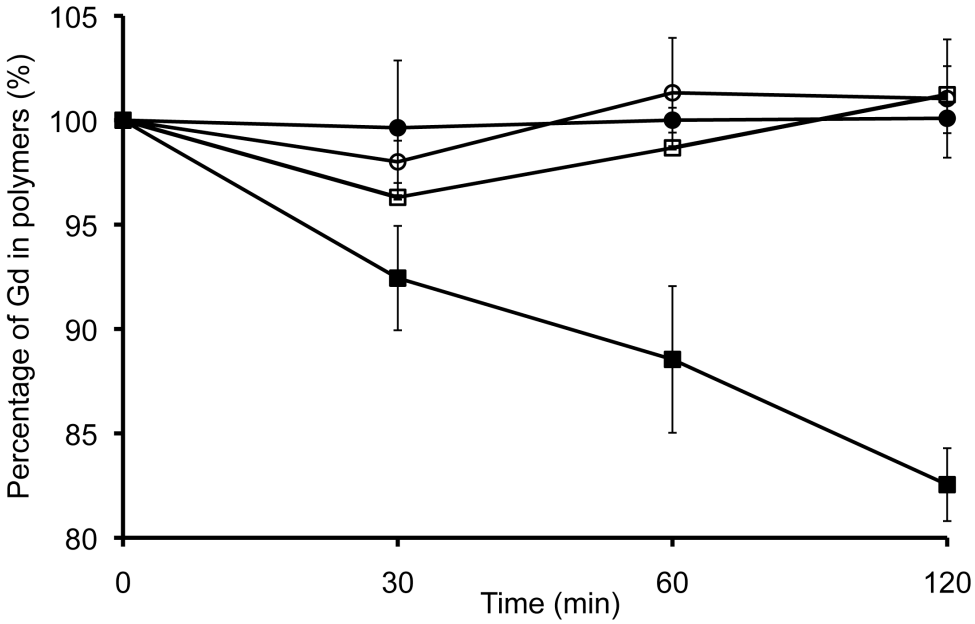

Figure 4.4. The Gd(III) content in GDCC (square) and GOLS (circle) before and in the incubation in PBS buffer with $ZnCl_2$ (50 μM, filled) and without $ZnCl_2$ (open) for 30, 60, and 120 min.

100 % to 92% at 30 min, 88 % at 90 min and 82 % at 120 min during the *in vitro* Zn^{2+}incubation. In contrast, negligible loss of Gd was observed with GOLS, similar to what was oberved with the control samples of GDCC and GOLS incubated with Zn(II) free PBS buffer. The results demonstrated the polydisulfide containing macrocyclic Gd(III) chelate (GOLS) possessed high kinetic inertness against transmetallation.

In Vivo MR Imaging

Figure 4.5 shows the T1-weighted 3D maximum intensity projection MR images of mice bearing orthotopic 4T1 mouse malignant tumor before and after intravenous injection of GOLS and Gd(HP-DO3A). The blood pool enhancement generated by GOLS was gradually decreased, but still visible at 10 min post injection. In comparison, the

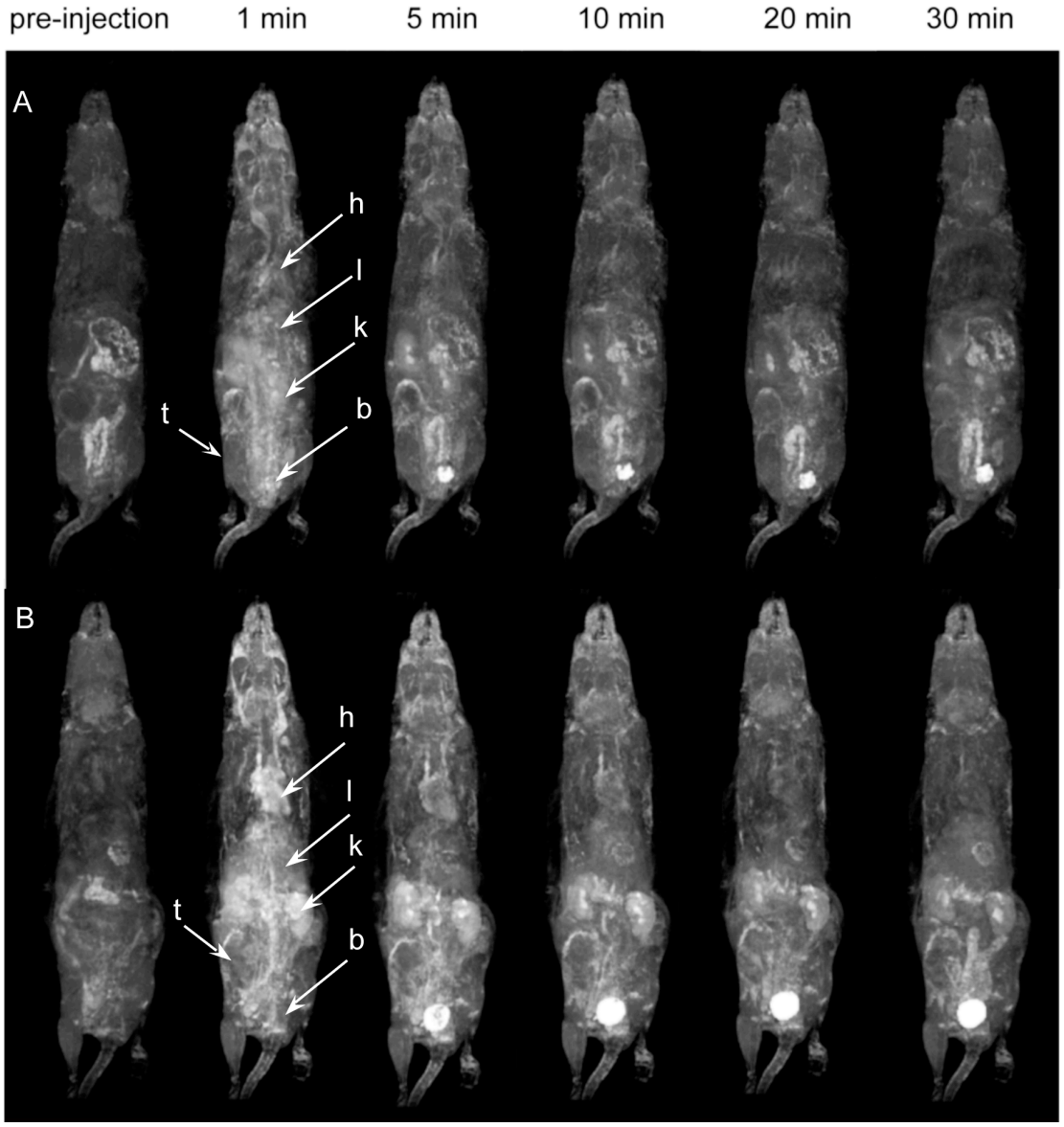

Figure 4.5. 3D maximum intensity projection images (coronal view) of mice bearing 4T1 breast cancer before and at 1, 5, 10, 20, and 30 min after injection of Gd(HP-DO3A) (A) and GOLS (B) at a dose of 0.1 mmol Gd kg^{-1}. The major organs are marked as h (heart), l (liver), k (kidney), b (bladder), and t (tumor).

Gd(HP-DO3A) generated blood pool signals that decreased sharply in 1 min post injection, and become negligible at 5 min post injection. Signal intensity in the kidneys decreased over time, while that in the urinary bladder increased for both agents, indicating the elimination of both agents through kidney filtration. The bladder enhancement was first observed at 1 min post injection for Gd(HP-DO3A), and 5 min for GOLS, indicating slightly slower excretion of the macromolecular agent. Figure 4.6 shows the axial T1-weighted 2D spin-echo tumor images before and at various time points after injection of GOLS and Gd(HP-DO3A). GOLS generated more significant and prolonged signal enhancement in the tumor than Gd(HP-DO3A). As shown in Figure 4.7, GOLS generated significantly higher CNR in blood than Gd(HP-DO3A) in the first 10 min post injection. GOLS also produced a more than twofold CNR increase in the tumor compared with Gd(HP-DO3A) for at least 30 min.

Biodistribution

Figure 4.8 shows the biodistribution of Gd(III) in the major organs and tissues, including the heart, spleen, lung, muscle, femur, skin, brain, liver, and kidney of mice, at 2 days and 10 days after intravenous injection of GOLS, GODC, GDCC, and Gd(HP-DO3A) at 0.1mmol Gd kg^{-1}. The polydisulfide agents GOLS, GODC, and GDCC had similar low Gd(III) distribution in the heart, spleen, lung, muscle, femur, skin, and brain at both time points to Gd(HP-DO3A). The agents showed higher Gd(III) concentration in the liver and kidney than in the other organs. The neutral polydisulfide agent GOLS showed much lower accumulation in the liver and kidneys than the negatively charged agent GODC and polydisulfide with linear Gd(III) chelates GDCC ($p < 0.05$) at 2 days

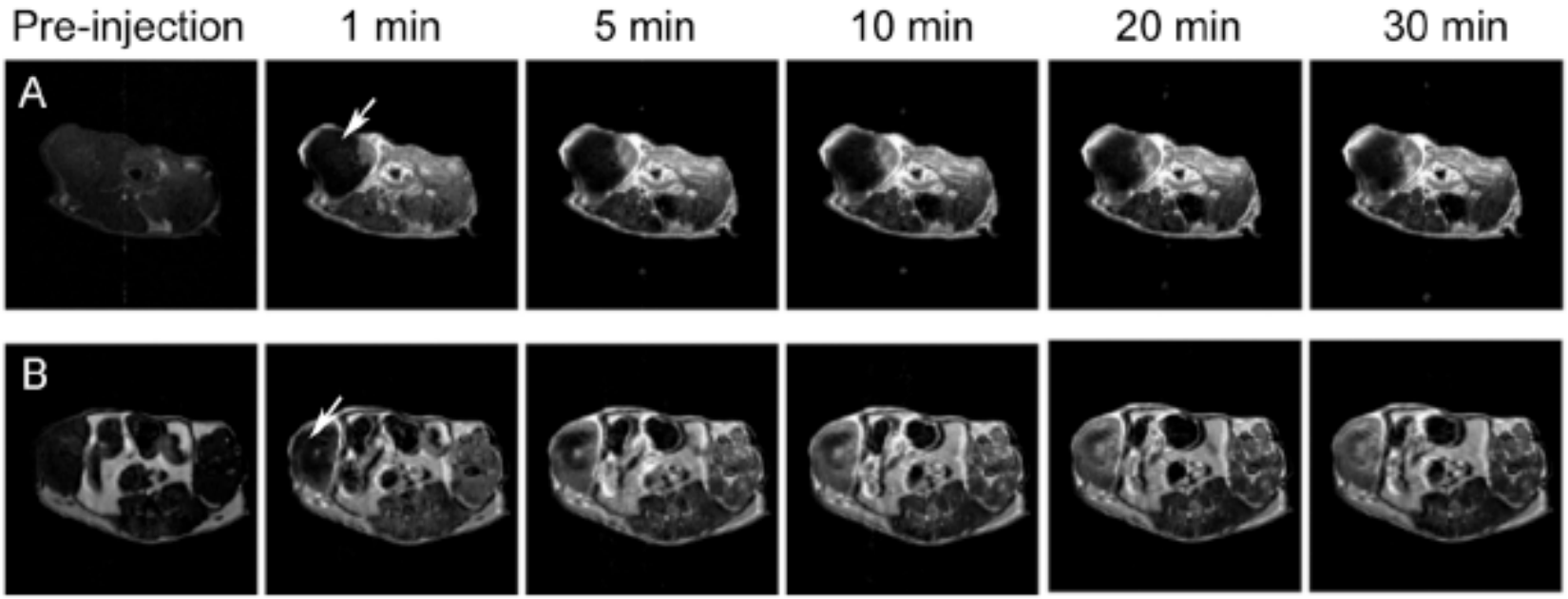

Figure 4.6. Axial 2D spin echo images of mice bearing 4T1 orthotopic breast tumor before and at 1, 5, 10, 20, and 30 min post injection of Gd(HP-DO3A) (A) and GOLS (B) at a dose of 0.1 mmol Gd kg^{-1}. The arrow points to the tumor.

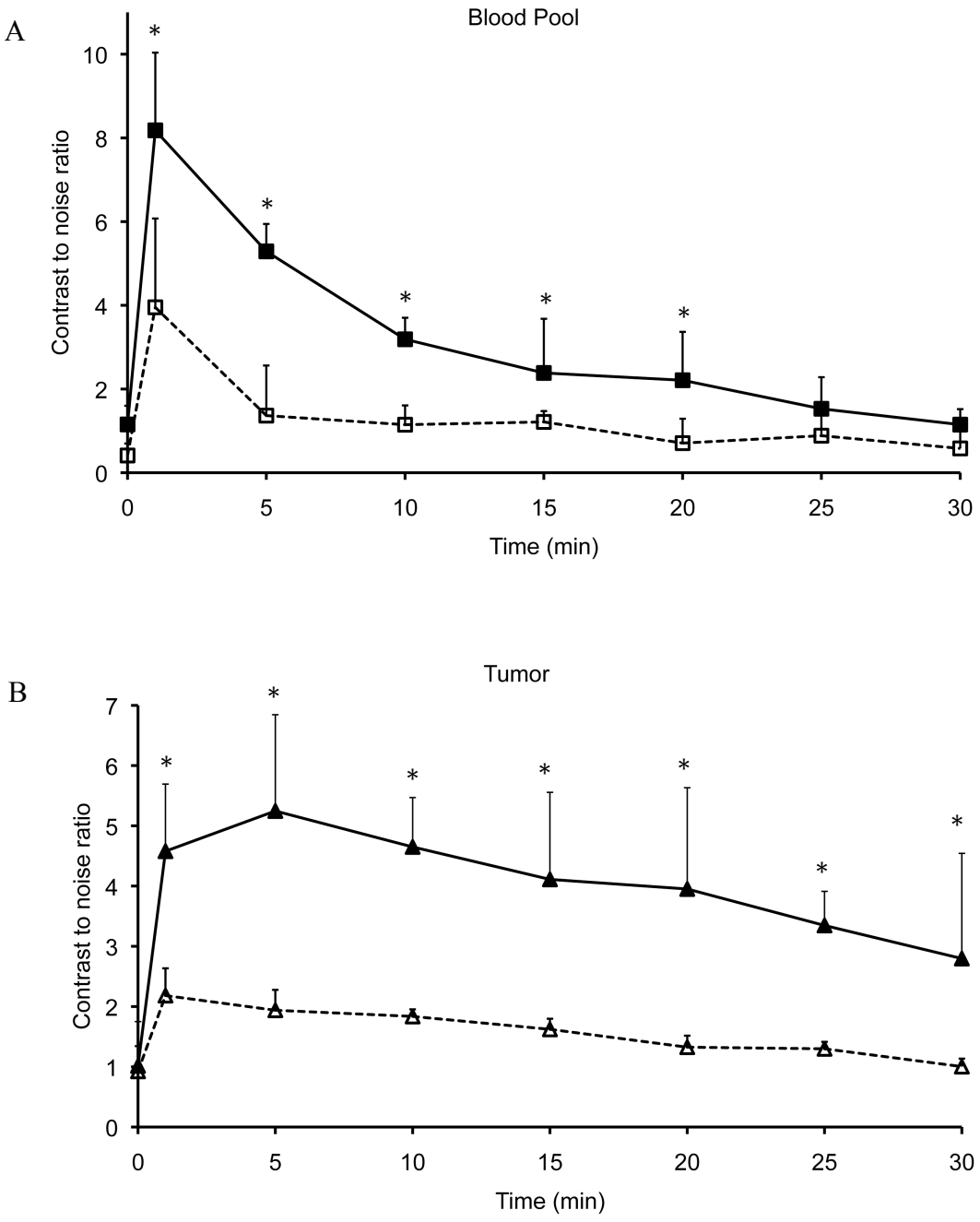

Figure 4.7. Contrast-to-Noise Ratio (CNR) of blood pool (A), and tumor (B) of mice bearing malignant breast cancer before and at different time points after administration of Gd(HP-DO3A) (open) and GOLS (filled) (*$p < 0.05$). Data presented as mean ± SD.

A

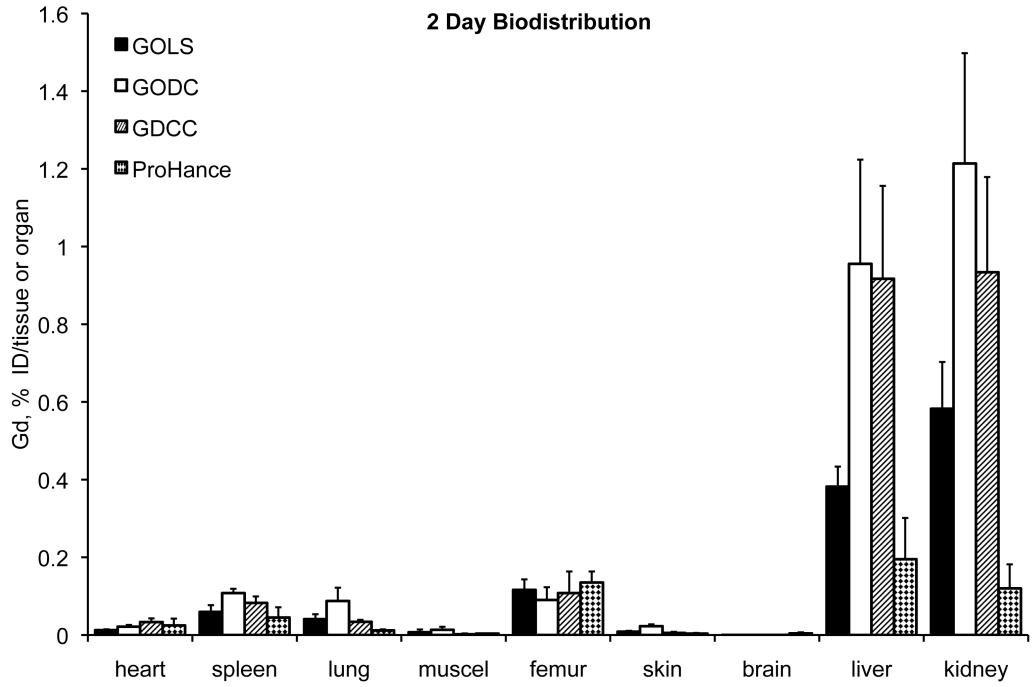

B

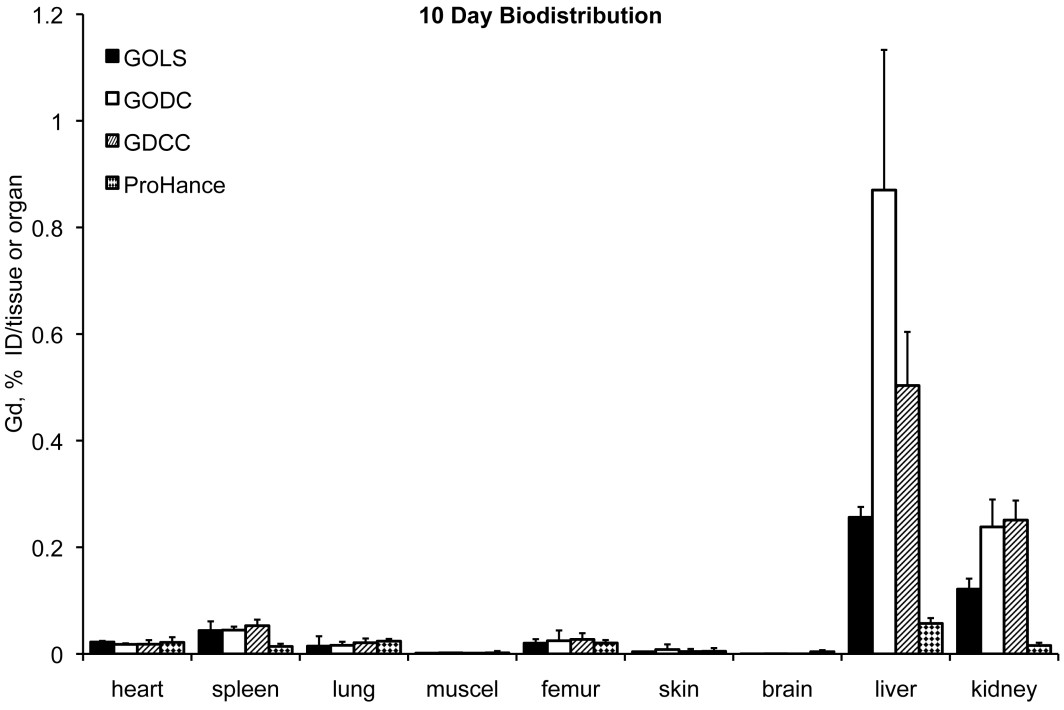

Figure 4.8. Biodistribution of Gd(III) in Balb/c mice 2 days (A) and 10 days (B) after intravenous injection of GOLS, GODC, GDCC, and Gd(HP-DO3A) at a dose of 0.1 mmol-Gd/kg. Data presented as mean ± SD

post injection, which further decreased at 10 days post injection. Approximately 0.3% and 0.1% of injected GOLS was measured in the liver and kidneys 10 days post injection, lower than that of GDCC (0.5% of injected dose/liver, 0.3% of injected dose/kidney) and GODC (0.9% of injected dose/liver, 0.3% of injected dose/ kidney) ($p < 0.05$). Overall, the neutral agent GOLS had much lower long-term body retention than GODC and GDCC.

In Vivo Chelation Stability

Figure 4.9 shows the concentrations of Gd(III), Zn(II), Ca(II), and Cu(II) in the urin samples collected before and at different time periods of 0–8, 8–16, 16–24, and 24–48 h after intravenous administration of GOLS, GODC, GDCC, and Gd(HP-DO3A). Most of the contrast agents were excreted through renal filtration within the first 8 h post injection. The Gd(III) urine levels were comparable among GOLS, GODC, and Gd(HP-DO3A). The linear agent GDCC had lower Gd(III) concentrations than the other agents. In correlation, there was an significant increase of Zn(II) concentration in the urine samples collected in the first 8 h post injection of GDCC ($p < 0.05$), indicating transmetallation of GDCC with endogenous Zn(II) ions. There was no change in Zn(II) concentration in the urine samples from the mice injected with the macrocyclic agents GOLS, GODC, and Gd(HP-DO3A). No significant change of the urine Cu(II) and Ca(II) content was observed during different time periods after injection of the contrast agents, indicating the chelation stability of the tested agents. The result demonstrated the high chelation stability of the neutral polydisulfide containing macrocyclic Gd(III) chelates against transmetallation with endogenous metal ions.

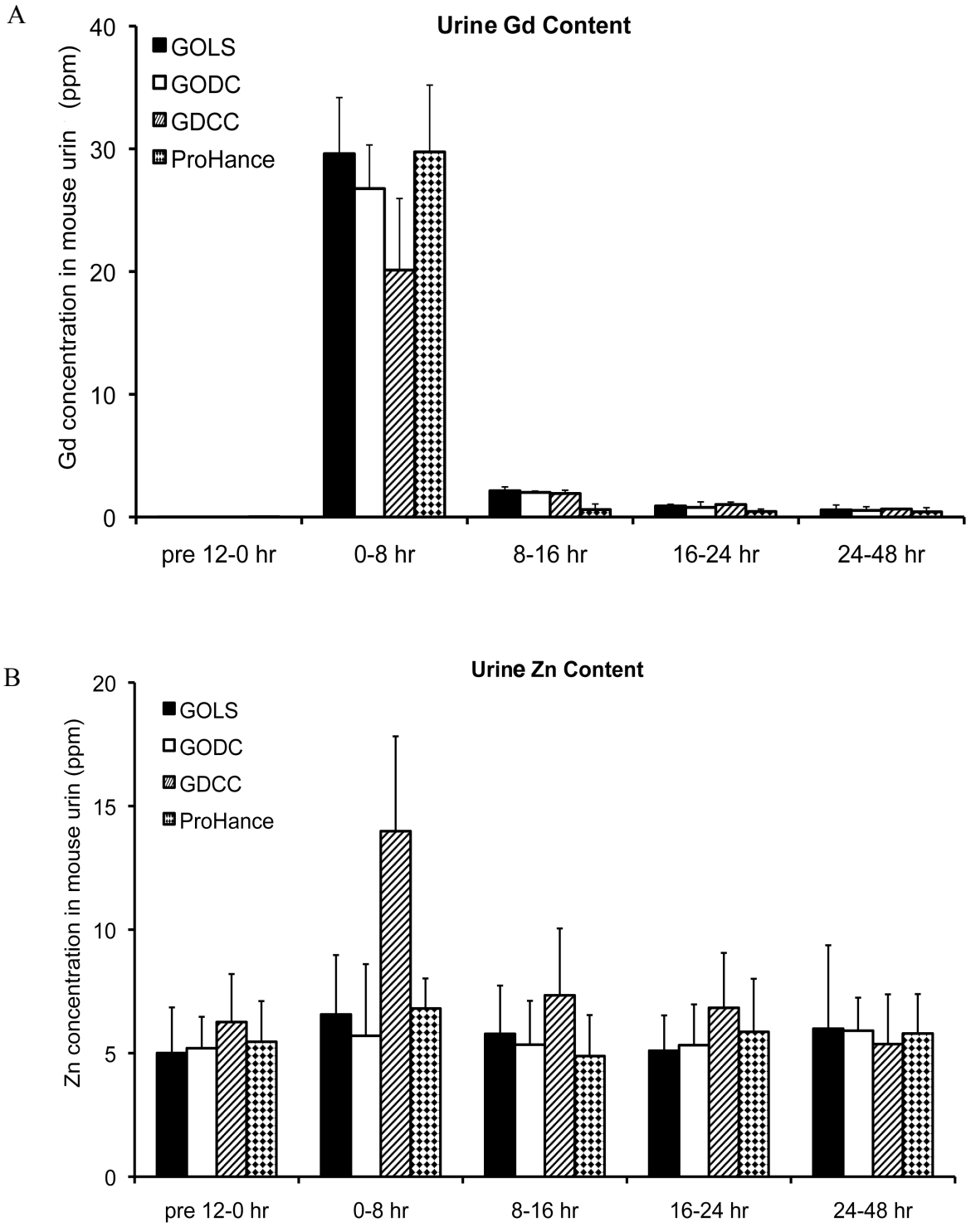

Figure 4.9. Concentrations of Gd(III) (A), Zn(II) (B), Ca(II) (C), and Cu(II) (D) measured in urine before and after administration of GOLS, GODC, GDCC, and Gd(HP-DO3A) at a dose of 0.1 mmol Gd kg^{-1}. Data presented as mean ± SD.

C

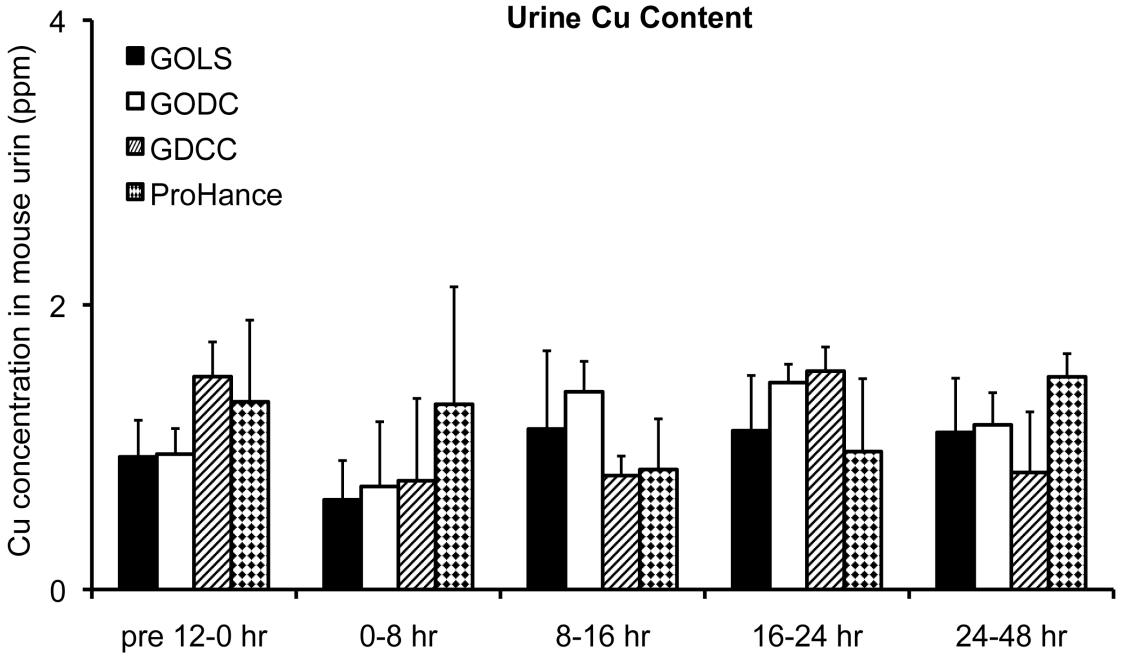

D

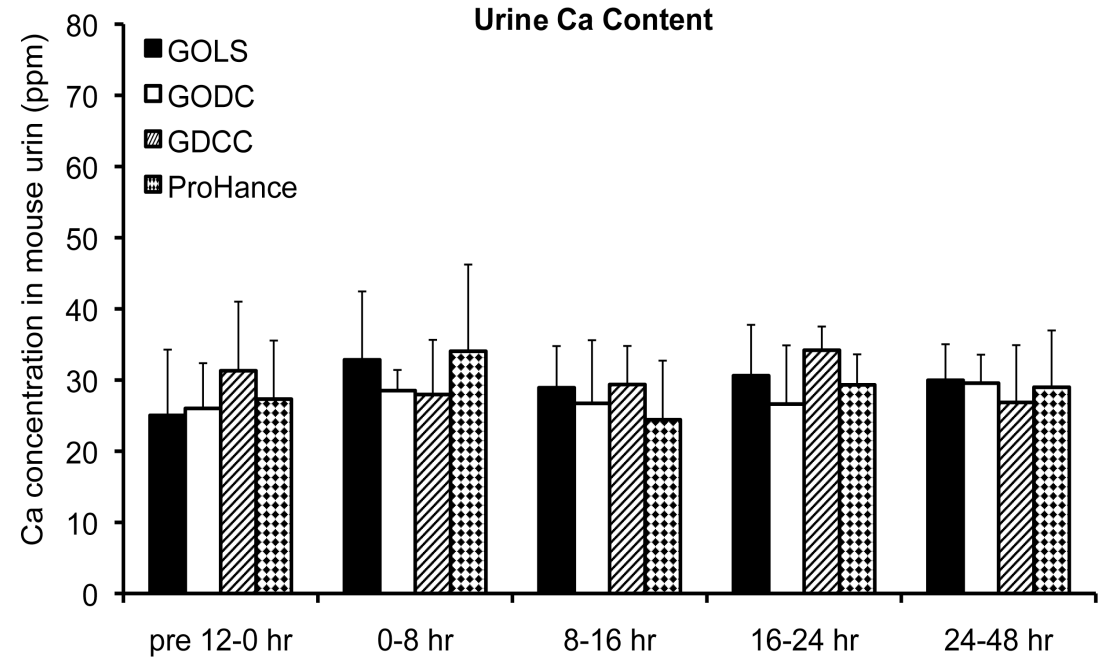

Figure 4.9. Continued.

Discussion

GOLS is a neutral alternative to the previously developed macrocyclic polydisulfide GODC. We have shown that negatively charged GODC is readily degraded in vivo and effective for blood pool and cancer MRI. However, the negative charges on GODC might complicate biodistribution and elimination of the agent due to non-specific charge interaction with tissue. The neutral agent GOLS was designed to eliminate those potential nonspecific tissue interaction. The T_1 and T_2 relaxivities of GOLS were slightly smaller than those of GODC (r1 = 8.25 mM^{-1} s^{-1} and r2 = 10.08 mM^{-1} s^{-1}), but much higher than the clinical agent Gd(HP-DO3A). Similar to GODC, the polymer chains of GOLS were readily reduced by L-cysteine, the most abundant free thiol in plasma (29,36). The in vivo study validated the degradation mechanism through analysis of the urine metabolites of GODC using mass spectrometry. It was shown in both in vitro and in vivo studies that GOLS and GODC demonstrated high kinetic inertness against transmetallation with endogenous metal ions, particularly Zn(II) ions. Since both agents contain Gd-DOTA monoamide chelates, their in vivo kinetic inertnesses are similar to the clinical macrocyclic agent Gd(HP-DO3A). They have a much higher kinetic inertness than GDCC, a polydisulfide agent based on linear chelates. High kinetic inertness of Gd(III)-based MRI contrast agents is a critical safety parameter for complete and intact excretion of the agents from the body.

GOLS demonstrated similar blood pool and tumor contrast enhancement to GODC, which was superior to the clinical agent Gd(HP-DO3A). The strong and prolonged blood pool enhancement of GOLS was a result of increased relaxivity and extended blood circulation. Strong bladder enhancement was observed at 5 min post

administration of GOLS, which was slower than that of Gd(HP-DO3A) but faster than that of GODC (10 min). This indicates the macromolecular feature and strong degradability of GOLS. The gradual increase of bladder signals indicated that GOLS could be readily excreted via renal filtration. The neutral macrocyclic chelate based biodegradable macromolecular MR contrast agent GOLS was advantageous for contrast-enhanced blood pool and tumor imaging over the clinical agent Gd(HP-DO3A), and was readily excreted via renal filtration.

GOLS exhibited similar retention in most organs and tissues to the clinical agent Gd(HP-DO3A), but slightly higher retention in the liver and kidneys. However, the retention of GOLS in the liver and kidneys was much lower than that of GODC and GDCC. The negatively charged GODC had significantly higher liver retention than GOLS, which could be attributed to the relatively slower in vivo excretion of GODC and non-specific interaction of the liver with negative charges of the agent. Nevertheless, the polydisulfide MRI contrast agents, including GDCC, had much lower long-term tissue retention than other non-degradable macromolecular MRI contrast agents, as shown in our previously publications (37,38). In addition, the liver and kidney retentions of the three polydisulfide agents were dramatically lower than those of some other reported macromolecular Gd(III) agents such as the second-generation Gd-DTPA polypropyleneimine dendrimer conjugate (7 kDa) (45% of injected dose in rats 14 days after injection) (39) and carboxymethyl hydroxyethyl starch-(Gd-DO3A) (47% of injected dose remained in the body 7 days post injection) (40). The result validated our design hypothesis that the neutral GOLS would minimize non-specific tissue interaction and result in more complete elimination than negatively charged GODC. The comparable

long-term tissue retention of GOLS to the clinical agent Gd(HP-DO3A) is an advantageous safety feature of the macromolecular blood pool contrast agent for further clinical development.

Conclusion

A neutral polydisulfide polydisulfide containing Gd(III) DOTA monoamide, GOLS, was synthesized and evaluated as a new generation of biodegradable macromolecular MRI contrast agent with high chelation stability. GOLS was readily reduced by endogenous thiols into smaller oligomers that were excreted from renal filtration. It possessed high kinetic inertness against transmetallation with endogenous metal ions both in vitro and in vivo. GOLS produced superior blood pool and tumor contrast enhancement to small molecular clinical contrast agents. Most importantly, GOLS resulted in minimal long-term tissue retention, comparable to a macrocyclic clinical contrast agent Gd (HP-DO3A). The neutral biodegradable macromolecular contrast agent GOLS has the potential to be developed as a safe and effective macromolecular blood pool MRI contrast agent for clinical cardiovascular imaging and cancer imaging.

References

1. Caravan P, Ellison JJ, McMurry TJ, Lauffer RB. Gadolinium(III) chelates as MRI contrast agents: structure, dynamics, and applications. Chem Rev. 1999;99(9):2293–2352.

2. Zhou Z, Lu ZR. Gadolinium-based contrast agents for magnetic resonance cancer imaging. Wiley Interdiscip Rev Nanomed Nanobiotechnol. 2013;5(1):1–18.

3. Chopra A, Shan L, Eckelman WC, Leung K, Latterner M, Bryant SH, Menkens A. Molecular Imaging and Contrast Agent Database (MICAD): evolution and progress. Mol Imaging Biol. 2012;14(1):4–13.

4. Caravan P. Strategies for increasing the sensitivity of gadolinium based MRI contrast agents. Chem Soc Rev. 2006;35(6):512–523.

5. Tang J, Sheng Y, Hu H, Shen Y. Macromolecular MRI contrast agents: structures, properties and applications. Prog Polym Sci. 2013;38(3-4):462–502.

6. Longmire MR, Ogawa M, Choyke PL, Kobayashi H. Dendrimers as high relaxivity MR contrast agents. Wiley Interdiscip Rev Nanomed Nanobiotechnol. 2014;6(2):155–162.

7. Lu ZR, Ye FR, Vaidya A. Polymer platforms for drug delivery and biomedical imaging. J Control Release. 2007;122(3):269–277.

8. Zhou Z, Lu ZR. Dendritic nanoglobules with polyhedral oligomeric silsesquioxane core and their biomedical applications. Nanomedicine. 2014;9(15):2387–2401.

9. Yadav NN, Xu JD, Bar-Shir A, Qin Q, Chan KWY, Grgac K, Li WB, McMahon MT, van Zijl PCM. Natural D-glucose as a biodegradable MRI relaxation agent. Magn Reson Med. 2014;72(3):823–828.

10. Barrett T, Kobayashi H, Brechbiel M, Choyke PL. Macromolecular MRI contrast agents for imaging tumor angiogenesis. Eur J Radiol. 2006;60(3):353-366.

11. Korkusuz H, Ulbrich K, Welzel K, Koeberle V, Watcharin W, Bahr U, Chernikov V, Knobloch T, Petersen S, Huebner F, Ackermann H, Gelperina S, Kromen W, Hammerstingl R, Haupenthal J, Gruenwald F, Fiehler J, Zeuzem S, Kreuter J, Vogl TJ, Piiper A. Transferrin-coated gadolinium nanoparticles as MRI contrast agent. Mol Imaging Biol. 2013;15(2):148–154.

12. Maeda H, Nakamura H, Fang J. The EPR effect for macromolecular drug delivery to solid tumors: improvement of tumor uptake, lowering of systemic toxicity, and distinct tumor imaging in vivo. Adv Drug Deliv Rev. 2013;65(1):71–79.

13. Srikar R, Upendran A, Kannan R. Polymeric nanoparticles for molecular imaging. Wiley Interdiscip Rev Nanomed Nanobiotechnol. 2014;6(3):245–267.

14. Aime S, Caravan P. Biodistribution of gadolinium-based contrast agents, including gadolinium deposition. J Magn Reson Imaging. 2009;30(6):1259–1267.

15. Cheng Z, Al Zaki A, Hui JZ, Muzykantov VR, Tsourkas A. Multifunctional nanoparticles: cost versus benefit of adding targeting and imaging capabilities. Science. 2012;338(6109):903–910.

16. Chan KWY, McMahon MT, Kato Y, Liu GS, Bulte JWM, Bhujwalla ZM, Artemov D, van Zijl PCM. Natural D-glucose as a biodegradable MRI contrast agent for detecting cancer. Magn Reson Med. 2012;68(6):1764–1773.

17. Mohs AM, Nguyen T, Jeong EK, Feng Y, Emerson L, Zong YD, Parker DL, Lu ZR. Modification of Gd-DTPA cystine copolymers with PEG-1000 optimizes pharmacokinetics and tissue retention for magnetic resonance angiography. Magn Reson Med. 2007;58(1):110–118.

18. Liu YJ, Feng LX, Liu TX, Zhang L, Yao Y, Yu DX, Wang LL, Zhang N. Multifunctional pH-sensitive polymeric nanoparticles for theranostics evaluated experimentally in cancer. Nanoscale. 2014;6(6):3231–3242.

19. Kim KS, Park W, Hu J, Bae YH, Na K. A cancer-recognizable MRI contrast agents using pH-responsive polymeric micelle. Biomaterials. 2014;35(1):337–343.

20. Raghunand N, Jagadish B, Trouard TP, Galons JP, Gillies RJ, Mash EA. Redox-sensitive contrast agents for MRI based on reversible binding of thiols to serum albumin. Magn Reson Med. 2006;55(6):1272–1280.

21. Do QN, Ratnakar JS, Kovacs Z, Sherry AD. Redox- and hypoxiaresponsive MRI contrast agents. ChemMedChem. 2014;9(6):1116–1129.

22. Ye DJ, Pandit P, Kempen P, Lin JG, Xiong LQ, Sinclair R, Rutt B, Rao JH. Redox-triggered self-assembly of gadolinium-based MRI probes for sensing reducing environment. Bioconjugate Chem. 2014;25(8):1526–1536.

23. Tian M, Wen XX, Jackson EF, Ng C, Uthamanthil R, Liang D, Gelovani JG, Li C. Pharmacokinetics and magnetic resonance imaging of biodegradable macromolecular blood-pool contrast agent PG-Gd in non-human primates: a pilot study. Contrast Media Mol Imaging. 2011;6(4):289–297.

24. Zhang HW, Wang LQ, Xiang QF, Zhong Q, Chen LM, Xu CX, Xiang XH, Xu B, Meng F, Wan YQ, Deng DYB. Specific lipase-responsive polymer-coated gadolinium nanoparticles for MR imaging of early acute pancreatitis. Biomaterials. 2014;35(1):356–367.

25. Cao CY, Shen YY, Wang JD, Li L, Liang GL. Controlled intracellular self-assembly of gadolinium nanoparticles as smart molecular MR contrast agents. Sci Rep. 2013;3:1024.

26. Lu ZR, Mohs AM, Zong Y, Feng Y. Polydisulfide Gd(III) chelates as biodegradable macromolecular magnetic resonance imaging contrast agents. Int J Nanomed. 2006;1(1):31–40.

27. Lu ZR, Parker DL, Goodrich KC, Wang X, Dalle JG, Buswell HR. Extracellular biodegradable macromolecular gadolinium(III) complexes for MRI. Magn Reson Med. 2004;51(1):27–34.

28. Ye Z, Wu X, Tan M, Jesberger J, Grisworld M, Lu Z-R. Synthesis and evaluation of a polydisulfide with Gd–DOTA monoamide side chains as a biodegradable macromolecular contrast agent for MR blood pool imaging. Contrast Media Mol Imaging. 2013;8(3):220–228.

29. Lu ZR, Wu X. Polydisulfide-based biodegradable macromolecular magnetic resonance imaging contrast agents. Isr J Chem. 2010;50(2):220–232.

30. Wu XM, Zong YD, Ye Z, Lu ZR. Stability and biodistribution of a biodegradable macromolecular MRI contrast agent Gd-DTPA cystamine copolymers (GDCC) in rats. Pharm Res. 2010;27(7):1390–1397.

31. Sieber MA, Lengsfeld P, Frenzel T, Golfier S, Schmitt-Willich H, Siegmund F, Walter J, Weinmann HJ, Pietsch H. Preclinical investigation to compare different gadolinium-based contrast agents regarding their propensity to release gadolinium in vivo and to trigger nephrogenic systemic fibrosis-like lesions. Eur Radiol. 2008;18(10):2164–2173.

32. Thomsen HS, Morcos SK. Nephrogenic systemic fibrosis and nonionic linear chelates. Am J Roentgenol. 2007;188(6):W580 author reply W581.

33. Hermann P, Kotek J, Kubicek V, Lukes I. Gadolinium(III) complexes as MRI contrast agents: ligand design and properties of the complexes. Dalton Trans. 2008;(23): 3027–3047.

34. Angle SR, Qian XL, Pletnev AA, Chinn J. General synthesis of pyrroloquinolizidines: synthesis of an unnatural homologue of the pyrroloindolizidine myrmicarin alkaloid 215B. J Org Chem. 2007;72(6):2015–2020.

35. Appelhans D, Stastny V, Komber H, Voigt D, Voit B, Lhotak P, Stibor I. Novel dendritic cores based on thiacalix[4]arene derivatives. Tetrahedron Lett. 2004;45(38):7145–7149.

36. Feng Y, Zong YD, Ke TY, Jeong EK, Parker DL, Lu ZR. Pharmacokinetics, biodistribution and contrast enhanced MR blood pool imaging of Gd-DTPA cystine copolymers and Gd-DTPA cystine diethyl ester copolymers in a rat model. Pharm Res. 2006;23(8):1736–1742.

37. Zong Y, Guo J, Ke T, Mohs AM, Parker DL, Lu ZR. Effect of size and charge on pharmacokinetics enhancement of biodegradable and in vivo MRI contrast polydisulfide Gd(III) complexes. J Control Release. 2006;112(3):350–356.

38. Zong YD, Wang XL, Jeong EK, Parker DL, Lu ZR. Structural effect on degradability and in vivo contrast enhancement of polydisulfide Gd(III) complexes as biodegradable macromolecular MRI contrast agents. Magn Reson Imaging. 2009;27(4):503–511.

39. Wang SJ, Brechbiel M, Wiener EC. Characteristics of a new MRI contrast agent prepared from polypropyleneimine dendrimers, generation 2. Invest Radiol. 2003;38(10):662–668.

40. Helbich TH, Gossman A, Mareski PA, Raduchel B, Roberts TPL, Shames DM, Muhler M, Turetschek K, Brasch RC. A new polysaccharide macromolecular contrast agent for MR imaging: biodistribution and imaging characteristics. J Magn Reson Imaging. 2000;11(6):694–701.

CHAPTER 5

SUMMARY AND FUTURE DIRECTIONS

Summary

The purpose of this research was to promote the clinical translation of macromolecular contrast agents for noninvasive MR blood pool imaging by developing biodegradable polymeric contrast agents of good safety and high efficacy. The work was an extension of our previous research on polydisulfide system, which demonstrated favorable cancer diagnosis efficacy and efficient in vivo degradation (1-4). However, the previous system was developed based on the kinetically labile linear Gd(III) chelates, whose safety concerns can potentially hinder their further clinical interpretation. To address this issue, we have developed two alternative polydisulfide systems based on two different chelate species: the manganese chelates and the more kinetically inert macrocyclic Gd(III) complexes.

Manganese-based Polydisulfides

Recently, the Gd(III)-based contrast agents have been found in association with nephrogenic systemic fibrosis (NSF), a severe disease affecting a small percentage of the patients with kidney deficiency who had a history of the exposure to Gd(III)-based

contrast agents, especially the linear nonionic chelates (5-10). Although the cause for NSF is still unclear, the design and development of effective non-gadolinium contrast agents with lower toxicity may alleviate the safety concerns over MRI contrast agents. Paramagnetic manganese(II) chelates or compounds are an alternative class of MRI contrast agents. As an endogenous metal, the manganese-based contrast agents exhibit unique biodistribution pattern and effective contrast enhancement in the myocardium, liver, and brain (11, 12). The main limitation of the manganese-based contrast agents is their relatively low relaxivities, which requires a large dose to generate sufficient contrast enhancement for diseased area. However, a high dose of manganese-based contrast agents may lead to unexpected toxic side effects. Chemical modifications of manganese based contrast agents may result in more effective non-gadolinium contrast agents by improving their relaxivities and optimizing their pharmacokinetics and biodistribution (13-17).

In this study, we aim to develop Mn(II)-based biodegradable macromolecular contrast agent as an alternative for Gd(III)-based contrast agents (18). Two types of polydisulfide Mn(II) complexes, Mn-DTPA cystamine copolymer, and Mn-EDTA cystamine copolymer, were synthesized and evaluated. The polymeric ligands were synthesized based on reported protocols, followed by Mn(II) complexation. The T_1 relaxivity of the polydisulfide Mn(II) complexes was increased as compared to that of $MnCl_2$ due to the increase of molecular size, which significantly prolonged their rotational tumbling time, resulting in relaxivity increase. Moreover, the relaxivities of these Mn(II)-based polydisulfides were comparable to that of the previously developed polydisulfide Gd-DTPA, possibly due to the faster water exchange rate of manganese

complexes than that of the gadolinium chelates which compensate the lower intrinsic paramagnetism of manganese (19). Comparing the relaxivity of the two Mn(II) polydisulfides, Mn-EDTA cystamine copolymers (6.41 $mM^{-1}s^{-1}$) had higher r_1 relaxivity than Mn-DTPA cystamine copolymers (4.74 $mM^{-1}s^{-1}$) because of the extra inner sphere water binding site the EDTA agent provides.

The degradation and kinetic stability of the two polydisulfide Mn(II) complexes were evaluated through in vitro incubation study. The two agents were gradually degraded in the presence of endogenous free thiol at plasma concentration. The kinetic stability study revealed potential transmetallation of Mn(II)-based contrast agents with calcium. In vitro incubation of the polydisulfides with calcium revealed lower extent of transmetallation associated with Mn(II)-EDTA cystamine copolymers than Mn(II)-DTPA cystamine copolymers.

The efficacy of the two agents in MR cancer diagnosis was studied on nu/nu athymic mice bearing MDA-MB-231 breast cancer xenografts. The Mn(II)-based polydisulfides generated less blood pool and tumor enhancement in comprison to Gd(III)-based contrast agents. Polydisulfide Mn(II) complexes also resulted in strong and prolonged contrast enhancement in the liver, while Gd-DTPA cystamine copolymers had much less contrast enhancement in the liver. Similar to other reported Mn(II) chelates, polydisulfide Mn(II) complexes resulted in prominent contrast enhancement in the liver and myocardium. Macromolecular Mn(II) complexes have a potential to be developed as effective contrast agents for MR imaging.

Gd-DOTA-based Polydisulfides

To address the potential safety issue with our previously developed polydisulfide Gd-DTPA, we have developed and evaluated two polydisulfide Gd-DOTA as a new generation of Gd(III)-based polydisulfides (20, 21). The agents were designed to maintain the polydisulfide backbone, but incorporate the macrocyclic chelates instead of the linear chelates to ensure high kinetic inertness of the system. The first macrocyclic polydisulfide we have developed was a copolymer of a lysine-based Gd-DOTA monoamide and 3-(2-carboxyethyldisulfanyl)propanoic acid (GODC), synthesized through condensation polymerization. As the previously reported polydisulfides, GODC was demonstrated to be readily degraded through the thiol-disulfide exchange mechanism. Our in vitro transmetallation study demonstrated significantly higher kinetic inertness of this new system over a previously developed polydisulfide Gd-DTPA, GDCC, indicating higher safety potential of the agent in clinical application. GODC showed significant advantage in tumor diagnosis than the clinical agents. However, the extra free carboxylic group on the monomer unit of GODC rendered the polymer charge negatively under physiological pH, and resulted in potentially unfavorable biological features. As demonstrated in our previous studies, the negatively charged polydisulfides showed slower degradation than the neutral polydisulfides. Since the plasma thiols are also negatively charged, the degradation through thiol-disulfide exchange reaction can be hindered via charge repulsions, resulting in comparably slower degradation, and consequently longer tissue retention of the agents. In addition, the charge repulsion effect can lead to increase of the hydrodynamic volume of GODC, which might further affect its elimination through renal filtration.

To extend the family of the macrocyclic polydisulfides, we have further developed a neutral alternative of GODC. Rather than using the negatively charged lysine linkages between the macrocyclic chelates and the polymeric backbone, neutral linkers of ethylenediamine were incorporated in the new polydisulfide Gd-DOTA conjugate, N^1-lysylethylenediamine Gd-DOTA monoamide and dithiobispropionic acid copolymers (GOLS). GOLS was prepared in a similar route as GODC through copolymerization of the Gd-DOTA conjugated monomer and a disulfide-contained monomer. The physiological properties of GOLS, such as molecular weight, hydrodynamic diameter, Gd(III) content, and relaxivity, were determined. Although GODC and GOLS showed similar molecular weight, the actual hydrodynamic volume was different as shown in the DLS results. The negatively charged GODC had a slightly larger size than GOLS due to charge repulsion on the polymeric backbones, which caused differences in relaxivity and degradability between the two macrocyclic polydisulfides. In comparison, GOLS had slightly lower relaxivity, but faster degradability than GOLS. In vitro kinetic stability evaluation showed high kinetic inertness of GOLS, similar to that of GODC. The efficacy of GOLS in MR tumor diagnosis was assessed on an orthotopic mouse breast cancer model. The agent generated advantage in tumor and blood pool imaging than clinical agents. The blood pool enhancment of GOLS appeared to decrease faster than GODC, possibly due to its faster degradation. The pharmacokinetics of GODC and GOLS were compared on mice. The distribution half life of GODC was slightly but not significantly longer than that of GOLS. No difference of elimination half life was observed between the two agents. The extent of tissue retention of the two agents was evaluated through short-term and long-term biodistribution study, in comparison to the polydisulfide Gd-

DTPA agent GDCC and the clinical agent ProHance®. The polymeric agents showed significantly higher liver and kidney retention after 10 days of administration. The order of tissue deposition was GODC > GDCC ≥ GOLS. The prolonged deposition of GODC might be a result of its negative charge. In vivo transmetallation was compared among GOLS, GODC, GDCC, and ProHance® via analysis of the metal metabolite content in mouse urines. The biodistribution study showed minimal tissue deposition of GOLS. The efficacy and safety evaluation suggested GOLS as a safe and effective polymeric candidate for clinical MR cardiovascular imaging and cancer prognosis.

Future Direction

Both the Mn(II) polydisulfides and the Gd-DOTA polydisulfides showed their strength on different areas of disease diagnosis, and are potentially safe to be applied clinically. The Mn(II)-based contrast agents are better imaging agents for the diagnosis of liver dysfunction and myocardium diseases. The Gd-DOTA polydisulfide have advantages on MR blood pool imaging, including MR angiography and cancer diagnosis. These agents are conveniently prepared and characterized.

Development of Polydisulfide Mn(II) Using Chelates with Higher Stability

We have shown in this study that polydisulfide Mn(II) complexes had better relaxivity, pharmacokinetics, clearance, and in vivo enhancement than $MnCl_2$. In comparison to some recently reported dendritic agents and colloidal systems (7-11, 26), our polydisufide-based Mn(II) contrast agents, designed to passively target tumor, showed relatively higher relaxivity and favorable pharmacokinetics. However, the main

limitation of currently available Mn(II) complexes is their low complexation stability, including both thermodynamic and kinetic stabilities. Further studies are needed to design Mn(II) chelates with high thermodynamic and kinetic stability in order to develop novel Mn(II)-based contrast agents and to expand their application in MR imaging of other tissues and organs. The magnetic property of Mn(II) based agents are also different from that of Gd(III)-based contrast agents. Mn(II) complexes often have much higher T_2 relaxivity, which can significantly reduce the signal in T_1-weighted imaging. This could be overcome by designing better imaging sequence to reduce T_2 effect in T1-weighted MRI in the future studies.

Development of Polydisulfide Gd-DOTA with Symmetrical Structure

The monomer of GODC and GOLS was unsymmetrical, causing the final product of both agents with three possible arrangements of the Gd-DOTA monoamide in the polymer chains: two α-amines of separate Gd-DOTA monoamide molecules connected to the same DTTSP molecule, two ε-amines connected to the same DTTSP molecule, and one α-amine and one ε-amine connected to DTTSP. Due to this unsymmetrical structure, cyclization byproducts can be formed during the polymerization. Although we expect minor affect of unsymmetrical structures, it is desirable to develop polymers with symmetrical structure to ensure consistent quality and repetition of the result. The symmetrical polymers should be easy to achieve. Firstly, a different Gd-DOTA contained monomer with symmetrical structures should be synthesized, then copolymerized with the disulfide-based monomer (symmetrical as well) to give the final product.

Application of Polydisulfide Gd-DOTA in Tumor Evaluation

Since the polydisulfide Gd-DOTA are advantageous in the diagnosis of cancer and blood pool imaging. These agents can have high strength on the more advanced MR analysis of tumor staging, which provides clues of treatment response of cancer, leading to effective and individualized treatment. In the experimental design, xenograft malignant tumor models will be developed, followed by periodical treatment. The tumor length (L), width (W) and height (H) will be measured daily before and after treatment using a caliper. The tumor volume will be calculated. The volume growth-time profile will be drawn, and its correlation with the predicted parameters from DEC-MRI will be compared. MR studies will be performed before treatment, and at different time points post administration of the treatment agents using the DCE-MRI sequences. The evaluation of DCE-MRI will be performed using physiological model mimicking the microenvironment of tumor. The prediction will be compared with the physical evaluation of tumor volume. The estimation of treatment response should be more accurate using the polydisulfide Gd-DOTA in compared with that of the clinical agents.

Development of Multifunctional Agents by Adding Targeting Groups or Treatment Agents

The application of the polydisulfide system can be extended beyond imaging agents by conjugating targeting peptides and cancer treatment groups. The current polydisulfides are designed to target tumor passively via the enhanced retention and permeation (EPR) effect. Adding targeting groups on the polydisulfide will further increase the potential of our polymeric system in tumor diagnosis and staging.

References

1. Ke T, Feng Y, Guo J, Parker DL, Lu ZR. Biodegradable cystamine spacer facilitates the clearance of Gd(III) chelates in poly(glutamic acid) Gd-DO3A conjugates for contrast-enhanced MR imaging. Magn Reson Imaging. 2006;24(7):931-940.

2. Lu ZR, Wu X. Polydisulfide based biodegradable macromolecular magnetic resonance imaging contrast agents. Isr J Chem. 2010;50(2):220-232.

3. Lu ZR, Ye F, Vaidya A. Polymer platforms for drug delivery and biomedical imaging. J Control Release. 2007;122(3):269-277.

4. Wu X, Jeong EK, Emerson L, Hoffman J, Parker DL, Lu ZR. Noninvasive evaluation of antiangiogenic effect in a mouse tumor model by DCE-MRI with Gd-DTPA cystamine copolymers. Mol Pharm. 2010;7(1):41-48.

5. Broome DR. Nephrogenic systemic fibrosis associated with gadolinium based contrast agents: a summary of the medical literature reporting. Eur J Radiol. 2008;66(2):230-234.

6. Cowper SE. Nephrogenic systemic fibrosis: a review and exploration of the role of gadolinium. Adv Dermatol. 2007;23:131-154.

7. Cowper SE, Rabach M, Girardi M. Clinical and histological findings in nephrogenic systemic fibrosis. Eur J Radiol. 2008;66(2):191-199.

8. Aime S, Caravan P. Biodistribution of gadolinium-based contrast agents, including gadolinium deposition. J Magn Reson Imaging. 2009;30(6):1259-1267.

9. Kribben A, Witzke O, Hillen U, Barkhausen J, Daul AE, Erbel R. Nephrogenic systemic fibrosis: pathogenesis, diagnosis, and therapy. J Am Coll Cardiol. 2009;53(18):1621-1628.

10. Kuo PH. Gadolinium-containing MRI contrast agents: important variations on a theme for NSF. J Am Coll Radiol. 2008;5(1):29-35.

11. Lee JH, Koretsky AP. Manganese enhanced magnetic resonance imaging. Curr Pharm Biotechnol. 2004;5(6):529-537.

12. Silva AC, Lee JH, Aoki I, Koretsky AP. Manganese-enhanced magnetic resonance imaging (MEMRI): methodological and practical considerations. NMR Biomed. 2004;17(8):532-543.

13. Bertin A, Steibel J, Michou-Gallani AI, Gallani JL, Felder-Flesch D. Development of a dendritic manganese-enhanced magnetic resonance imaging

(MEMRI) contrast agent: synthesis, toxicity (in vitro) and relaxivity (in vitro, in vivo) studies. Bioconjug Chem. 2009;20(4):760-767.

14. Kobayashi H, Brechbiel MW. Dendrimer-based nanosized MRI contrast agents. Curr Pharm Biotechnol. 2004;5(6):539-549.

15. Pan D, Caruthers SD, Hu G, Senpan A, Scott MJ, Gaffney PJ, Wickline SA, Lanza GM. Ligand-directed nanobialys as theranostic agent for drug delivery and manganese-based magnetic resonance imaging of vascular targets. J Am Chem Soc. 2008;130(29):9186-9187.

16. Pan D, Senpan A, Caruthers SD, Williams TA, Scott MJ, Gaffney PJ, Wickline SA, Lanza GM. Sensitive and efficient detection of thrombus with fibrin-specific manganese nanocolloids. Chem Commun (Camb). 2009;(22):3234-3236.

17. Tan M, Ye Z, Jeong EK, Wu X, Parker DL, Lu ZR. Synthesis and evaluation of nanoglobular macrocyclic Mn(II) chelate conjugates as non-gadolinium(III) MRI contrast agents. Bioconjug Chem. 2011;22(5):931-937.

18. Ye Z, Jeong EK, Wu X, Tan M, Yin S, Lu ZR. Polydisulfide manganese(II) complexes as non-gadolinium biodegradable macromolecular MRI contrast agents. J Magn Reson Imaging. 2012;35(3):737-744.

19. Zetter MS, Dodgen HW, Hunt JP. Measurement of the water exchange rate of bound water in the manganese(II)-adenosine triphosphate complex by oxygen-17 nuclear magnetic resonance. Biochemistry. 1973;12(4):778-782.

20. Ye Z, Wu X, Tan M, Jesberger J, Grisworld M, Lu ZR. Synthesis and evaluation of a polydisulfide with Gd-DOTA monoamide side chains as a biodegradable macromolecular contrast agent for MR blood pool imaging. Contrast Media Mol Imaging. 2013;8(3):220-228.

21. Ye Z, Zhou Z, Ayat N, Wu X, Jin E, Shi X, Lu ZR. A neutral polydisulfide containing Gd(III) DOTA monoamide as a redox-sensitive biodegradable macromolecular MRI contrast agent. Contrast Media Mol Imaging. 2016;11(1):32-40.

APPENDIX

The content of Chapter 2, Chapter 3, and Chapter 4 have been published, and are reprinted with permission from the following journals.

1. Chapter 2 is reprinted from JMRI (2012) March 35(3):737-44, 22848. Polydisulfide manganese(II) complexes as non-gadolinium biodegradable macromolecular MRI contrast agents. Ye Z, Jeong EK, Wu X, Tan M, Yin S, Lu ZR. © Owned by the authors, published by 2011 Wiley-Liss, Inc. With kind permission by Journal of Magnetic Resonance Imaging (JMRI).

2. Chapter 3 is reprinted from CMMI (2013) May/June 8(3):220-8, 1520. Synthesis and evaluation of a polydisulfide with Gd-DOTA monoamide side chains as a biodegradable macromolecular contrast agent for MR blood pool imaging. Ye Z, Wu X, Tan M, Jesberger J, Grisworld M, Lu ZR. © Owned by the authors, published by 2013 John Wiley & Sons, Ltd. With kind permission by Contrast Media & Molecular Imaging (CMMI).

3. Chapter 4 is reprinted from CMMI (2015) July, 1655. A neutral polydisulfide containing Gd(III) DOTA monoamide as a redox-sensitive biodegradable

macromolecular MRI contrast agent. Ye Z, Zhou Z, Ayat N, Wu X, Jin E, Shi X, Lu ZR. © Owned by the authors, published by 2015 John Wiley & Sons, Ltd. With kind permission by Contrast Media & Molecular Imaging (CMMI).